UILU-ENG 91-3605

Report No. 159

FINITE ELEMENT SIMULATIONS OF FATIGUE CRACK GROWTH AND CLOSURE

by

Wei Sun

A Report of the

MATERIALS ENGINEERING—MECHANICAL BEHAVIOR

College of Engineering, University of Illinois at Urbana-Champaign

December 1991

Abstract

A modified elastic-plastic finite element program was used to simulate fatigue crack growth and closure. The study has identified some of the factors that contribute to crack closure. It has provided an evaluation of stress, strain and displacement fields near crack tips and their contribution to crack closure. The thesis contains three parts:

In the first part, the mechanism of crack closure under plane strain condition was explained. It is identified that material ahead of the crack tip contracts in the transverse direction, and this mechanism provides residual material on crack surfaces to cause crack closure. Stress-strain history and material displacements as the crack advances are presented to support this model.

In the second part, a distinction is drawn between residual stresses in the absence of crack closure and those due to plasticity induced closure. A new crack tip parameter, S_{tt}, is defined as the applied stress level corresponded to the development of tensile stresses immediately ahead of crack tips. The results demonstrated the importance of this parameter, as the stresses ahead of crack tips could remain compressive even when the crack surfaces opened.

The notch effect on crack closure is studied in the third part of the thesis. Crack opening levels were obtained for crack growing from notches. A set of closure prediction equations was proposed to determine crack growth rate from notches for variable notch shape, applied maximum load level, R ratio and crack length from notch roots on different materials. The model has applied to a steel and an aluminum alloy, and the prediction of crack growth rate from notches were very satisfactory.

Acknowledgement

The research was supported by the Fracture Control Program, College of Engineering, University of Illinois at Urbana-Champaign. Computer access was gained by grants from National Center for Supercomputing applications, University of Illinois at Urbana-Champaign.

My advisor, Professor Huseyin Sehitoglu, is gratefully acknowledged for his guidance and encouragement throughout this study. Professor Darrell Socie, Professor Frederick Lawrence, and Professor James Stubbins are sincerely thanked for their advice.

A special thank to my family members, my father, Huan-Ran Sun and my sister Jun Sun for their encouragement. Finally and most importantly, the strength to conceive and complete the work was provided by my husband, Suyi Liu. He has been giving me the most important thing I need, surport, help and love.

Table of Contents

List of Figures

Nomenclature

A	Constants in S_{open}/S_{max} equation
a	Crack length including half notch width, $a = \ell + c$
Δa	Crack growth increment
B	Constants in S_{open}/S_{max} equation
b	Minor axis of elliptical notch
β	Geometrical coefficient to calculate limit load for CT specimen
c	Half notch width
C'	Material constant in crack growth equation
CCT	Center cracked tension specimen
CT	Compact tension specimen
D	Constants in S_{open}/S_{max} equation
da/dN	Crack growth rate
$d\bar{\varepsilon}P$	Equivalent plastic strain increment
$d\varepsilon_{ij}^{p}$	Plastic strain rate tensor
dS_{ij}^{c}	Deviatoric back stress rate tensor
$d\mu$	Scalar in Ziegler's equation
E	Elastic modulus
F	Constants in S_{open}/S_{max} equation
G	Material constant for power law hardening
H	Hardening modulus
J2	Second invariant of stress
ΔK	Stress intensity range
ΔK_{eff}	Effective stress intensity range

K_t	Theoretical elastic tress concentration factor
ℓ	Crack length measured from notch root (CCT specimen)
m	Exponent in Paris equation
N	Material constant of power law hardening
P_{max}	Maximum applied load level
P_{min}	Minimum applied load level
P_o	Limit load for CT specimen
P_{open}	Crack opening load level at which the residual stresses behind crack tip are overcome
P_t	Applied tensile load level at which all stresses in the uncracked ligament become tensile
P_{tt}	Applied tensile load level at which stresses immediately ahead of crack tip become tensile
R	Applied load ratio
r_p	Notch plastic zone size
s_{ij}	Deviatoric stress
s^c_{ij}	Deviatoric back stress tensor
S_{max}	Maximum applied stress level
S_{min}	Minimum applied stress level
S_{open}	Crack opening stress level at which the residual stresses behind crack tip are overcome
S^{stable}_{open}	Stabilized crack opening stresses
S_t	Applied tensile stress level at which all stresses in the uncracked ligament become tensile
S_{tt}	Applied tensile stress level at which stresses immediately ahead of crack tip become tensile

$\bar{\sigma}$	Von Mises equivalent stress
$\sigma_{o,}$	Yield strength,
T	Specimen thickness
u	Displacement
U	Effective stress ratio
W	Specimen Width
x, y, z	Coordinate Axis (x=crack growth direction, z=thickness direction)

Chapter 1:

Introduction

1.1. Background

Crack closure phenomenon was discovered by Elber in early 1970's [1-3]. He proved the occurrence of crack closure in the wake of a growing fatigue crack by monitoring the nonlinear load-crack tip displacement behavior. The fatigue crack surfaces contacted before the minimum load was reached even during tension-tension cyclic loading, and they remained closed during the loading reversal until the residual stresses on the crack surfaces were overcome. Since the fatigue crack may grow only when the crack surfaces are fully open, an effective stress intensity range, ΔK_{eff}, was defined to characterize crack growth rates instead of the stress intensity range, ΔK.

The first mechanism forwarded to explain the crack closure phenomenon was plasticity induced crack closure. Based on this mechanism, crack closure occurs as a consequence of crack tip plasticity. When a cracked specimen is loaded, the plastic zone develops ahead of the crack tip as the yield strength of the material is exceeded. As the crack grows through the plastic zone, this part of material is unloaded. The plastically 'stretched' material causes the crack surfaces to come in contact before minimum load is reached. Upon further unloading, compressive residual stresses develop behind the crack tip. When these compressive residual stresses on the crack surfaces are overcome during the loading reversal, the crack surfaces are fully open.

In recent years much attention has been focused on fatigue crack closure phenomenon, and crack closure is now a widely studied branch of fatigue research. It is well known that crack closure has the first order influence on the fatigue crack growth rate. The concept of closure may account, at least in part, for previously unexplained behaviors such as mean stress effects, thickness effects, crack growth thresholds, short crack effects, crack growth retardation or acceleration during variable amplitude loading and recently time dependent fatigue loading.

Other mechanisms for crack closure have been proposed, such as crack path roughness induced closure, oxide induced closure and phase transformations induced closure [4-5]. Roughness induced closure results from the mismatch of fracture surface asperities on unloading, which occurs as the result of combined Mode I - Mode II propagation. It can be particularly pronounced near threshold in planar glide materials such as the high strength aluminum alloys. Oxide induced closure is caused by the oxides between the crack surfaces, this type of closure can be caused by other crack fillings, such as fretting debris, liquids or other corrosion products. They can be considered as external agents that reduce the effective stress intensity factor range. In certain metastable alloys the stresses at the crack tip can trigger a phase transformation. If there is a volume increase in transformation, crack closure can develop as the crack penetrates the transformed region.

However, plasticity induced crack closure mechanism provided insight into the understanding of fatigue crack growth phenomena in metallic materials in most cases, including small scale, intermediate and large scale yielding cases. Although, crack growth within the threshold stress intensity regime is known to occur primarily due to roughness and oxide induced closure, there is evidence on the significance of plasticity induced closure in the threshold regime [6]. Closure concepts have been used to explain R-ratio effects and overload effects in early

studies, and have been recently used to explain state of stress effects, notch size effects, applied stress level effects and accelerated growth of short cracks [7-11].

Numerous of experimental results [12-28] have been obtained on crack closure. Experiments have attempted to measure closure directly using strain gages, crack opening displacements [23-24], high resolution microscopy [21] and laser interferometric techniques [22, 28]. The high resolution microscopy and interferometry techniques are capable of observing the crack tip events. Unfortunately, these techniques are confined to surface measurements and it is very difficult to obtain experimental information on residual displacements and stresses near crack tips, especially in the middle of thick bodies. Numerical [19-20, 29-39] and analytical [40-43] studies have also been reported. Yet, the details of the closure mechanism, such as the mechanism of material transfer to the crack front in thin or thick specimens, the residual stress variations during a loading cycle, and the material effect on crack closure levels, have not been well understood. Further numerical studies are needed to provide insight into factors that contribute to crack closure. The present study is an extension of the research on crack closure starting with Paul Lalor and Craig McClung under the guidance of Dr. H. Sehitoglu at University of Illinois.

1.2. Purpose and Scope of Present Study

The current research concentrated on the influence of external factors on plasticity induced closure behavior and fatigue crack growth. An elastic-plastic finite element program was modified for this study. Several mechanisms are proposed based on the results from the finite element analysis. The detail of the finite element code and its modifications are described in Chapter 2.

The mechanism of crack closure under plane strain condition is proposed in Chapter 3. This mechanism will explain where the residual material on the crack

surfaces comes from under plane stress and plane strain conditions. Two other different mechanisms have been discussed and compared with the new model, and evidences supporting the new mechanism are provided.

Characterization of fatigue crack growth processes requires an understanding of fatigue crack tip stress-strain fields including residual stress fields. Previous closure studies placed attention on residual stresses only behind the crack tip. It is realized that residual stresses ahead of the crack tip are also important and aid our understanding of crack closure and crack growth behavior. This research provided a systematic study of the stress distributions behind and ahead of the crack tip under cyclic loading, and the results will be shown in Chapter 4.

It has been reported that small cracks growing from notches exhibit faster growth rates than long fatigue cracks. A set of crack opening prediction equations is proposed in Chapter 5. The crack growth rate from notches can be determined based on these equations. The model can account for variable notch shape, applied maximum load level, R ratio and crack length from notch root for different materials. The model has been applied to predict crack growth behavior from notches in a steel and an aluminum alloy.

Chapter 2:

Finite Element Modeling

2.1. Background

A specialized two dimensional elastic-plastic finite element code with provision of cyclic crack growth was used for this study. The code was initially generated by Lalor and Sehitoglu [29-30] in 1986 and was modified by McClung and Sehitoglu [31-33] in 1987. A small deformation formulation was employed, and the direct Newton-Raphson method was used for the iteration to the correct solution of the nonlinear equations at each load increment.

The material model was based on the concepts of incremental, rate independent plasticity. Kinematic hardening and Von Mises yield criteria were employed, therefore, Bauschinger effect can be accounted during cyclic loading. The elastic modulus, E, is 200,000 MPa, and the value of the hardening modulus, $H = d\bar{\sigma}/d\bar{\varepsilon}^P$ was chosen as constants equal to 0.01E and 0.07E. The yield strength, σ_0, is 430 MPa. In the power law hardening model, $d\bar{\sigma}/d\bar{\varepsilon}^P$, the plastic modulus can be written as a function of stresses:

$$H = (GJ_2^N)^{-1} \qquad (2.1)$$

where $J_2 = 1/2\, S_{ij}S_{ij}$, S_{ij} is the stress deviator. G and N are material constants, where $G = 1.664 \times 10^{-15}$ and N=2.1 in this study. The inelastic strain rate is related to the stress in the following form:

$$d\varepsilon_{ij}^{p} = \frac{3}{2}\frac{d\bar{\varepsilon}^{p}}{\sigma_o}(S_{ij} - S_{ij}^{c}) \qquad (2\text{-}2)$$

where $d\bar{\varepsilon}^{p}$ is equivalent plastic strain increment, S_{ij} is the deviatoric stress tensor and S_{ij}^{c} is the deviatoric back stress tensor. The evolution of back stress is given in Ziegler's form:

$$dS_{ij}^{c} = d\mu\,(S_{ij} - S_{ij}^{c}) \qquad (2\text{-}3)$$

where $d\mu$ is the scalar determined from the consistency condition.

Four noded isoparametric elements were chosen to have linear strain distributions. Higher order elements are not feasible, from the computer time standpoint, because many cycles are simulated with the model and the history of deformations are stored. Truss elements were attached along the crack line, and the crack could grow though the mesh by releasing these truss elements. The stiffness of a given truss element was set to an extremely large value when the crack was 'closed' at that location, and set to a negligibly small value when the crack was 'open'.

2.2. Modeling Issues

Two different geometries were studied, one was a center cracked tension (CCT) specimen (Figures 2.1) and another was a compact tension (CT) specimen (Figures 2.2). The circular and the elliptical notch were considered for the CCT specimen. The ratio of major and minor axis, c/b, is 1 for the circular notch and 3 for the elliptical notch. The theoretical stress concentration factor, K_t, can be calculated as:

$$K_t = 1 + 2.\frac{c}{b} \qquad (2\text{-}4)$$

Therefore, K_t equals 3 for the circular notch and 7 for the elliptical notch. The dimensions of the mesh for the CCT specimen were unitless, since loads were directly applied as stresses along the remote boundary. The half width of the specimen, W, was 1000 units and the half width of the center notches, c, was 32 units. The width of the circular notch and the elliptical notch were the same. The mesh along the crack line was refined, and the size of the element was 2 units (Figures 2.1(a) and 2.1(b)). The mesh contained 864 elements and 936 nodes. In order to increase the resolution in front of the notches, a set of meshes with larger notches and finer elements ahead of the notch were generated. The half width of the notch was 64 units and the element size in front of the notch was 1.33 units. The degrees of freedom are the same for the two sets of meshes.

A one-inch CT specimen was studied. The specimen width, W, was 2 inches (50.8 mm), the thickness, T, was 1 inch (25.4 mm), and the height was 2.4 inches (61 mm). The initial crack length, a, was 1.2 inches (30.5 mm). Two finite element meshes were generated. The coarse mesh contains 803 elements and 878 nodes, and the element size along the crack line is 0.0015 inches (0.038 mm). The fine mesh contained 997 elements and 1083 nodes, and the element size along the crack line was 0.00075 inches (0.019 mm). A concentrated load was applied to the CT specimen. The limit load, P_o, was determined according to fully plastic solutions [44] and is given by:

$$P_o = 1.455\ \beta\ (W - a)\ T\ \sigma_o \qquad (2.5a)$$

for plane strain and by

$$P_o = 1.071\ \beta\,(W - a)\,T\,\sigma_o \qquad (2.5b)$$

for plane stress, where β is defined as

$$\beta = \left[\left(\frac{2a}{W-a}\right)^2 + 2 \times \frac{2a}{W-a} + 2\right]^{1/2} - \left[\frac{2a}{W-a} + 1\right] \qquad (2.5c)$$

The difference between the CCT specimen and the CT specimen is the size of the plastic zone. The plastic zone ahead of the crack tip is very small compared to the crack length and the width of the CT specimen, since the concentration factor for a CT specimen is very large, which could be as high as 30. The result obtained on this specimen can be considered as under small scale yielding. The plastic zone can be fairly large compared with the crack length and the CCT specimen width, and may reach the edge of the specimen when a high stress is applied. Therefore, the results from a CCT specimen can be considered as outside the small scale yielding regime.

Twenty to thirty loading cycles were applied to the specimen so that the crack opening stresses can reach stabilized values. It took 25 loading increments for each reversal when R = 0 and 50 increments when R = -1 for the CCT specimen. Forty load increments was used for R = 0 and 80 increments for R = -1 for the CT specimen. The crack is released at the first increment of the unloading reversal. Previous study [33] has shown that there is no significant effect of node release scheme on crack opening stress levels.

This study examined both ideal cracks and fatigue cracks. A schematic of a crack ahead of a notch is shown in Figure 2.3. In the ideal crack case, a certain number of truss elements in the crack wake were released before the load was

applied. During cycling the crack surfaces were not allowed to contact each other. It is possible that a negative crack surface displacement occurred at minimum applied load. To obtain a fatigue crack, one truss element was released and the crack was advanced at maximum load on each loading cycle. Crack surfaces contacted and sustained compressive stresses during fatigue crack growth simulations. Crack opening level, S_{open}, is defined as the applied load level at which all the compressive residual stresses in the wake of the crack have been overcome. The closure level, S_{clos}, is the stress level at which the first contact of crack surfaces occur. There is no consensus about the mechanism of crack advance in the research community. Often, crack growth rate averages over a large number of cycles are reported. In the numerical model, it is not possible to choose crack increments comparable to experimental crack growth rate per cycle, as this would result in enormous computation times. The size of the crack increments, though, is not likely to change the closure levels provided that the model is fine enough to capture the plastic deformation near the crack tip.

It was found that the tangent-stiffness solution under plane strain condition exhibited much too stiff response when high loads were applied, especially for the CT specimen. The stresses and strains were very high at the crack tip, and convergence was difficult. The reduced integration modification by Nagtegaal, Parks and Rice [45] has been incorporated in the formulation to avoid this mesh locking problems in the plane strain case. The modified strain increment in plane strain finite element code is defined as follows:

$$\dot{\varepsilon}_{ij} = \frac{1}{2}(\dot{u}_{i,j} + \dot{u}_{j,i}) + \frac{1}{3}\delta_{ij}\left(\int_{V_\alpha} \dot{u}_{k,k}\,dV_\alpha - \dot{u}_{k,k}\right) \qquad (2\text{-}6)$$

where $\dot{u}$ is displacement increment, V_α is the volume of the α^{th} element.

The results have been checked against ABAQUS finite element code for the stationary crack cases, the stresses and strains between our code and ABAQUS agreed within 2%. An extensive comparison between our code and the high resolution experimental measurements of Davidson have been recently published by McClung and Davidson [46]. The agreement between the numerical and experimental crack tip strain fields, and crack opening displacements for cracks growing over a wide range of S_{max}/σ_o ratios was remarkable. These results confirm the utility of the finite element model as an indispensible tool for crack closure research.

The simulations were possible with grants from the National Center for Supercomputer Applications at University of Illinois over the last few years. The simulations were conducted using a CRAY-XMP48 supercomputer located in National Center for Supercomputer Applications at University of Illinois. Typical execution times were of the order of 0.5 to 1 CPU hour per simulation with a total usage of approximately 90 hours per year.

Chapter 3:

Modeling of Plane Strain Fatigue Crack Closure

3.1. Background

Plasticity induced crack closure plays a very important role in influencing fatigue crack growth rates. Although it is often associated with plane stress conditions, there is experimental evidence that crack closure indeed occurs, though to a lesser extent, under plane strain conditions [16-18]. Numerical solutions also showed results on crack closure under plane strain [19-20, 29, 38, 34-35]. Dugdale model is often used to describe the physical mechanism of closure in plane stress, however, this model is not applicable to plane strain. In the plane stress case, the inelastic strains in the y-direction (applied load direction) are tensile while the inelastic strains in the z direction (thickness direction) are compressive. In this case the residual material comes from contraction in the z-direction. This mechanism cannot occur in plane strain, because strain in the z direction is zero under plane strain. Contraction in the z-direction is impossible. Despite the significance of the problem, closure mechanisms in plane strain have been forwarded only recently. The question of where the residual material on crack surfaces come from has been addressed in two of the three models discussed below.

Fleck and Newman [47] proposed that plastic strain component in the z-direction is nonzero and provides material on crack surfaces. In plane strain case, total strain in the thickness direction, ε_z, is zero. The plastic strain and elastic strain in this direction are not zero, they have equal magnitude and opposite sign, e.g. ε_z^p

$= -\varepsilon_z^e \neq 0$. This is a plausible mechanism. The schematic shown in Figure 4(a) indicates the crack and the compressive permanent (plastic) strain in the z-direction. Fleck and Newman did not give the magnitude of plastic strain in the z-direction in their study. Depending on the stress levels in the x, y, and z directions at minimum load from this study, the elastic component, ε_z^e, could be compressive and the plastic component, ε_z^p, may be tensile instead of compressive as implied in Figure 3.1(a). The corresponding residual displacements may not cause any appreciable crack closure if ε_z^p is positive. The magnitude of ε_z^p will be discused for a number of cases in a later section.

Another plausible mechanism of crack closure in plane strain was forwarded by Ritchie et al. [48] in response to a discussion of their paper by Prof. McEvily. Ritchie et al. proposed that as the crack grows into the compressive stress zone presented in front of the crack tip under reversed deformation, the stresses are only partially relieved and the remaining compressive stresses contribute to crack closure in plane strain. The compressive stresses at minimum load are indicated in Figure 3.1(b). If the crack were to advance at minimum load by an amount Δa, it would close immediately due to the presence of compressive stresses along its wake. The crack will open during loading when the applied load overcomes the compressive stresses. If the crack is advanced Δa at maximum load, the tensile stresses at the crack tip are sustained and no compressive stresses are generated during the crack advance. Therefore the proposed mechanism relied on the presence of compressive stress field during crack advance, Δa at minimum load. Whether crack advance is possible below the crack opening load or through the compressive stress fields is open to question.

Analogous to the plane stress case where the residual material comes from thickness contraction, progressive contraction of the material at the crack tip in the x-direction (along the crack growth direction) has been identified in plane strain by

the Sehitoglu-Sun Model [49-50]. The deformation of a material element at the crack tip is depicted in Figure 3.1(c). Specifically, the ε_x^p component of strain is compressive and this strain component causes a permanent decrease in the ligament size in the x-direction ahead of the crack tip. Upon the crack advances, since plastic incompressibility condition is satisfied, this would manifest itself as residual material on the crack flanks. Upon unloading, crack contact develops. The magnitude of the ε_x^p is significantly higher than the ε_z^p component and its contribution to crack closure is far more significant. This contraction occurs progressively with cycles and ε_x^p component increases in negative direction. The ε_x^p levels and u_x (displacement in the x direction) will be given for a number of cases later.

3.2. Further Understanding of Crack Closure in Plane Strain

The compact tension specimen was analyzed for this study. Three R ratios 0.3, 0, and -1 were considered under plane strain and plane stress conditions.

3.2.1. Stress-Strain Histories Near Crack Tip

The history of deformation at a material point which is initially three elements away from the initial crack tip is studied. The schematic indicating the original position of the crack tip and the location of the material point is given in Figure 3.2(a). The load cycling as a function of step number is indicated in Figure 3.2(b). Material point is reached after three cycles. Step #40 indicates the maximum load of the first cycle, step #120 of the second cycle, step #200 of the third cycle, and step #280 of the fourth cycle. The crack tip coincides with material point at step #200. The crack tip passes the material point by step #280. Steps #80, #160, #240, and #360 denote the minimum load for the first to the fourth cycle, respectively. Similar results would be obtained if the material point is selected as further away

from the initial crack tip position. In that case the number of cycles to reach the material point would become larger.

The stress-strain behavior in plane strain for σ_y - ε_y, σ_x - ε_x and σ_z - ε_z^p are given in Figures 3.3(a), 3.3(b) and 3.3(c). The stresses are normalized by the yield strength of the material. Only the first four cycles are shown. The results would be qualitatively similar if twenty cycles were considered. The results in Figures 3.3(a) and 3.3(b) are for R = -1 loading at $P_{max}/P_o = 0.4$. The result shown in Figure 3.3(c) is for R=0 loading at $P_{max}/P_o = 0.5$. The ε_x^p component progressively increases in the compressive direction, and the ε_z^p component is compressive at maximum load, but tensile at minimum load. Only plastic strain in the z-direction is shown in Figure 3.3(c) since the total strain in the z-direction is zero. The scale for this figure is different than Figures 3.3(a) and 3.3(b) because the magnitude of the plastic strain in the z-direction is very small compared to the strain in other directions.

Stress in the y-direction versus plastic strain in the z-direction is given in Figure 3.3(d) for the plane stress case. Stress in the z-direction is zero in this case, therefore σ_y is chosen as the vertical scale. The ε_x^p component is compressive and the magnitude is very large compared to the plane strain case although the stress component is much lower than the plane strain case.

The plastic strains in the x and z directions for plane strain at minimum load, when the crack tip reaches the material point and passes it, are summarized in Figure 3.4 for R = 0.3, 0 and -1. Note that the ε_z^p is positive for the P_{max}/P_o levels above 0.3. This is consistent with a positive component shown at step #240 in Figure 3.3(d). The magnitudes given in Figure 3.4 are obtained after 20 cycles while Figures 3.3(a) - 3.3(d) are after three cycles. Therefore, the plastic strain would not match exactly. The magnitude and direction of stress in the x, y and z directions (at minimum load) influence the sign of ε_z^e and hence ε_z^p. A positive ε_z^p cannot

provide residual material to crack surfaces. However, the component ε_x^p is compressive in all cases considered and could provide residual materiel to crack surfaces upon crack advance.

3.2.2. Displacements in the X-Direction

The displacements in the x-direction, u_x, on the crack plane in the first loading cycle are indicated in Figure 8 for the plane stress and plane strain cases. The u_x is given with respect to the crack tip, therefore $u_x = 0$ at the crack tip. The horizontal axis denotes the distance measured from the crack tip, x - a. The location of the crack tip and edge of the specimen are indicated in these diagrams. The displacements ahead of the crack tip are positive, while the displacements behind the crack tip are negative. Note that the displacements indicated in Figure 3.5 correspond to maximum load levels of $P_{max}/P_0 = 0.2$ and 0.5. The shape of the displacements are similar for the plane strain and plane stress case.

A different picture emerges under cyclic loading conditions. The displacements in the x-direction are influenced by cyclic loading. The x - displacement changes after 20 cycles are indicated in Figure 3.6(a) for the plane strain case. In the case of plane strain, the material ahead of the crack tip undergoes contraction in the x-direction consistent with the closure mechanism proposed by Sehitoglu and Sun. As noted in Figure 3.6(a), at the minimum load, the distance between the crack tip and the edge of the specimen is shortened. The location where a negative displacement gradient is present corresponds to compressive strains in the x direction since $\varepsilon_x = \partial u_x/\partial x$. There is a region of positive displacement for material behind the crack tip, and displacement gradients are small far behind the crack tip. Due to these positive displacements with respect to the crack tip, crack tip blunting occurs in plane strain conditions. The blunting

effect decreases the crack closure levels. It is evident that the blunting effect is more pronounced for the $P_{max}/P_o = 0.5$ case compared to the $P_{max}/P_o = 0.2$ case.

Note that the displacement profiles in the plane stress case are different from the plane strain case as shown in Figure 3.6(b). In this case the displacement gradients, $\partial u_x/\partial x$, are small, which are consistent with small strains in the x direction. The ε_x is tensile in front of the crack tip and is approximately zero behind the crack tip. The contribution to closure from the ε_x^p strain component is not significant in this case. Also, at minimum load the contraction of material with respect to crack tip is negligibly small.

3.2.3. Crack Tip Displacements and Dimensional Changes

Crack opening displacements for $P_{max}/P_o = 0.5$ plane strain case are indicated for three cycles and twenty cycles in Figures 3.7(a) and 3.7(b). The solid line indicates the crack opening displacements at maximum load and the broken line denotes the displacements at minimum load. Closure occurs over only one element in the case of three cycles and the crack opening load is close to the minimum load of the cycle. Note that the crack extended 0.0045 inch (0.114 mm) after 3 cycles. A crack advance of 20 cycles corresponds to 0.03 inch (0.762 mm). In this case, closure has occurred over 8 elements which corresponds to a distance of 0.0105 inch (0.267 mm). The crack tip opening displacements at maximum load over the 0.0105 inch are lower than crack opening displacements obtained after 3 cycles. The results clearly indicate that for R=0 loading the length of the closed crack is as low as 1% of the total crack length. When experiments are conducted at an R ratio of 0.3 the length of the closed crack is even a smaller fraction of the total length. The capabilities of the remote measurement techniques of crack closure are severely limited in capturing the phenomena at this small size scale.

The crack opening displacement for the stationary crack case (the third cycle and the 20th cycle) are shown in Figure 3.8. The crack opening displacement for this case obtained by maintaining the crack tip stationary and cycling the specimen three cycles and twenty cycles without allowing contact of crack surfaces. Comparison of Figure 3.8 and Figure 3.6(b) indicates that the residual displacements are smaller than 0.0003 inch (0.007 mm) immediately behind the crack tip. Residual displacements are considered as the difference between the stationary crack opening displacements and the fatigue crack opening displacements after 20 cycles. Therefore, attempts to detect dimensional changes of the specimen or to directly measure residual displacements would have limitations.

A view of dimensional changes at the crack tip illustrated in Figures 3.9(a) and 3.9(b). The undeformed mesh is shown in Figure 3.9(a) and is comprised of elements of size 0.0015 inch (0.038 mm) near the crack tip. In Figure 3.9(b) the deformed mesh is shown at minimum load (zero load) after 20 cycles. The location of the crack tip is noted with a small arrow. Note that the displacements u_x and u_y are magnified by x20 and x3, respectively. The arrow on the left depicts the motion of material in the positive x direction immediately behind the crack tip. This results in the blunting effects on crack surfaces consistent with Figure 3.7(a) - 3.7(c). The second arrow on the right denotes motion to crack surfaces in the negative x-direction. Crack closure in plane strain may be viewed as a competition between the blunting effect and transverse motion of material in the negative x-direction.

3.3. Summary of Crack Closure in Plane Stress and Plane Strain

Since the mechanism is different, the crack closure levels are different for plane stress and plane strain. Normalized crack opening loads, P_{open}/P_{max}, as a function of maximum load normalized by the limit load, P_{max}/P_o, are presented in

Figures 3.10(a) - 3.10(c) for R = -1, 0, and 0.3 cases. The opening loads for plane strain are significantly lower than those for plane stress. The results indicate that the P_{open}/P_{max} decreases with increasing maximum load, and the opening load approaches the minimum load level as the maximum load exceeds 60 percent of limit load for plane strain.

Schematic profiles of crack surfaces under plane strain and under plane stress conditions during a load cycle are illustrated in Figures 3.11. The stress distribution near crack tips during loading and unloading reversal are indicated in the same figure. Note that the left side pictures indicate the crack profile and stress distributions near the crack tip under plane strain conditions. The crack profiles and stress distributions for plane stress are depicted on the right side. At maximum load the crack displacements for plane strain are higher than for plane stress. The stresses ahead of the crack are tensile and the tensile stress field exists also at a distance behind the crack tip (a). During unloading, crack surfaces come in contact at the crack tip first for the plane stress case, however, the first crack contact occurs behind the crack tip in plane strain (b). This is sometimes referred to as discontinuous crack closure and has been confirmed experimentally [34, 51]. The stresses behind the crack tip are compressive for both cases. At minimum load, only a part of fatigue crack surfaces come in contact for the plane strain case. However, the contact distance extends all along the fatigue crack length for the plane stress case (c). The contact zone increases and the compressive stress zone extends behind the crack tip at minimum load. When the applied load level reaches the crack opening load level during loading (d), the crack opens all along its length. The displacements in the x direction are indicated in plane strain (c-d, lhs). Corresponding x-displacements are small for plane stress (c-d, rhs). The compressive stresses behind the crack are relieved at P_{open} and stresses are zero or slightly tensile along crack surfaces. The crack is advanced one element size, Δa, at

maximum load and the crack profile is indicated in the schematic (e). The tensile stresses reach their maximum levels, and the stresses for plane strain are higher than for plane stress. The crack surfaces and stress distributions above are given for R = 0 loading conditions. The results for R = -1 and 0.3 would be similar, and the magnitudes and location of stress fields may vary.

Based on changes of stress distributions near the crack tip during a loading cycle shown in Figures 3.11, stresses behind the crack are compressive until the opening load level is reached, while stresses ahead of the crack tip remain compressive. It is unlikely that the crack could advance before opening load is reached, when both the stress fields behind the crack tip and ahead of the crack tip are in compression. Therefore, the proposal that the presence of compressive stresses on the advancing crack front (shown in Figures 3.1(b)) is the cause of closure is difficult to conceive.

The observations of crack closure suggest that remote measurements of crack closure, such as the back face strain gage method, have to be used with great caution as its ability to detect the local crack contact is rather limited under plane strain conditions. The experimental techniques of Davidson [21] and Sharpe [22], and the surface replication techniques of Nisitani [23] and Sehitoglu [24] have the resolution to detect these changes; unfortunately, these techniques make surface measurements where plane stress conditions exist.

It is difficult to compare the numerical results with experimental P_{open}/P_{max} values. Experimental results of Fleck [16] on CT specimens, using the push rod technique, confirm the presence of closure in plane strain. The crack opening levels reported by Fleck [16, 34] are in general agreement with the results here. Interpretation of CT specimen data in literature is difficult, because often the maximum load levels and the crack lengths are not explicitly given in the research papers. If the experiments are conducted under constant P_{max} conditions, the

model suggests that the closure levels are constant and are independent of crack length over a wide regime of crack growth rates. The model results indicate that as the crack length becomes larger and the remaining ligament undergoes intermediate and eventually net section yielding, then the P_{max}/P_o ratio increases and the P_{open}/P_{max} decreases. Experimental results reported by Allison et al. [25], Vasquez et al. [26-27], and the survey conducted by McClung [52] confirm the nearly constant P_{open} levels. At high crack growth rates, or when the net section stresses approached the yield strength, the experimental P_{open} levels decreased with increasing crack length as noted in the data by Fleck [16] and Staal and Ellen [53].

3.4. Conclusions

1. Three models forwarded to explain the mechanism of closure in plane strain are discussed. A model based on ε_z^p component is shown not to be a significant factor in plane strain closure. A model based on generation of compressive stress over the crack advance region is considered but found not to be realistic if cracks were to extend in tensile stress fields.

2. The model that proposes transverse contraction of ε_x^p strain effect at crack tips will give rise to material transfer to crack surfaces and crack closure in plane strain. A study of inelastic strain accumulation in the x direction and the corresponding negative displacement gradient in the x-direction in front of the crack tip confirm this mechanism.

3. The results demonstrate that under cyclic loading the stress, strain, and displacement fields near crack tips are considerably modified compared to the monotonic loading case. The crack blunting mechanism is due to ε_x^p strain effect. Crack closure models which do not reflect these effects will be deficient.

4. The closure in plane strain is shown to occur over a wide range of P_{max}/P_o levels. Closure is studied further by considering the stress - strain fields,

stationary crack and fatigue crack displacements, and dimensional changes in the vicinity of crack tips. The dimensional changes reported are small and only local (not remote) measurements could capture them.

Chapter 4:

Residual Stress Fields During Fatigue Crack Growth

4.1. Background

An understanding of fatigue crack tip stress-strain fields, including residual stress fields, is needed to characterize the fatigue crack growth processes. Residual stresses are relevant to threshold values of stress intensity, transient changes in crack growth due to sudden changes in applied loading, fatigue crack closure phenomena, and crack growth under different constraint conditions (plane stress versus plane strain).

Closure studies placed attention on residual stresses behind the crack tip, and the applied load level required to overcome these residual stresses has been identified as the crack opening load [29, 31, 37, 38]. Still, residual stresses develop within the forward plastic zone when closure of crack surfaces does not occur, and less attention has been devoted to these stress fields. These residual stresses and those arising from plasticity induced crack closure are deciding factors in fatigue crack growth rates. The residual stresses change with applied S_{max}/σ_o ratio (S_{max} is maximum applied stress, σ_o is yield strength), R ratio, and plane stress versus plane strain conditions. A systematic evaluation of these stresses has not been reported.

A few of experimental studies on residual stress fields for growing fatigue cracks and stationary cracks have been reported. The x-ray diffraction technique, used for these studies [54-62], lacks the resolution immediately at crack tips;

however, it provides useful information on the average residual stress fields. The residual stress field has been reported upon removal of applied load [54-60] in addition to the stress field ahead of a fatigue crack tip at maximum load [55, 60]. Higher strength materials resulted in higher residual stresses [56]. The residual stresses at minimum load have been found in the range from $-0.3\sigma_0$ to $-0.7\sigma_0$ for R = 0 loading condition. These stresses appear to be much lower compared to calculations using crack tip displacements [16, 21] and compared to finite element results from early studies [29, 31-32, 38]. The residual stress magnitudes were in the range of $-1\sigma_0$ to $-3\sigma_0$ based on finite element studies, but a systematic study of these stresses has not been reported.

The residual stresses at the crack tip evolve from two contributions: (i) residual stresses due to reversed deformation in the absence of crack closure effects, and (ii) residual stresses due to the crack closure phenomena. In the case of ideal cracks, all the residual stresses originate from the reversed plasticity at the crack tip constrained by the surrounding material. In the case of fatigue cracks, residual stresses are added from plasticity induced closure. When the applied load is increased from the minimum load, a fraction of the applied load overcomes these residual stresses that would exist in the absence of closure. Another fraction of the applied loading overcomes the residual stresses due to plasticity induced closure. Davidson [54] discussed the difficulty to apportion the residual stresses ahead of the crack tip and the crack wake effects experimentally. The residual stresses due to these two effects are not independent, and experimental measurements will yield the combined effect. Careful numerical studies can isolate these two effects as discussed below. By studying the stress fields for ideal cracks versus fatigue cracks, a distinction can be made between these two effects. This distinction allows an unambiguous determination of crack closure contribution to residual stress fields as a function of R-ratio and constraint

conditions. Debate on whether crack closure occurs in the plane strain [17-18, 63-67] or whether the observed R-ratio and overload effects come about solely due to the residual stress ahead of the crack tip [68-69] continues. This chapter will resolve most of these questions. Specifically, the results show that closure in plane strain conditions indeed occurs, though the residual stresses ahead of the crack tip play even a more significant role.

4.2. Stress Distributions for Notches and Ideal Cracks versus Fatigue Cracks Under Cyclic Loading.

The schematics given in Figures 4.1(a) and 4.2(b) describe the typical stress distribution at the ideal and the fatigue crack tip and the stress-strain behavior (σ_{yy} - ε_{yy}) at a material point ahead of an ideal crack and a fatigue crack, respectively. In the case of a fatigue crack, compressive stresses developed behind the crack tip. For an ideal crack, compressive stresses were confined to the crack tip forward plastic zone. The material at the crack tip has a prior deformation history which is also indicated. When the crack tip is at a distance from the material point, the material behavior is elastic. As the crack tip approaches the material point the strains accumulate in the tensile direction. The σ_{yy} component at the crack tip becomes tensile when the applied stress reaches the crack tip tensile stress level, S_{tt} (P_{tt}). S_{tt} is used for the CCT geometry and P_{tt} for the CT geometry. The S_{tt} (P_{tt}) level could be as high as 70% of S_{max} (P_{max}) for fatigue cracks. The S_{tt} (P_{tt}) level for an ideal crack is lower than that of a fatigue crack, yet it could be as high as 40% of S_{max} (P_{max}) under R = 0 condition. This is illustrated in Figure 4.1(c). The portion of applied stress range that overcomes residual stresses in the crack wake (crack closure contribution) and the portion that overcomes the residual stresses for the ideal crack tip (in the absence of crack closure) are illustrated in Figure 4.1(c). During this study, it is proved that the crack closure contribution to S_{tt} (P_{tt}) in the

plane stress dominates over the crack closure contribution to S_{tt} (P_{tt}) in the plane strain. On the other hand, the residual stresses due to reversed deformation are higher in the plane strain compared to the plane stress. This study will emphasize the contributions to S_{tt} (P_{tt}) systematically for a broad range of conditions, and provided further insight into our understandings of crack closure and residual stresses in plane strain versus plane stress condition.

4.2.1. CCT Specimen, S_{max}/σ_o=0.8, R=-1 case

The stress distributions ahead of the circular and elliptical notch are given in Figures 4.2(a) and 4.2(b) for plane stress cyclic loading conditions, respectively. The notch root stress, S_{tt}, becomes tensile at -0.56 S_{max} for the circular notch and at -0.76 S_{max} for the elliptical notch. The stress field ahead of notch root, S_t, becomes tensile at 0.20 S_{max} for the circular notch and 0.12 S_{max} for the elliptical notch. The results are also presented for an ideal crack in Figure 4.2(c) and the stress level at which the crack tip stress becomes positive is -0.76 of S_{max}, similar to the elliptical notch case. The stress field ahead of the crack tip, S_t, becomes to tensile at 0.20 S_{max}. The crack length, ℓ, in Figure 4.2(c) is chosen as 1.5 times of the half notch width. Now, consider the stress distribution ahead of a fatigue crack when it grows to the same length as the ideal crack. The minimum stresses for the ideal crack and for the fatigue crack were -1.5 σ_o and -1.2 σ_o, respectively. Crack surfaces open when applied stress is -0.12 S_{max} for the fatigue crack from the circular notch and -0.16 S_{max} for the fatigue crack from the elliptical notch. The S_{tt} level for a fatigue crack is reached at a higher stress, -0.08 S_{max}, as shown in Figures 4.3(a) and 4.3(b). The S_t level is 0.16 S_{max} and 0.20 S_{max} for the fatigue crack grown from the circular notch and the elliptical notch. When ℓ/c = 1.5 the results for a crack growing from a circular notch or elliptical notch are similar. The S_{tt} levels in Figures 4.3(a) and 4.3(b) for a fatigue crack far exceed those shown for the ideal crack case in Figure

4.3(c). The contribution to S_{tt} from the crack closure effect is {-0.08 - (-0.76)}S_{max} = 0.68 S_{max} and the contribution to S_{tt} from the residual stress effect in the absence of closure is {-0.76 - (-1)} S_{max}= 0.24 S_{max}. Therefore, the crack closure contribution to S_{tt} (= 0.68 S_{max}) is greater than the crack tip reversed deformation contribution to S_{tt} (0.24 S_{max}).

Results for plane strain conditions are presented in Figures 4.4. The trends are similar to the plane stress case, however, the magnitude of crack tip stresses at the maximum and minimum load are higher in the plane strain case. In Figures 4.4(a) and 4.4(b) the stress distributions and the S_{tt} and S_t levels for a circular notch and an elliptical notch are given. The stress distributions for an ideal crack and for a fatigue crack are shown in Figures 4.4(c) and 4.4(d). The compressive stress at the minimum load is -3.2 σ_o for the ideal crack tip, while it is -2.3 σ_o for the fatigue crack tip. The compressive residual stress decreased immediately to zero behind the ideal crack tip; for the fatigue crack, the compressive stresses are as high as -1.0 σ_o when ℓ/c is -0.5. The stress level at which the crack tip stress becomes tensile in an ideal crack and in a fatigue crack are -0.44 S_{max} and 0.24 S_{max}, respectively. The crack opening load is 0.20 S_{max} for the fatigue crack started from the circular notch. The contribution to S_{tt} level from crack closure effect is {0.24 - (-0.44)} S_{max} = 0.68 S_{max} and the contribution from residual stress in the absence of closure is {-0.44 - (-1)} = 0.36 S_{max}.

To illustrate the results further, consider Figures 4.5(a) and 4.5(b) where the residual stress contribution to S_{tt} in the absence of closure and the crack closure contribution to S_{tt} is shown for plane stress and plane strain cases. It is evident that the residual stress effect in the absence of crack closure (light shaded region) is more significant in plane strain compared to plane stress. However, the crack closure contribution to S_{tt} (dark shaded region) is significant and cannot be ignored.

4.2.2 Transient variations of S_t, S_{tt}, S_{open}

Crack opening stresses S_{open}, and crack tip tensile stress S_{tt} levels are very similar. Depending on the stress distribution in the vicinity of the crack tip, the S_{tt} level may be slightly higher or slightly lower than S_{open}.

The evolution of S_{open}, S_{tt}, and S_t as the fatigue crack grows from the elliptical notch under plane stress an plane strain are given in Figures 4.6(a) and 4.6(b), respectively. S_{open} at the first load cycle is -0.76 S_{max} for plane stress and -0.68 S_{max} for plane strain. S_{tt} at the first load cycle is -0.72 S_{max} for plane stress and -0.52 S_{max} for plane stress. As the crack grows, S_{open} and S_{tt} increase and tend to stabilized values. S_{tt} is higher than S_{open} during the loading history in this case, and the difference between S_{open} and S_{tt} is very small. S_t is stabilized when the crack starts to grow, which equals -0.08 S_{max} for plane stress and 0.16 S_{max} for plane strain.

The results of the difference among S_{open}, S_{tt} and S_t for cracks from an elliptical or a circular notch are similar. The stress field of the notch itself has a very diminishing effect when ℓ/c ratio exceeds 1.0.

4.2.3 CCT Specimen, S_{max}/σ_o=0.8, R=0 case

The stress distribution ahead of the circular and the elliptical notch are given in Figures 4.7(a) and 4.7(b) for plane stress cases. S_{tt} is 0.44 S_{max} for the circular notch and 0.16 S_{max} for the elliptical notch. S_t is 0.52 S_{max} for the circular notch and 0.60 S_{max} for the elliptical notch. The stress distributions near an ideal crack and a fatigue crack are shown in Figures 4.8(a) and 4.8(b). The crack tip tensile load levels are 0.16 S_{max} and 0.48 S_{max} for the ideal crack and the fatigue crack, respectively. The crack opening load level for the fatigue crack is 0.40 S_{max}, two load increments after the crack is open, the crack tip stress becomes tensile. S_t is 0.64 S_{max} for the ideal and fatigue crack. The residual stress at minimum load was

near -1.0 σ_o for the ideal and fatigue crack. The residual stress decreased to zero behind the crack tip, gradually for the fatigue crack case, and almost immediately for the ideal crack case.

The stress distributions ahead of notches are shown in Figures 4.9(a) and 4.9(b) for plane strain. Crack tip tensile load is 0.48 S_{max} for the circular notch and 0.24 S_{max} for the elliptical notch. S_{tt} for an ideal crack is 0.32 S_{max}, and 0.36 S_{max} for a fatigue crack as shown in Figures 4.10(a) and 4.10(b). It is also noted that the stress amplitude is higher but the plastic zone size is smaller for plane strain than for plane stress cases. The crack opening stress is 0.40 S_{max}, which is one load increment higher than S_{tt}. S_t is 0.48 S_{max} for the circular notch, which is same as S_{tt}, and 0.52 S_{max} for the elliptical notch. The residual stress at minimum load is near -1.5 σ_o, which is lower than the residual stress of -2.3 σ_o in the ideal crack case. The results shown in Figures 4.11(a) and 4.11(b) summarize the findings. The S_{tt}/S_{max} ratio decreases with increasing applied maximum stress in plane stress. This decrease is due to the reduction of crack closure with increasing S_{max} and the lowered effect of crack tip residual stresses. Under R = 0 conditions, the crack closure contribution to S_{tt} was diminished in the plane strain case.

4.2.4. CT Specimen, P_{max}/P_o = 0.5, R = 0 and -1 Case

The stress distribution near the ideal crack tip and fatigue crack tip under plane stress conditions is indicated in Figure 4.12(a) and 4.12(b), respectively. The crack length is 1.23 inches (= 0.615W). The stress at the crack tip at maximum load was lower for the fatigue crack case. The minimum stress at the crack tip was similar for both cases and is near -1.0 σ_o. However, there is an extension of residual compressive stress zone in the fatigue crack wake. This zone extends at a distance ahead of the crack tip in the ideal crack case. The crack tip becomes tensile when applied load is P_{tt} = 0.20 P_{max} for the ideal crack, and at P_{tt} = 0.55 P_{max} for the

fatigue crack. The crack opening load is $P_{open} = 0.5\ P_{max}$. The Pt level is 0.65 Pmax for both the ideal crack and the fatigue crack.

The stress distribution near the crack tip under plane strain conditions is indicated in Figures 4.13(a) and 4.13(b). The tensile stresses at the crack tip were higher for the ideal crack case, while the compressive stresses at the crack tip were higher in the fatigue crack case. The region of compressive stress in the fatigue crack wake is noted in Figure 4.13(b). The crack tip becomes tensile when applied load is $P_{tt} = 0.25\ P_{max}$ for an ideal crack, and at $P_{tt} = 0.30\ P_{max}$ for a fatigue crack. The P_{tt} levels for the ideal crack and the fatigue crack are very close, which suggests that residual stress effect in the absence of closure is significant in the plane strain case. Furthermore, we note the significant difference between P_{open} and P_{tt} level for plane strain R = 0 case. Here, the use of P_{open} for characterizing crack growth would have major drawbacks, since the material at the crack tip was experiencing a compressive stress of -2.0 σ_o (the P_{open} line) even when the crack surfaces opened. The description of crack growth using P_{tt} would be more meaningful here.

To illustrate the results further, consider Figures 4.14(a), 4.14(b) where P_{tt}/P_{max} is plotted versus P_{max}/P_o. The residual stress contribution to P_{tt} is shown for plane stress and plane strain cases for R = 0 conditions. The contributions are indicated in the absence of closure and due to the crack closure induced residual stresses. We did not provide any stress distributions for the R = -1 case; however, the summary of results for plane stress and plane strain cases is given in Figures 4.14(c) and 4.14(d), respectively. The contribution from the 'residual stress effect in the absence of crack closure (due to reversed deformation only)' in plane strain is very significant compared to the 'crack closure contribution'. We also note that crack closure was the dominant contribution to S_{tt} in plane stress case.

4.3. Discussion of Results

This chapter evaluated the contribution of residual stresses, due to reversed deformation only and due to plasticity induced crack closure, on crack tip stress behavior. The demarcation between these residual stresses is established to gain a further understanding on the origin of fatigue crack residual stress fields. The residual stresses were reported for plane stress and plane strain conditions. Experimental methods to measure residual stresses inside the specimens (where plane strain conditions prevail) are rather limited and this study shows that the residual stresses are higher in plane strain compared to plane stress.

The stress fields determined in this study are considerably more complex than those reported in experiments. Crack tip residual stresses have been reported of the order of 0.3 to 0.7 σ_0 based on X-ray studies [54-61]. Using stereoimaging the sensitivity of measurements near crack tip is significantly improved, and at maximum load crack tip stresses were as high as 2.3 to 3.5 times the yield stress [70]. Unfortunately, corresponding residual stresses at minimum load have not been reported. In the current study, the reported values of compressive residual stress (at minimum load) are of the order of 1.2 σ_0 in plane stress and 3.2 σ_0 in plane strain under R = -1 conditions. The residual stresses for the ideal cracks are higher than for the fatigue cracks. However, the residual stresses are confined to a region in front of the ideal crack. For real fatigue cracks, the residual compressive stresses exist over a significant portion of the crack wake.

The S_{open}/S_{max} levels, S_{tt}/S_{max} levels and S_t/S_{max} levels are presented in Table 1 through Table 4. The result indicated that the S_{tt}/S_{max} decreases with increasing maximum stress. This behavior is similar with S_{open}/S_{max} levels as reported in Chapter 3. It is noted that the S_t/S_{max} does not exhibit the maximum applied stress dependence as the crack opening stress. The reversed plastic zone is depend on applied stress, at certain percentage of the maximum applied stress, the

stress within the reversed plastic zone becomes to tensile. This percentage does not change with the value of the maximum applied stress. Also the S_{tt}/S_{max} does not change with the notch shape nor the crack length.

Comparing S_{tt} in different notches and cracks, it is noted that the S_{tt} levels for the elliptical notch are very similar with S_{tt} for the ideal crack in plane stress, and are slightly lower for the ideal crack in plane strain. In the plane stress case, the crack tip tensile load, S_{tt}, decreases with increasing applied load. For plane strain, S_{tt} or P_{tt} does not vary as significantly with increasing applied load.

In early studies on crack closure on CCT specimens, the crack opening levels for plane stress were higher than plane strain at low S_{max}/σ_o values, while at high S_{max}/σ_o levels, the crack opening stress level for plane stress was lower. Both Newman [38] and Lalor and Sehitoglu [29] reported such results. No explanations for this crossover were available at that time. This crossover behavior in S_{open} was confirmed in this study, and the reason for this behavior is now explained as follows. Considering results from CCT specimen under R = -1, it is found that for the S_{max}/σ_o = 0.4 case the crack opening levels were 0.44 S_{max} and 0.24 S_{max} for plane stress and plane strain, respectively. For the S_{max}/σ_o = 0.8 case, the crack opening levels were -0.16 S_{max} and 0.20 S_{max} for plane stress and plane strain, respectively. When the residual stress effect in the absence of crack closure was subtracted off, it was determined that the closure contributions were 1.0 S_{max} and 0.84 S_{max} for plane stress under S_{max}/σ_o = 0.4 and 0.8, respectively. For corresponding plane strain cases, the closure contributions were 0.28 S_{max} and 0.68 S_{max}, respectively. Since 0.28 S_{max} < 1.0 S_{max} and 0.68 S_{max} < 0.84 S_{max}, plasticity induced closure is more significant in plane stress compared to plane strain over the whole range of S_{max}/σ_o.

The results also showed that crack closure indeed occurred in plane strain. It is noted, however, that the residual stresses due to crack closure in plane strain

was confined to a short distance behind the crack tip, and their contribution to overall residual stress fields was small. In a recent study on the origin of closure mechanisms in plane strain [71-72], it was confirmed that the residual material (appended on crack surfaces) in plane strain comes from the contraction of the material in the transverse (crack growth) direction. The volume of the material transferred to crack faces was smaller in plane strain compared to the material transferred to crack faces (due to contraction in the z or thickness direction) under plane stress conditions. The results reported in this study confirmed these early findings, and the smaller zone of contact in the crack wake was noted in plane strain relative to plane stress.

The data shown in the figures suggested that there were important differences between the S_{tt}, P_{tt} levels between the CCT and CT specimens. This difference was significant, and pointed out to testing conditions that would result in drastically different S_{tt} versus P_{tt} levels, therefore different crack growth behaviors. One reason for the difference lies in the difference in plastic zone behavior of the two specimens. For the CT specimen, when $P_{max}/P_o < 0.8$, the plastic zone size ahead of the crack tip was very small compared to the uncracked ligament of the specimen, and the elastic strain field severely constrained the crack tip. In the CCT specimen, the plastic zone at the maximum load was comparable to the uncracked ligament size even when $S_{max}/\sigma_o < 0.8$. Then, the constraint was reduced on the crack tip and the compressive residual stress effect in the absence of closure was decreased. One reason for the higher constraint and higher stresses in the CT specimen was the presence of high transverse (in-plane) stresses, as outlined in References 25 and 52.

Simple methods forwarded in early studies, for determining the residual stresses, were useful; however, these cannot capture the details of the complex crack tip behaviors studied here. The Dugdale based model proposed by Budiansky

and Hutchinson [42], and the model proposed by Fleck [16] using the crack displacements, were noteworthy. Both models, however, predicted that the residual stresses decreased to zero very rapidly in the crack wake contrary to the results presented here. Furthermore, it is important to make a further distinction between this work and those previous reported studies on growing cracks by Budiansky and Hutchinson, Rice [42, 73]. Simple analysis of crack tips predicts that material ahead of the crack suffered tensile yielding as soon as the crack tip opened. Although true for infinitely sharp cracks, this behavior would not occur in cracks with finite tip radius, growing in ductile materials. The 'ideal' cracks, studied in our work do not experience closure; however, experience yielding and develop a finite tip radius, and the remote stress could be as high as 0.4 S_{max} before these ideal crack tips suffer tensile stressing. Similarly, fatigue cracks develop a finite tip radius; hence, their behavior, after the crack opens, differs from infinitely sharp cracks.

The results have implications in understanding of several factors that influence fatigue crack growth behavior due to reversed deformations in the absence of crack closure and when significant closure effects were present. It is known that high R-ratios, high S_{max}/σ_o levels, and physically small crack cases are conducive to decrease in the influence of closure. Therefore, when the closure effects were small, the crack driving force parameters should have incorporated S_{tt}; since, crack growth in these cases would still depend on the tensile stress range at the crack tip. When the closure effects were significant, S_{tt} retained its meaning as a measure of the effective driving force via releasing of residual stresses behind the crack and those at the crack tip. Therefore, the results could be used in development of realistic models of fatigue crack growth accounting for residual deformations, stresses and strains at crack tips. The knowledge of these stress fields would be necessary whether the developed models were phenomenological using

remote quantities or based on micro-mechanical failure considerations (such as localized shearing, tensile decohesion).

4.4. Conclusions

The normalized stresses and loads, S_{tt}/S_{max} (P_{tt}/P_{max}) and S_t/S_{max} (P_t/P_{max}) were determined for CCT and CT geometries under plane strain and plane stress, R = 0, -1 conditions. The following conclusions are drawn:

1) Upon determining S_{tt} for an ideal crack and a fatigue crack, it was found that S_{tt} for a fatigue crack combines: (a) the residual stress effect in the absence of crack closure, and (b) the residual stresses generated due to crack closure. The residual stress in the absence of crack closure developed due to reversed deformation at the crack tip. This effect was always more significant in plane strain than in plane stress. On the other hand, the residual stress effect due to crack contact was more significant in plane stress compared to plane strain.

2) The S_{tt} was similar to crack opening load S_{open} for the CCT geometry. Therefore, the use of S_{open} indicated tensile stress conditions at the crack tip. The P_{tt} was higher than the crack opening load P_{open} for the CT geometry in plane strain. This difference in behavior of CCT and CT specimens was attributed to non-similitude of residual stress distributions. These results proved the need to consider, P_{tt}, in addition to crack opening load, P_{open}, in representation of crack driving force.

3) The crack closure effect was always more significant in plane stress compared to in plane strain. It was verified that the apparent high S_{open} levels in plane strain at high applied stresses reported in early studies on CCT specimen under R = -1, was not a 'true' crack closure (contact) effect. It was a consequence of higher residual stress buildup under reversed deformation in plane strain.

4) Compressive residual stresses were determined in the range -1.2 σ_0 to -3.2 σ_0 for ideal cracks and for fatigue cracks in the CT specimen. The magnitude of the residual stresses for fatigue cracks were lower than for the ideal cracks in the CCT geometry. However, the compressive stresses extended over a large volume including the crack wake for fatigue cracks while they were confined to the plastic zone for ideal cracks for both CCT and CT geometries.

5) It is imperative to develop crack propagation models that capture the residual stress in the crack wake and at the crack tip, as both would influence the S_{tt} (P_{tt}) hence the crack growth behavior.

6) It is found that S_t/S_{max} is independent with maximum applied stress, notch shape and crack length. It is only influenced by R-ratio and constraint conditions.

Chapter 5:

A Unified Model for Crack Growth from Notches

5.1. Background

It has been observed experimentally that fatigue cracks growing from the notch may grow at unusually high crack growth rates when the crack length is much smaller than the notch width [19, 74-88]. These small cracks propagate initially at a high crack growth rate, decelerate to a minimum rate, and then match the long crack data trend. A considerable fraction of the crack propagation lifetime could be spent in the regime where transient changes in crack growth behavior occur. The transient regime of crack growth is proportional to the elastic stress field of the notch to a first approximation. In view of the significance of the problem, models of crack growth from notches should be accurate in their estimate of crack driving force hence the crack growth rates.

One explanation of the accelerated crack growth rate at notches is the phenomena of 'crack closure'. When a crack initiates from a notch root, the plastic wake field has not been fully developed. Therefore, the crack surface can open at very low applied load levels, and the effective stress intensity range is higher compared to a long crack. As the crack grows the plastic wake develops, the crack tip generates its own stress fields which dictate the closure behavior and the influence of the notch becomes gradually smaller.

Sehitoglu [86] proposed a model of crack closure for cracks growing from notches. The model accounted for the crack length, applied stress and R-ratio effects accurately. The model predicted the gradual increase in the crack opening

load as the crack advanced from the notch root, and transient changes in opening level even when the notch root plasticity is absent. As with other Dugdale type models, the limitation of the model has been the plane stress deformation, and the elastic-perfectly plastic idealization of material behavior.

McClung [33, 90] proposed a simple model to predict crack opening stresses as cracks grew from notch roots using finite element analysis. The local stress component at the y-direction at each point along the crack line in an uncracked body was considered as the remote stress at this point. There was a crack opening stress corresponding to every remote stress level when the crack tip reached such a material point. This model was very simple, and worked well on results from a sharp notch. However, the prediction only held for plane stress conditions, and when the plastic zone at the notch root was increased, or when the stress distribution at the notches was altered in plane strain, the results may under-predict crack growth rates.

Leis [81] proposed a variation of crack opening stress level within the plastic zone of the notch. Initially, the opening stress level was equal to the minimum stress, as the inelastic boundary was approached the opening level reached the nominal value. This approach has the correct features, however this study shows that approach to the nominal value is rather complicated and is not bounded by the notch inelastic boundary [76-86].

A ligament closure model was developed by Newman [10, 11, 91] to calculate the crack opening stress for small cracks growing from notches. The material at the crack wake and in front of the crack tip was treated as rigid-perfectly plastic bar elements with a flow stress taken as the ultimate tensile strength, and the material in the far field was considered as an elastic continuum. The results were applied to predict crack growth rate from circular holes in steels and aluminum alloys. The idealization of material behavior in the ligament model, and the use of plane

deformation equations (and their modification to plane strain by elevation of flow stress by $\sqrt{3}$) are considered approximate.

Ogura et. al. [20] studied crack growth from notches with a finite element analysis under plane strain condition. They noted the decreasing effective stress range ratio, U, with increasing crack length until a stabilized value was reached. Their applied stress level varied from 0.15 σ_0 to 0.30 σ_0, and the stabilized U value increased slightly with increasing applied stress level. Their results indicated that the increase in S_{open} occurred over a distance of 1 mm from the notch root which exceeded the notch plastic zone.

An early model for notch fatigue crack growth behavior developed by Hammouda and Miller [92-93] is noteworthy. They postulated that cracks grew at high crack growth rates within the notch plastic zone, and the rates decreased as elastic-plastic boundaries of the notch were approached. Again, the assumptions regarding constitutive behavior and plane deformations restrict the generality of the model, furthermore, the bounding of the transient high crack growth rates by the elastic plastic boundary is not necessary. El Haddad et al. [76] proposed the use of notch strain range in a modified stress intensity range expression and a modification of the crack length with the material constant, ℓ_0. This model would predict higher crack growth rates from notches, however, once the choice of ℓ_0 is made for a material, this model can not account for the influence of stress level, and constraint conditions. Tanaka and Nakai [82] proposed a model to predict the crack closure level when short cracks grew below the ΔK threshold and became non-propagating cracks. Other data have been presented [19, 77-81, 83-86] which indicate that accelerated crack growth rates occur well beyond the notch plastic zone. Therefore, the notch plasticity alone could not account for accelerated growth rates.

Keyvanfar [94] studied crack growth in residual stress fields in notched and welded coupons and compared his results to crack growth behavior in the absence of residual stress fields. Initial crack growth rates were higher within the tensile residual stress field. When the crack entered the compressive residual stress field the growth rates were lower compared to the baseline results. It is worth noting that his residual stress gradients were not confined to the plastic zone of the notch and extended far ahead of the notch. These results are in conceptual agreement with the hypothesis that under constant amplitude cycling of notched members the elastic stress field of the notch, even in the absence of notch plasticity, will have a first order effect on crack growth rates.

The need exists to develop notch fatigue crack growth models which approach the steady state solutions as the crack grows, noting that the steady state depends on the applied stress level, R-ratio and crack length. In this chapter, a series of general equations are proposed for the crack opening stress changed with applied load, R-ratio, notch shape, crack length from the notch root and material properties. The equations are valid over a broad range of notch plasticity levels and in the important cases when the notch behavior is elastic. The crack growth rate predictions were compared with experimental data on cracks growing from notches in two materials- a 1020 steel and a 2024-T351 aluminum alloy.

5.2. Basic Results from Finite Element Analysis

CCT specimen was studied with the circular and the elliptical notch. Two bilinear and a power low material hardening models were considered. Stress distributions ahead of notches and near crack tips were examed, and crack opening stress levels were obtained under plane stress and plane strain conditions.

5.2.1. H/E=0.07, Plane Stress Case

The stress distributions ahead of the notch are shown in Figure 5.1(a) for the circular notch and in Figure 5.1(b) for the elliptical notch under different applied tensile stress levels. The vertical axis was stress normalized by yield strength, σ_o, and the horizontal axis was distance normalized by half notch width, c. It was noted that the stress at the circular notch root was rather low, which was only about 1.05 σ_o for $S_{max}/\sigma_o = 0.4$ and 1.2 σ_o for $S_{max}/\sigma_o = 0.8$. The sharp corners in the stress distributions indicated boundaries of the plastic zones and these corners were evident when the bilinear stress-strain relation was employed. The notch plastic zone size was in the range 0.1 to 1.0 c depending on the maximum stress level. The stress variation within the plastic zone of the circular notch was small compared to the elliptical notch case. Stresses at the elliptical notch root were higher, they reached 1.2 σ_o for $S_{max}/\sigma_o = 0.4$ and 1.8 σ_o for $S_{max}/\sigma_o = 0.8$ case respectively. Stresses decreased gradually with increasing distance from the notch root.

It is instructive to compare the notch stress distribution with that of a very short fatigue crack emanating from the notch. The stress distribution ahead of a very short fatigue crack ($\ell/c = 0.06$) after one loading cycle is shown in Figure 5.2(a) for the crack started from the elliptical notch. The stress at the crack tip was 1.4 σ_o and 2.2 σ_o when $S_{max}/\sigma_o = 0.4$ and 0.8 respectively. Note that in Figure 5.2(a) the distance, x, was measured from the crack tip, and not from the notch surface. The results indicated that crack tip stresses exceeded those given for the notch field, and the plastic zone size reached the notch plastic zone field as early as $\ell/c = 0.06$. Upon comparing Figures 5.1(b) and 5.2(a), it is noted that the plastic zone boundary of the $\ell/c = 0.06$ fatigue crack was comparable to the notch plastic boundary. Furthermore, since the crack was advanced in the model a distance $\Delta x/c \leq 0.6$, it

was the stresses immediately ahead of the crack tip that were responsible for crack closure and not the stresses remote from the crack tip.

The stress distribution ahead of a fatigue crack tip after 20 loading cycles is shown in Figure 5.2(b). The crack length, ℓ/c, was 1.25. The stress at crack tip was increased to 1.5 σ_o for $S_{max}/\sigma_o = 0.4$ and 2.4 σ_o for $S_{max}/\sigma_o = 0.8$, respectively. The plastic zone size for the long fatigue crack and the stress distributions resembled closed the stress distribution for the short crack in Figure 5.2(b). In view of the results in Figures 5.2 where $\ell/c = 0.06$, we note that crack grown from the elliptical notch crack behavior was close to its steady (long crack) behavior.

The crack opening stress levels are shown in Figures 5.3(a) and 5.3(b) for R = -1 case as solid lines with symbols. The crack opening stresses were low when cracks just started to grow from notch roots. The crack opening stresses for the circular notch were 0.0 S_{max} and -0.44 S_{max} for S_{max}/σ_o equal to 0.4 and 0.8, respectively. Then, they increased gradually as the crack grew until stabilized opening stresses were reached. The beginning crack opening stresses from the elliptical notch in Figure 5.3(b) were much lower, which were -0.52 S_{max} for $S_{max}/\sigma_o = 0.4$ and -0.66 S_{max} for $S_{max}/\sigma_o = 0.8$. As the crack grew, the crack opening stresses increased rapidly and reached the stabilized values. The stabilized crack opening stresses from the circular notch and the elliptical notch were very similar. Figures 5.3(c) and 5.3(d) indicate the crack opening stress under R = 0. The behavior was similar to R = -1 case; however, note the dependence of the opening stress level on S_{max}/σ_o was somewhat less in R = 0 case and the difference between S_{open} at low ℓ/c and stable value of S_{open} was smaller compared to R = -1 case.

An equation which relates the crack opening stress to crack length, stress concentration factor of notch, applied load and R ratio was proposed based on the finite element results.

$$\frac{S_{open}}{S_{max}} = \left\{\frac{S_{open}^{stable}}{S_{max}} - \left[A\left(\frac{S_{max}}{\sigma_o}\right) + B\right] \exp\left[\frac{-\ell/c}{\left(\frac{S_{max}}{\sigma_o}\right)^D}\right]\right\} (1-F) + FR \qquad (5.1)$$

where

$$\frac{S_{open}^{stable}}{S_{max}} = 0.49 + 0.01R - (0.1 - 0.3R)\frac{S_{max}}{\sigma_o}$$

$$A = -0.255 - 1.375R + (0.085 - 0.075R)\, K_t$$

$$B = 0.298 + 0.563R + (-0.043 - 0.198R)\, K_t$$

$$D = 1.700 + 1.475R + (0.100 - 0.225R)\, K_t$$

$$F = \exp(-10^6 \times \ell/c)$$

The predicted crack opening stress is shown in Figures 5.3 compared with the finite element results. The dashed lines indicate results from Equation (5.1). Equation (5.1) predicts the stable value of S_{open}/S_{max} as ℓ/c becomes large and the R ratio as ℓ -> 0. The stable value of S_{open} is dependant on both R-ratio and S_{max}/σ_o. Constants A, B, D are dependent on R and K_t, elastic stress concentration factor of the notch.

It is important to insure that the normalization of ℓ with half notch size c in Equation (5.1) is valid. This check was carried out by conducting analyses with identical loading parameters but three different notch sizes in Reference [96]. The crack opening curves were found to be geometrically similar with respect to the notch sizes.

5.2.2. H/E=0.01 Plane Stress Case

The stress distributions ahead of notch roots are shown in Figures 5.4 for the circular and the elliptical notch. Since the hardening modulus was rather low in this case, stresses did not increase significantly after the yield stress was exceeded. The stresses at the circular notch root were approximately 1.05 σ_o for applied

stresses range from 0.4 σ_o to 0.8 σ_o. It was noted that stresses did not decrease but increased as the distance from the notch root increased within plastic zones. The stress at the elliptical notch root was about 1.1 σ_o for S_{max}/σ_o = 0.4 and about 1.25 σ_o for S_{max}/σ_o = 0.8. The stresses increased as the distance from the notch root increased until a maximum value was reached, which was at the location of x/c = 1.0 for S_{max}/σ_o = 0.8 and x/c = 0.1 for S_{max}/σ_o = 0.4. Note that stresses increased within the plastic zone for all applied stresses. Since these were fields of the stress component in the y-direction, the maximum value was still at the notch root if the equivalent stress was plotted. This kind of stress distribution had been observed ahead of notches and blunting cracks from stress analysis. Closure and life models using elastic stress fields to predict plasticity at notch roots cannot recognize this behavior. The stress distribution ahead of the fatigue crack tip is shown in Figures 5.5. The maximum stresses were at the fatigue crack tip (x/c = 0) for ℓ/c = 0.06. The plastic zone size was not changed after one loading cycle, although the stress distribution immediately ahead of the crack tip was changed.

The crack opening stress levels from finite element analysis are shown in Figures 5.6 by solid lines with symbols. Again, the crack opening stresses for the elliptical notch was lower than for the circular notch when the crack was short for R = -1 case. The crack opening stress of the first cycle was -0.10 S_{max} and -0.56 S_{max} under S_{max}/σ_o = 0.4 and 0.8 for the circular notch, and is -0.56 S_{max} and -0.76 S_{max} under S_{max}/σ_o = 0.4 and 0.8 for the elliptical notch. The stabilized opening stresses were same for two notches, which were 0.42 S_{max} for S_{max}/σ_o = 0.4 and 0.02 S_{max} for S_{max}/σ_o = 0.8. When R = 0, the crack opening stresses for first few cycles were similar at different applied load from the circular notch, since the stress distribution near the notch root was very similar at different applied loads. For the elliptical notch, the crack opening stress differed with increasing applied stress for

the first few cycles. The prediction equation is same as the one for H/E = 0.07, but the expression for $S_{open}^{stable}/S_{max}$ and constants, A, B, and D are different.

$$\frac{S_{open}}{S_{max}} = \left\{\frac{S_{open}^{stable}}{S_{max}} - \left[A\left(\frac{S_{max}}{\sigma_o}\right) + B\right] \exp\left[\frac{-\ell/c}{\left(\frac{S_{max}}{\sigma_o}\right)^D}\right]\right\} (1-F) + FR \qquad (5.2)$$

$$\frac{S_{open}^{stable}}{S_{max}} = 0.95 + 0.13R - (0.70 - 0.30R)\frac{S_{max}}{\sigma_o}$$

$$A = -1.138 - 1.138R + (0.163 + 0.163R)\,K_t$$

$$B = 0.902 + 0.507R - (0.089 + 0.164R)\,K_t$$

$$D = 3.400 + 2.575R - 0.125R\,K_t$$

The results from the prediction are shown in Figures 5.6 by dashed lines. The agreement between Equation (5.2) and the finite element results was remarkably good over a wide range of conditions. The main difference between H/E = 0.01 and 0.07 behaviors was the sensitivity of the S_{open}^{stable} to the S_{max}/σ_o. This sensitivity was much higher for H/E =0.01 case compared to the H/E = 0.07 case.

5.2.3. H/E=0.01, Plane Strain Case:

The stress distributions ahead of notch roots are shown in Figures 5.7 for plane strain case. The magnitude of the stress at the notch root was higher in plane strain than in plane stress. For S_{max}/σ_o = 0.8 case, the stress was 1.35 σ_o at the circular notch root and 1.8 σ_o at the elliptical notch root. The maximum value of the stress component in the y-direction was not at the notch roots for these cases. The plastic zone size for plane strain was significant smaller than for plane stress, therefore, it was difficult to capture the reversed plastic zone shape for cases with applied load, S_{max}/σ_o < 0.6, by using the finite element mesh in this study. The

stress distribution ahead of the fatigue crack tip is shown in Figures 5.8. When the crack size, ℓ/c, was 0.06, the stress at the crack tip was 2.9 σ_o for the crack growing from the elliptical notch. When the crack length, ℓ/c, reached 1.25 after 20 cycles, the stress at the crack tip increased to 3.2 σ_o. We note the close resemblance of stress distributions in Figures 5.8(a) and 5.8(b). Again, the effect of the notch plasticity alone was not fully responsible for crack tip behaviors when $\ell/c = 0.06$.

The crack opening stresses are shown in Figures 5.9 for R = -1 as the solid lines with symbols. Since the reversed plastic zone for R = 0 was too small, only R = -1 case was considered for plane strain. The crack opening stresses as the crack starts from the notch was -0.36 S_{max} and -0.52 S_{max} for the circular notch, and -0.56 S_{max} and -0.72 S_{max} for the elliptical notch at $S_{max}/\sigma_o = 0.7$ and 0.9, respectively. These values were higher than those in plane stress. The stabilized crack opening stresses in plane strain were higher than those in plane stress. The crack opening stresses for plane strain is written similarly to plane stress:

$$\frac{S_{open}}{S_{max}} = \left\{\frac{S_{open}^{stable}}{S_{max}} - \left[A\left(\frac{S_{max}}{\sigma_o}\right) + B\right] \exp\left[\frac{-\ell/c}{\left(\frac{S_{max}}{\sigma_o}\right)_D}\right]\right\} (1-F) + FR \qquad (3)$$

The stabilized opening stresses and the constants in plane strain are:

$$S_{open}^{stable}/S_{max} = 1.12 - 1.20\, S_{max}/\sigma_o$$

$$A = -0.10\, K_t$$

$$B = 0.346 + 0.71\, K_t$$

$$D = 2.475 + 0.075\, K_t$$

Note that the effect of R-ratio was not incorporated in the equation since only R = -1 case was considered. The results from the equation are shown with "---- " line in Figures 5.9.

5.2.4. Power Law Hardening, Plane Stress Case

The stress distribution ahead of circular notch and elliptical notch are shown in Figures 5.10(a) and 5.10(b) for power law hardening cases. Note that the applied stresses are normalized by the yield strength same as bilinear cases, σ_o = 430 MPa, although the actual yield surface size in the model is 277 MPa for this case. The stresses at the circular notch root is 0.8 σ_o and 1.2 σ_o for S_{max}/σ_o = 0.4 and 0.7 respectively. Again stresses are normalized by the yield stress of bilinear relation (430 MPa) here, there is a plastic zone ahead of notch root at S_{max}/σ_o = 0.4 even though the stress at notch root is under σ_o on the plot. The plastic zone sizes can not be determined from the stress distributions directly since the power law hardening model is employed. The stresses at elliptical notch root are higher than at circular notch root, which is 1.3 σ_o to 1.7 σ_o for S_{max}/σ_o = 0.4 to 0.7. The stress distribution ahead of fatigue crack tip is shown in Figures 5.11. When the crack starts to grow from notch roots (ℓ/c = 0.06), the stress distribution immediately ahead of the short crack tip is higher than those ahead of notch roots. However, the stress distribution a little away from the crack tip do not change. The stress at crack tip is 1.2 σ_o to 1.7 σ_o for crack starts from circular notch, and 1.5 σ_o to 2.0 σ_o for crack from elliptical notch at S_{max}/σ_o = 0.4 to 0.7 respectively. The stresses at a long fatigue crack tip (ℓ/c = 1.25) varies from 1.3 σ_o to 2.0 σ_o for S_{max}/σ_o = 0.4 to 0.7. The stress at long crack tip is lower or similar to that at the short crack from elliptical notch due relaxation of stresses. The stresses decreases rapidly with increasing distance from crack tip for the short crack from the elliptical notch, but gradually for long fatigue crack.

The crack opening stresses are shown in Figures 5.12 as solid lines with symbols for circular notch, elliptical notch under R = -1 and 0. The difference of crack opening stresses for the first cycle at variable applied load is very small compared to bilinear relation cases. S_{open}/S_{max} at the first cycle for S_{max}/σ_o = 0.4 and 0.7 is -0.08 S_{max} and -0.28 S_{max} for circular notch, -0.40 S_{max} and -0.56 S_{max} for elliptical notch under R = -1. The stabilized opening stress is -0.04 S_{max} and 0.52 S_{max} for S_{max}/σ_o = 0.4 and 0.7 respectively. For R = 0 cases, the difference between opening stresses for elliptical notch and for circular notch is very small.

The equation to predict crack opening stresses is in the same form as Equation (5.2) and (5.3), and the stabilized opening stresses and constants A, B and D are shown below:

$$\frac{S_{open}}{S_{max}} = \left\{\frac{S_{open}^{stable}}{S_{max}} - \left[A\left(\frac{S_{max}}{\sigma_o}\right) + B\right] \exp\left[\frac{-1/c}{\left(\frac{S_{max}}{\sigma_o}\right)^D}\right]\right\} (1-F) + FR \qquad (5.4)$$

$$S_{open}^{stable}/S_{max} = 0.80 - 0.58R - (0.3 - 1.67R)\, S_{max}/\sigma_o$$

$$A = -0.357 + 1.518R + (0.019 - 0.039R)\, K_t$$

$$B = 0.501 - 0.844R - (0.007 + 0.055R)\, K_t$$

$$D = 2.65 + 1.90R + (0.05 - 0.10R)\, K_t$$

The prediction results are shown in Figures 5.12 as dashed lines. They fit the finite element results very well for most of cases.

5.2.5. Material Effect on Crack Closure

Based on the current work, it was found that crack opening stress levels were strongly influenced by material hardening behaviors. Two bilinear stress strain relations with hardening modulus, H/E=0.07 and 0.01, and power law

hardening have been considered. Originally, the model with H/E = 0.07 and the power law hardening model were both used to simulate material behavior of 1070 steel. Therefore, the difference between stress strain curves from these hardening models was very small. However, the difference of opening levels from these two materials were significant.

Summary of stabilized crack opening stresses for all three hardening models are shown in Figure 5.13 for R = -1 under plane stress. At low applied stresses, the highest crack opening stress is obtained from the power law hardening case, and the lowest crack opening stress is obtained from H/E = 0.07 case. At high applied loads, the highest value of crack opening stress occurred in H/E = 0.07 case, and the lowest value coincided with the power law case.

There are two important reasons for the different behaviors observed in these cases. As revealed in systematic studies by McClung and Sehitoglu [31-32], the crack opening behavior is a competition between the the forward plastic deformation, that is responsible for crack opening, and the reversed plastic deformation, that is responsible for the residual displacements. As the R-ratio is increased or as the applied S_{max}/σ_o ratio is increased the forward strain exceeds the reversed strain at the crack tip resulting in lowered crack opening levels. The constitutive response of a material could also influence the forward versus reverse flow hence change the crack opening behavior. Figures 5.14 indicate the stress strain response at a material point, as the crack approaches this material point and reaches it, in a material obeying a bilinear hardening, H/E = 0.07 and in a material undergoing power law hardening. The stress strain response for high applied stress, S_{max}/σ_o = 0.7 are shown in Figures 5.14(a) for H/E = 0.07 and 5.14(b) for power law hardening. We note that the forward strain in the H/E = 0.07 case is less than 0.025 while for the power law case is near 0.04. The minimum, or reversed strain level, in the H/E = 0.07 case is -0.005 while for the power law case it is as

high as 0.01. A somewhat different picture emerges when the forward and reversed strains are considered for the case $S_{max}/\sigma_o = 0.4$. The forward strain for H/E = 0.07 case is slightly higher than the power law case while the reversed strain is also more tensile compared to the power law case. This explains the lower opening load level for the H/E=0.07 case.

Furthermore, we note that at a high applied stresses, $S_{max}/\sigma_o = 0.7$, the total strain range was higher for the power law hardening than the bilinear hardening as the material point is reached. Furthermore, the mean strain at this cycle was significantly higher for the power law hardening than the bilinear hardening case as shown in Figures 5.15(c) and 5.15(d).

It is important to understand the further differences between bilinear hardening and power law hardening models. Although symmetric remote stress was applied, tensile mean stresses developed for H/E = 0.07 case, while mean stresses at the crack tip were nearly zero for the power law hardening case. These results may have implications in explaining the way in which the crack growth rates or lives change under mean stresses from one material to another [97-103].

5.3. Applications to Crack Growth from Notches:

The relationship of crack growth rate and the stress intensive range is well known as the Paris equation. When closure occurs, the stress intensity range is modified as $U\Delta K$:

$$da/dN = C' (U \Delta K)^m \qquad (5.5a)$$

where

$$U = (1 - S_{open}/S_{max}) / (1 - R) \qquad (5.5b)$$

The predictions were applied to three sets of experimental data, which included two sets of data for 1020 Steel and one set of data for 2024-T351 Aluminum alloy. Other data in the literature was also studied, but often the applied stress, crack length information was not reported which make the predictions difficult.

5.3.1. 1020 Steel

Sehitoglu [86, 87] tested crack growth rate from a blunt notch (K_t = 4) under different applied stress levels. C' and m were equal to 8.03 x 10^{-9} and 3.202, respectively. His results are shown in Figures 5.15(a) - 5.15(c) by symbols. The notch plastic zone sizes, r_p, are indicated in Figures 5.15. Bilinear relation with H/E = 0.07 was suitable for this material. The long crack growth rate was predicted by using $S_{open}^{stable}/S_{max}$, and the short crack growth rate was predicted by using $\frac{S_{open}}{S_{max}}$ in Equation (5.1). The short crack growth rate were much higher than the long crack growth rate when the crack reached the plastic zone boundaries, transient changes in the crack growth behavior and gradual linking with the long crack growth data occurred outside r_p.

Crack growth rates from different notches were examined by McClung and Sehitoglu [104]. The stress concentration factors for the notches were 3, 5 and 5.9, respectively. The applied stress S_{max}/σ_o was 0.54 and R ratio was -1. The constant in crack growth equation C' was 1.59 x 10^{-8} and m was 3.33. The experimental crack growth data and the prediction using Equations (5.1) and (5.3) are shown in Figures 5.13(d) - 5.13(f). The experimental data are indicated by symbols, the dashed lines indicate prediction for long crack growth rate and the solid lines indicate the

prediction for the short crack growth rate using Equation (5.1). The short crack growth prediction accounted for the transient changes in Sopen levels. The plastic zone size is noted in Figures 5.15(d) - 5.15(f) with the symbol r_p. The notch plastic zone size increased with increasing K_t at low applied stresses, and decreased with increasing K_t at high applied stresses. It coincides that the plastic zone size did not change with K_t when the applied stress, S_{max}/σ_o, was 0.54. The minimum in da/dN occurred at a crack length outside the plastic zone of the notch.

5.3.2. 2024-T351 Aluminum Alloy

Leis and Forte [77] tested crack growth rate from notches on 2024-T351 aluminum alloy under edge strain (displacement) control conditions. The hardening modulus was very low for aluminum alloy, therefore, results from H/E = 0.01 could be applied to this material. The CCT specimen was tested, and stress concentration factors for notches were 3, 5 and 7. C' and m in the crack growth equation were 5.83×10^{-16} and 9.044, respectively. The solution of stress intensity K was given in Reference [77] for strain control testing. Crack growth rates, da/dN, were presented vs. crack length and vs. maximum stress intensity, K_{max}, respectively in the paper. The applied stress was always changing during the experiment since strain control experiment was performed, it could be calculated since the crack length and K_{max} were known.

Finite element simulation was performed for one case with displacement control condition. The crack was allowed to grow to exceed half the specimen size over 40 cycles. It was found that the applied maximum stress did not change significantly at first 20 cycles, then it decreased gradually for the second 20 cycles. The crack opening stresses were very similar with that of the stress control condition since stress changes were not very high. Therefore, the opening stresses

for short crack and long crack were obtained according to Equation (5.2) for changing applied stress conditions.

The predictions compared to experimental data are shown in Figures 5.16 The applied maximum edge strain varies from 0.22% to 0.47%, the equivalent stress varied from 0.35 σ_0 ~ 0.45 σ_0 for ε_{max} = 0.22%, and 0.70 σ_0 ~ 0.90 σ_0 for ε_{max} = 0.47%. The notch plastic zone sizes, r_p, are indicated in Figures 5.14. The growth rates are higher than long crack prediction when crack reached the notch elastic plastic boundaries. Both long crack and short crack predictions were not as smooth as those for 1020 steel because the applied maximum stress was not constant in this case. We note in Figures 5.16(a) and 5.16(b) that if transient crack growth behavior was not accounted, the crack growth rates would be underestimated by two orders of magnitude. This would translate to a considerable error in lifetime calculation. It is noted that the prediction did not fit the experimental data of high applied strain amplitude cases (0.47%, 0.39%) compared to low applied strains. When the applied edge strain was 0.47%, the predicted growth rate was much higher than the experimental data. This is because when the maximum applied stress was around 0.9 σ_0, the notch plastic zone was very large. When the crack started from the notch, the residual stress fields developed more quickly in the experiments than in FEM simulations so that the opening stress increased to the stabilized value at very short crack length.

5.4. Summary of Results

The short crack behavior is more difficult to study in experiments than the long crack due to the resolution of the measurements, especially when the notch size is very small. Several models to predict crack grown from notches have been proposed. Hammouda and Miller [92, 93] studied plastic deformation for fatigue cracks and uncracked notches. The crack growth rate increased with increasing

plastic deformation, which was sum of notch plastic deformation and LEFM (linear elastic fracture mechanics) plastic deformation at the fatigue crack tip. When considering the crack growth rate from the notch the crack was slowing down due to decreasing stress field of the notch, but also increasing in rate due to increasing crack tip plasticity as a consequence of increasing crack length. This model suggests that the notch effect on crack growth occurs within the notch plastic zone. Dowling [105] assumed that the crack growth problem could be separated into two parts, one was an edge crack growing in the notch field, another one was a center crack growing independent of the notch. A transition crack length was determined by setting K solutions for the two parts equal to each other. The transition crack length was only function of notch size and notch shape, and was much smaller than plastic zone when the applied load was higher than $0.4\sigma_0$. The current study showed that the short crack effect at notches occurred beyond the transition length and also beyond the notch root plastic zone. The results demonstrated that the opening stresses were higher when the crack just started from the blunt notch than the sharp notch and they reached the stabilized values more rapidly for the sharp notch. This behavior is consistent with the more gradual elastic stress gradients ahead of blunt notches compared to the sharp notch. Also, the study lends further support to the hypothesis that a short crack effect develops within the notch elastic field. For example, if we consider S_{max}/σ_0 = 0.4 case in Figure 5.1(b), the notch plastic zone is about 0.2c. Considering Figure 5.3(b) the S_{open} level stabilized at about 0.75c, which was three times the notch plastic zone size. It is obvious in Figures 5.15 and 5.16 that the the short crack behavior occurred beyond the notch plastic zone size.

The current analysis of notch effect on the short crack was based on the crack closure concept. The model proposed in this paper has two advantages compared to other closure models. One of the advantages is its accuracy. The simple model to

predict crack opening stresses as crack grows from a notch proposed by McClung was based on the stress distribution of notched uncracked body. This simple model predicted that crack opening levels change very gradually for blunt notches since the stress gradients were shallow for blunt notches. The prediction worked well for the elliptical notch because the magnitude of stress gradients were as high as opening level gradients. For the circular notch, the stress gradients at the notch root were small, the prediction was too conservative as crack grew from the notch. When the applied load was low, for example, at $S_{max}/\sigma_o = 0.4$, the plastic zone was very small, and the predictions of S_{open} deviated from the simple model. If the stress distribution of a small crack at the notch root was used, this method would yield more accurate results. However, if a lower hardening modulus were considered, the difference between finite element results and the simple model could become more significant. Crack opening stresses varied rapidly even when stress gradients were shallow. The maximum value of the stress component in the loading direction was not at the notch roots but at a distance from the notch root due to multiaxiality effects. The crack opening stress, however, was lowest immediately at the notch root.

The stabilized opening stress in Leis's model was function of R ratio only, and the opening stress increased linearly from minimum applied stress at the notch root to S_{open}^{stable} at the boundary of notch plastic zone. Previous study [33] showed that the S_{max} had effect on the opening stress, furthermore S_{open}^{stable} was reached when the crack length was much longer than the notch plastic zone size. Elastic-perfectly-plastic material idealization was used in Sehitoglu's and Newman's model. It is known that opening stresses are influenced by the material hardening behavior. These effects were considered in the current model, and the equations proposed reproduced the finite element results closely. We note the agreement of our results with early work by McClung and Sehitoglu [90] who

considered a material with H/E = 0.07 under plane stress for R ratio as -1 cases, and Ogura et. al. who analyzed a material with H/E = 0.075 under plane strain.

The stress distributions near the notch root and the fatigue crack tip have been studied in current research. The results indicated that stress ahead of the crack tip was higher than that ahead of the notch root. When the crack grew from the notch root, the magnitude of stress components would increase from that of a notch to a fatigue crack. The stress immediately ahead of the crack tip increased when the crack started from the notch root, but the change of the stress field at a distance away was not significant. The stress field changed gradually as the crack grew while the plastic wake built up along crack surfaces. Therefore, the crack opening stress changed depending on the stress distribution ahead of the crack tip.

According to the opening stress equations, when the crack length was zero, the constant F was 1, then the crack opening stress was equal to R ratio, the result was shown analytically by Sehitoglu [36]. When the crack length became large enough, the crack opening stress approached the S_{open}^{stable}. The term of $[A\ (\frac{S_{max}}{\sigma_o}) + B]$ in the equation indicated the difference between the crack opening level when the crack just started from the notch root and the stabilized value, and the term of $\exp[\frac{-l/c}{(\frac{S_{max}}{\sigma_o})^D}]$ indicated how fast the crack opening stress reached its stabilized value.

Finally, it is noted that the prediction equations are written explicitly in terms of maximum stress, crack length and the R-ratio. It is possible to cast these results using stress intensity range. This was not done intentionally because when the crack length increases the S_{open} saturates, and for an S_{max} = constant test the crack opening levels will ultimately become independent of the stress intensity. The experimental results of Sharpe and Su [43], Mc-Clung and Sehitoglu [102] and

the recent overview by McClung [49] confirm the validity of developing stress opening relations which are independent of ΔK or crack length when the crack is growing under steady state conditions.

5.5. Conclusions

1. The crack opening stress levels are as low as minimum applied stresses when cracks start from notch roots, then they increase with increasing crack length until stabilized values are reached.

2. Crack closure is a main factor responsible for the notch effect on crack growth behavior. A set of prediction models was proposed to determine crack opening stresses when cracks grow from notches for variable notch shapes, applied maximum load levels, R ratios and crack length from notch roots for different materials.

3. The result indicated that transient changes in crack growth rate were not limited to the notch plastic zone, and rapid changes in crack opening loads and in crack growth rates occur outside the notch plastic zone.

4. The maximum stresses ahead of crack tips even within the notch plastic zone, $\ell/c = 0.06$, approached their steady state value, $\ell/c = 1.25$. Since closure is influenced by the plastic deformation immediately ahead of crack tips, the influence of the notch on crack tip stress fields is small; however, since crack contact cannot occur over the notch, the notch size, c, has an influence on closure behavior.

5. The model was applied to prediction of crack growth rates from notches in 1020 Steel and 2024-T351 Aluminum Alloy, and the prediction of the experimental data was very satisfactory over three orders of magnitude in crack growth rates.

Chapter 6:

Summary of Results

Finite element method is a very useful tool for studying mechanical factors that influence fatigue crack growth and closure. Three important findings of this thesis are summarized below.

The first finding is a model forwarded to explain the mechanism of crack closure under plane strain condition. Debate on this issue has been going on from the early days of crack closure research with no convincing model to explain plane strain closure. The proposed model identifies material transfer in the transverse direction (crack growth direction) to crack surfaces. This material transfer occurs in a direction normal to the material transfer in plane stress condition. The study of inelastic strain accumulation in the x-direction and the corresponding negative displacement gradient in the x-direction in front of the crack tip confirmed plane strain closure. The results also confirm that the length of the fatigue crack over which closure occurs is as low as 1% of the total crack length in plane strain, casting significant doubt on the accuracy of remote closure measurement techniques.

The second finding of this research is concerned with the residual stresses at the crack tip due to reversed deformation in the absence of crack closure and due to the residual stress on the wake of the crack surfaces. It was found that crack tip tensile stress level is a very important parameter for crack closure. The residual stress effect due to reversed deformation ahead of the crack tip in the absence of crack closure was always more significant in plane strain than in plane stress.

Similarly, the crack closure effect is always more significant in plane stress compared to plane strain.

The third finding of this research is that the accelerated crack growth occurred beyond the notch plastic zone which was consistent with the crack closure transient behavior. The crack opening stress levels for crack growing from notches were determined. A set of closure prediction equations was proposed to determine crack growth rate from notches based on the finite element analysis. The equations can count for the effect of variable notch shape, applied maximum load level, R ratio and crack length from notch roots from different materials on crack closure, thus on crack growth rates. The model has been applied to crack growth data from a steel and an aluminum alloy, and the predicted crack growth rates from notches were in excellent agreement with experiments.

Chapter 7:

Future Issues

Questions remain as to the general applicability of the continuum representation of the material when the crack tips, even for long cracks, are surrounded by one or finite number of grains. The microstructural effects, and the development of the plastic wake in short cracks of the order of the grain size require study. For example, the current finite element model underpredicts the crack tip strains of very small cracks as noted by McClung and Davidson [46] when the experiments are focussing on deformations within a grain. The large Mode II displacements reported on cracks growing near the threshold is probably a result of the anisotropy of the material in front of the crack tip. In the regime of crack nucleation and in the near threshold crack growth behavior regime, it is known that the size scale comparable to a grain size should be modelled. The finite element approaches incorporating crystal plasticity concepts are currently being developed to account for these inhomogenous deformations.

Table 1. Summary of Crack Opening Stress, S_{open}, Crack Tip Tensile Stress, S_{tt}, and Crack Tensile Stress, S_t, Under Plane Stress Condition from CCT Specimen

	R=-1			
	S_{max}/σ_o	S_{open}/S_{max}	S_{tt}/S_{max}	S_t/S_{max}
Ideal Crack	0.4		-0.56	0.32
Fatigue Crack	0.4	0.44	0.44	0.44
Ideal Crack	0.5		-0.64	0.32
Fatigue Crack	0.5	0.32	0.40	0.44
Ideal Crack	0.6		-0.68	0.28
Fatigue Crack	0.6	0.20	0.24	0.40
Ideal Crack	0.8		-0.76	0.12
Fatigue Crack	0.8	-0.16	-0.08	0.20

	R=0			
	S_{max}/σ_o	S_{open}/S_{max}	S_{tt}/S_{max}	S_t/S_{max}
Ideal Crack	0.5		0.28	0.60
Fatigue Crack	0.5	0.68	0.68	0.68
Ideal Crack	0.6		0.24	0.64
Fatigue Crack	0.6	0.56	0.56	0.56
Ideal Crack	0.8		0.16	0.64
Fatigue Crack	0.8	0.40	0.48	0.64

Table 2 Summary of Crack Opening Stress, S_{open}, Crack Tip Tensile Stress, S_{tt}, and Crack Tensile Stress, S_t, Under Plane Strain Condition from CCT Specimen

	R=-1			
	S_{max}/σ_o	S_{open}/S_{max}	S_{tt}/S_{max}	S_t/S_{max}
Ideal Crack	0.4		-0.12	0.12
Fatigue Crack	0.4	0.24	0.16	0.16
Ideal Crack	0.5		-0.16	0.16
Fatigue Crack	0.5	0.28	0.28	0.28
Ideal Crack	0.6		-0.32	0.16
Fatigue Crack	0.6	0.28	0.28	0.28
Ideal Crack	0.8		-0.44	0.12
Fatigue Crack	0.8	0.20	0.24	0.24
Ideal Crack	0.9		-0.44	0.12
Fatigue Crack	0.9	-0.04	0.00	0.12

Table 3. Summary of Crack Opening Load, P_{open}, Crack Tip Tensile Load, P_{tt}, and Crack Tensile Load, P_t, Under Plane Stress Condition from CT Specimen

	R=-1			
	P_{max}/P_o	P_{open}/P_{max}	P_{tt}/P_{max}	P_t/P_{max}
Ideal Crack	0.2		-0.50	0.35
Fatigue Crack	0.2	0.60	0.50	0.60
Ideal Crack	0.4		-0.70	0.00
Fatigue Crack	0.4	0.50	0.50	0.60
Ideal Crack	0.6		-0.75	-0.35
Fatigue Crack	0.6	0.40	0.45	0.60
Ideal Crack	0.8		-0.80	-0.45
Fatigue Crack	0.8	0.30	0.35	0.55

	R=0			
	P_{max}/P_o	P_{open}/P_{max}	P_{tt}/P_{max}	P_t/P_{max}
Ideal Crack	0.2		0.40	0.50
Fatigue Crack	0.2	0.65	0.65	0.65
Ideal Crack	0.4		0.20	0.65
Fatigue Crack	0.4	0.55	0.65	0.65
Ideal Crack	0.5		0.20	0.65
Fatigue Crack	0.5	0.50	0.55	0.65
Ideal Crack	0.6		0.15	0.60
Fatigue Crack	0.6	0.40	0.50	0.70
Ideal Crack	0.8		0.10	0.55
Fatigue Crack	0.8	0.30	0.35	0.65
Ideal Crack	1.0		0.05	0.50
Fatigue Crack	1.0	0.15	0.20	0.50

Table 4. Summary of Crack Opening Load, P_{open}, Crack Tip Tensile Load, P_{tt}, and Crack Tensile Load, P_t, Under Plane Strain Condition from CT Specimen

	R=-1 P_{max}/P_o	P_{open}/P_{max}	P_{tt}/P_{max}	P_t/P_{max}
Ideal Crack	0.2		0.325	0.45
Fatigue Crack	0.2	0.30	0.35	0.35
Ideal Crack	0.3		0.30	0.45
Fatigue Crack	0.3	0.25	0.35	0.35
Ideal Crack	0.4		0.20	0.40
Fatigue Crack	0.4	0.05	0.25	0.35
Ideal Crack	0.5		0.10	0.45
Fatigue Crack	0.5	0.00	0.15	0.40
Ideal Crack	0.6		0.05	0.45
Fatigue Crack	0.6	0.00	0.10	0.40

	R=0 P_{max}/P_o	P_{open}/P_{max}	P_{tt}/P_{max}	P_t/P_{max}
Ideal Crack	0.2		0.275	0.40
Fatigue Crack	0.2	0.30	0.30	0.30
Ideal Crack	0.4		0.325	0.40
Fatigue Crack	0.4	0.25	0.35	0.45
Ideal Crack	0.5		0.25	0.45
Fatigue Crack	0.5	0.10	0.30	0.45
Ideal Crack	0.6		0.25	0.40
Fatigue Crack	0.6	0.05	0.30	0.45

Table 5. Summary of Prediction Equations for Different Hardening Models

$$\frac{S_{open}}{S_{max}} = \left\{\frac{S_{open}^{stable}}{S_{max}} - \left[A\left(\frac{S_{max}}{\sigma_o}\right) + B\right]\exp\left[\frac{-1/c}{\left(\frac{S_{max}}{\sigma_o}\right)^D}\right]\right\}(1-F) + FR$$

H/E = 0.07, plane stress:

$$\frac{S_{open}^{stable}}{S_{max}} = 0.49 + 0.01R - (0.1 - 0.3R)\frac{S_{max}}{\sigma_o}$$

$A = -0.255 - 1.375R + (0.085 - 0.075R)\,K_t$

$B = 0.298 + 0.563R + (-0.043 - 0.198R)\,K_t$

$D = 1.700 + 1.475R + (0.100 - 0.225R)\,K_t$

$F = \exp(-1x10^6/c)$

H/E = 0.01, plane stress:

$$\frac{S_{open}^{stable}}{S_{max}} = 0.95 + 0.13R - (0.70 - 0.30R)\frac{S_{max}}{\sigma_o}$$

$A = -1.138 - 1.138R + (0.163 + 0.163R)\,K_t$

$B = 0.902 + 0.507R - (0.089 + 0.164R)\,K_t$

$D = 3.400 + 2.575R - 0.125R\,K_t$

Power Law, plane stress:

$$\frac{S_{open}^{stable}}{S_{max}} = 0.80 - 0.58R - (0.3 - 1.67R)\frac{S_{max}}{\sigma_o}$$

$A = -0.357 + 1.518R + (0.019 - 0.039R)\,K_t$

$B = 0.501 - 0.844R - (0.007 + 0.055R)\,K_t$

$D = 2.65 + 1.90R + (0.05 - 0.10R)\,K_t$

H/E=0.01, Plane strain

$$\frac{S_{open}^{stable}}{S_{max}} = 1.12 - 1.20\frac{S_{max}}{\sigma_o}$$

$A = -0.10\,K_t$

$B = 0.346 + 0.71\,K_t$

$D = 2.475 + 0.075\,K_t$

$$\frac{S_{open}}{S_{max}} = \left[\frac{S^{stable}}{S_{max}} - \left[A\,\frac{S_{max}}{\sigma_o} + B\right]1.\right](1-f) + \cancel{FR}^{\,0}$$

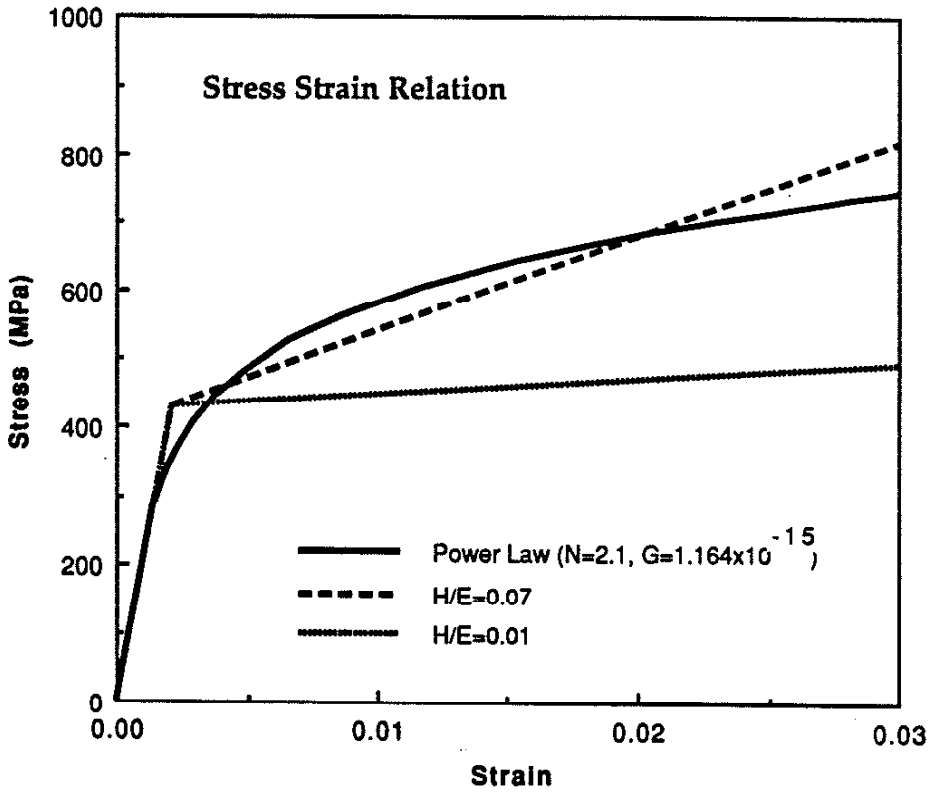

Figure 2.1. Cyclic stress strain relation for three hardening models.

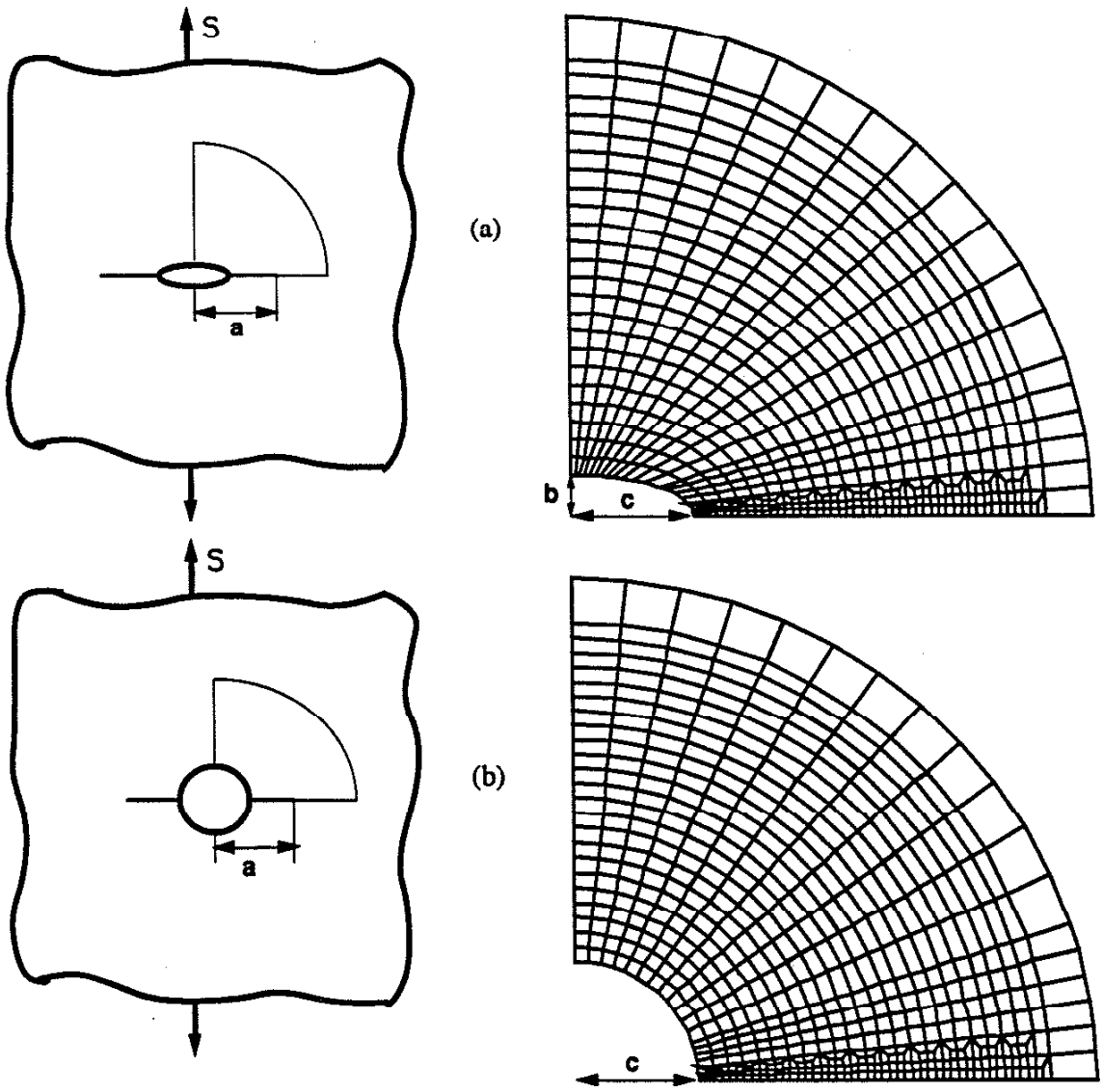

Figure 2.2 Finite element mesh for CCT specimen

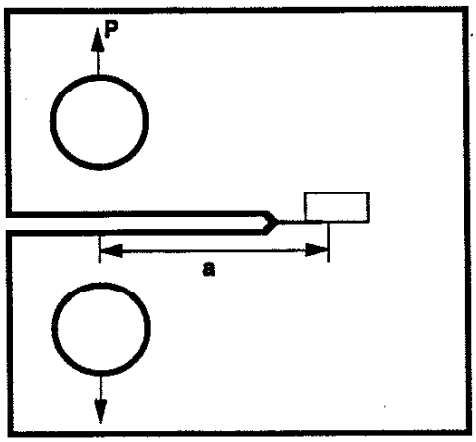

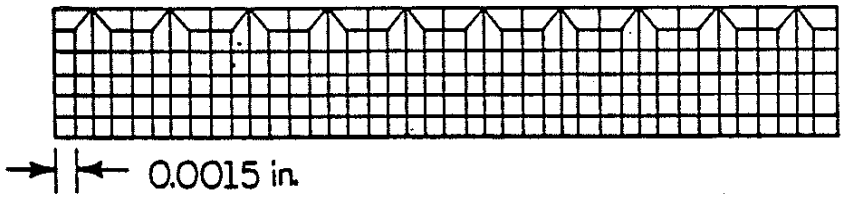

(a)

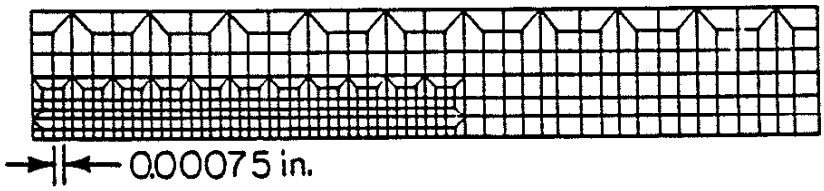

(b)

Figure 2.3. Finite element mesh for CT specimen

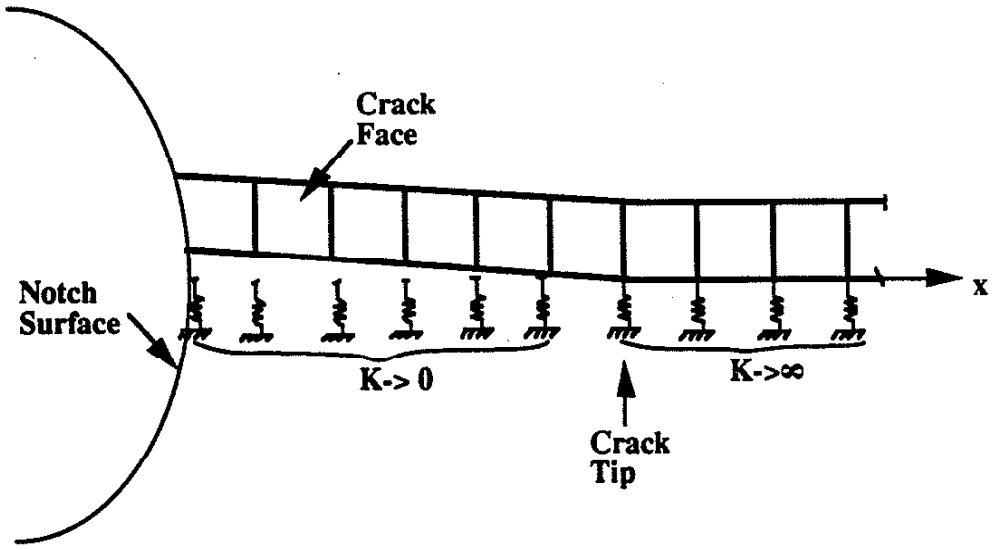

Figure 2.4 Schematic of Crack ahead of a notch.

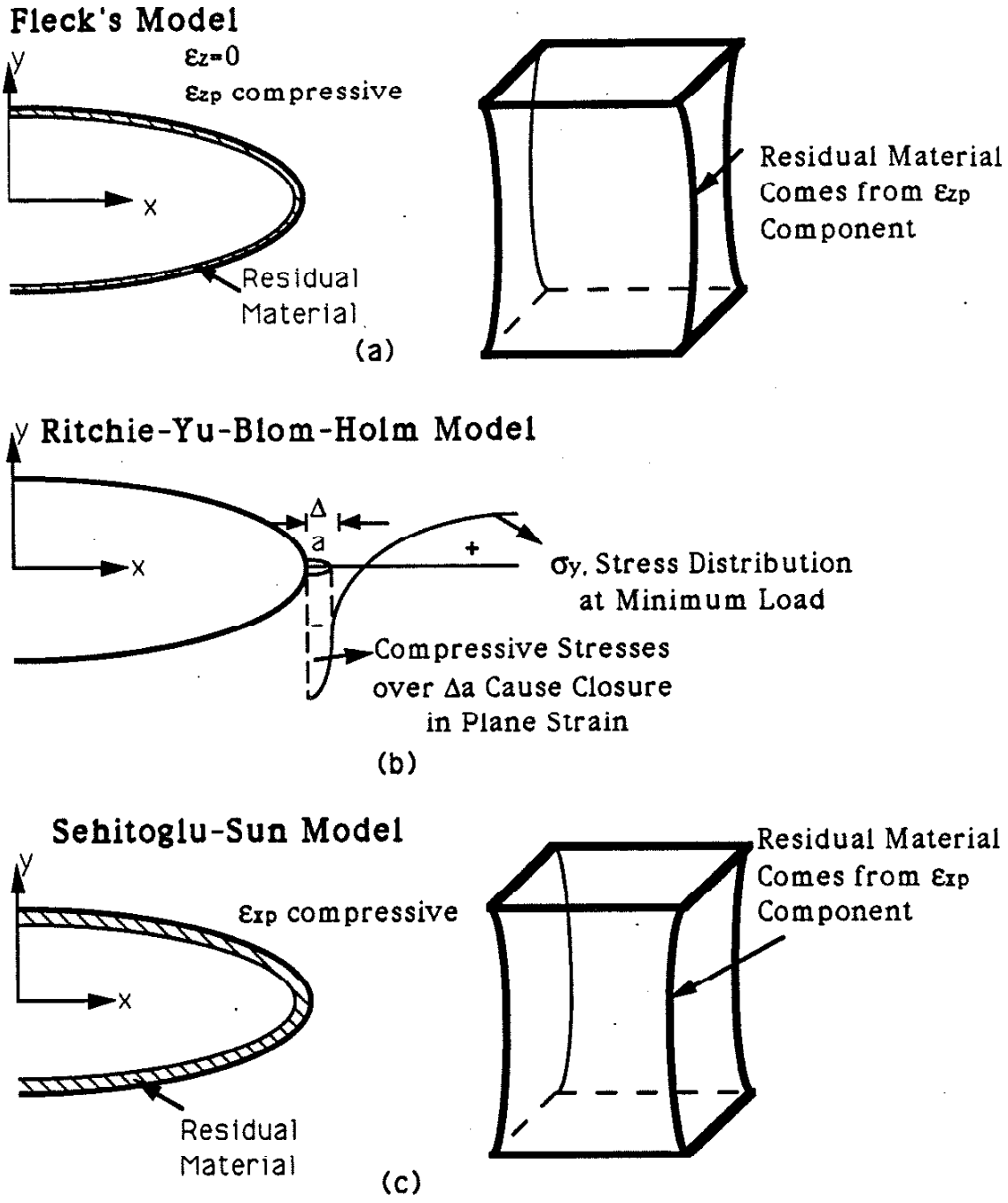

Figure 3.1 Summary of some of the proposed mechanisms of plane strain fatigue crack closure. (a) the plastic strains in thichness direction provide material for closure; (b) the compressive stresses on the crack surfaces during crack advance cause crack closure; (c) the plastic strains in transverse direction provides material for crack advance.

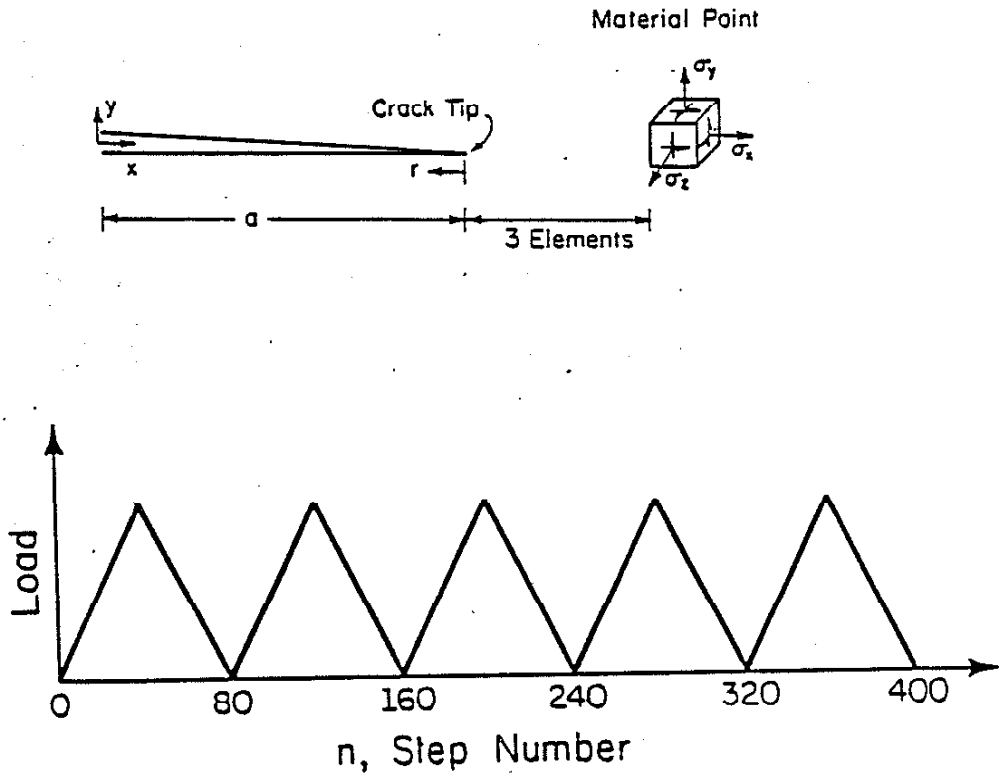

Figure 3.2 The location of the crack tip and location of the material point which is three elements away. The waviation of load with step number in the FEM model is also depicted. The crack tip reaches the material point at step #200. The load versus step number holds for all three R ratios considered.

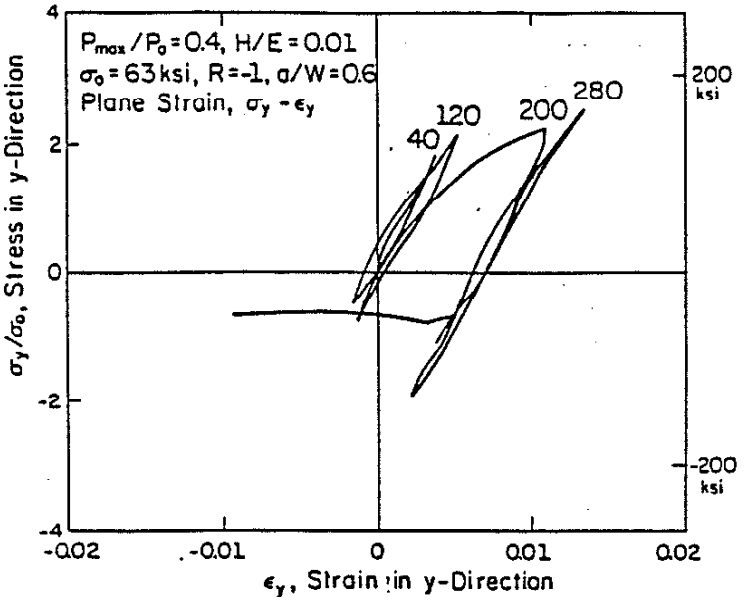

(a)

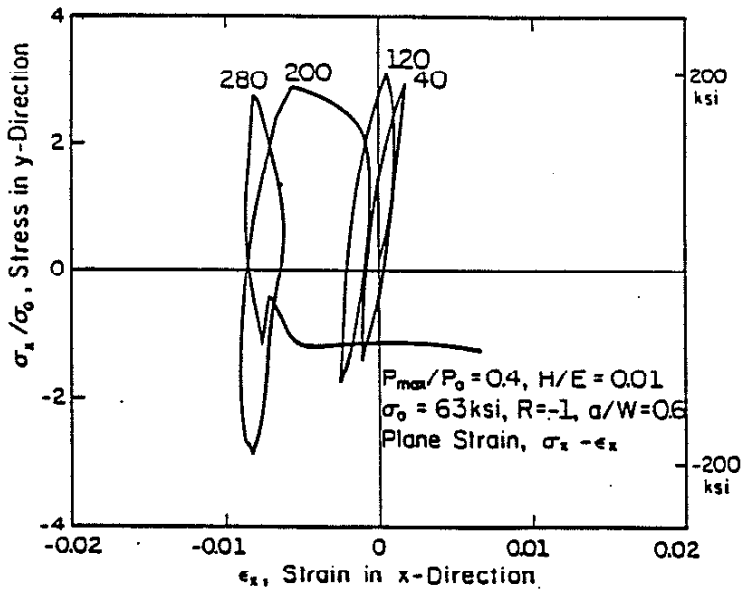

(b)

Figure 3.3 The stress-strain behavior in plane strain as the crack tip approaches the material point, reaches it and passes it. The crack tip reaches the material point in three cycles. (a) in the y-direction; (b) in the x-direction.

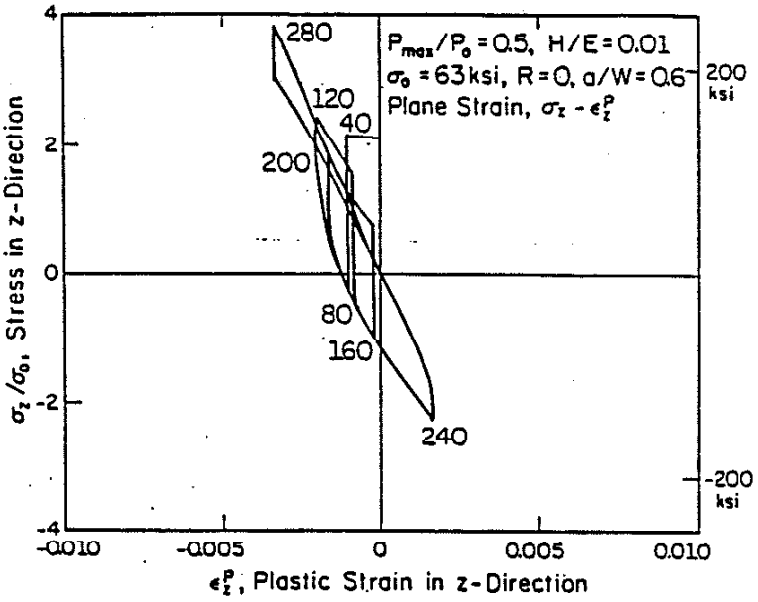

(c)

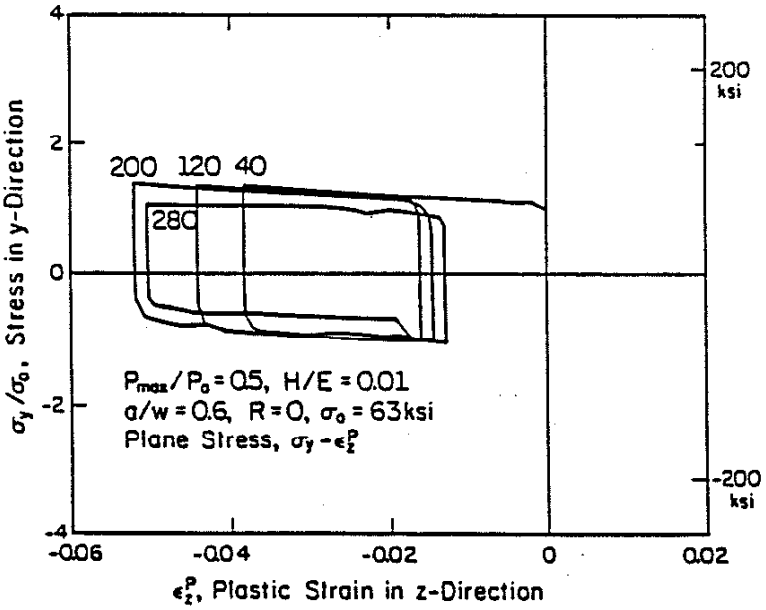

(d)

Figure 3.3 The stress-strain behavior in plane strain as the crack tip approaches the material point, reaches it and passes it. The crack tip reaches the material point in three cycles. (c) stress-plastic strain in the z-direction; (d) plane stress.

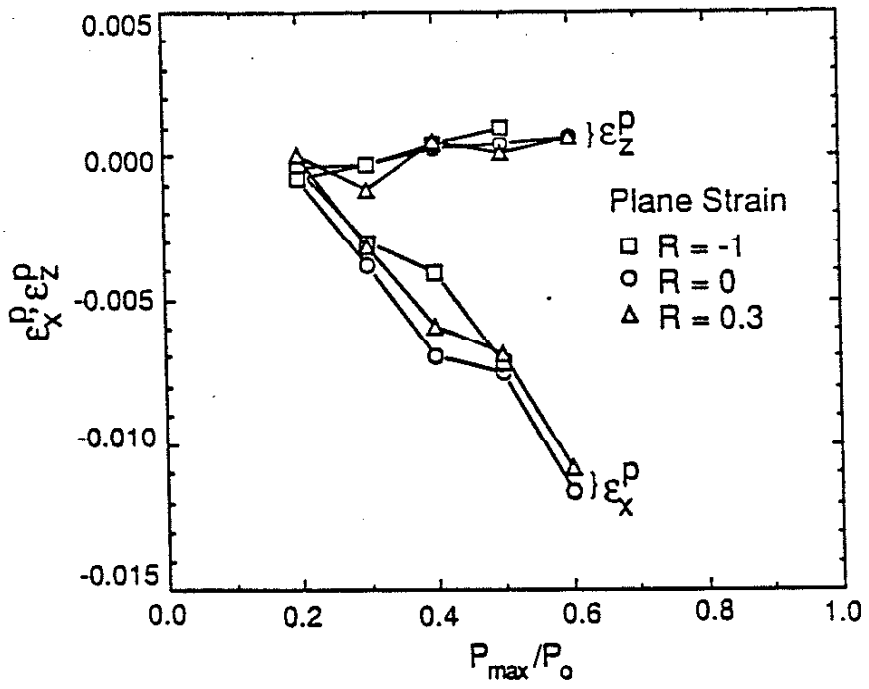

Figure 3.4 The variation of ε_z^p and ε_x^p with increasing maximum load under R = -1, 0, and 0.3 loading conditions.

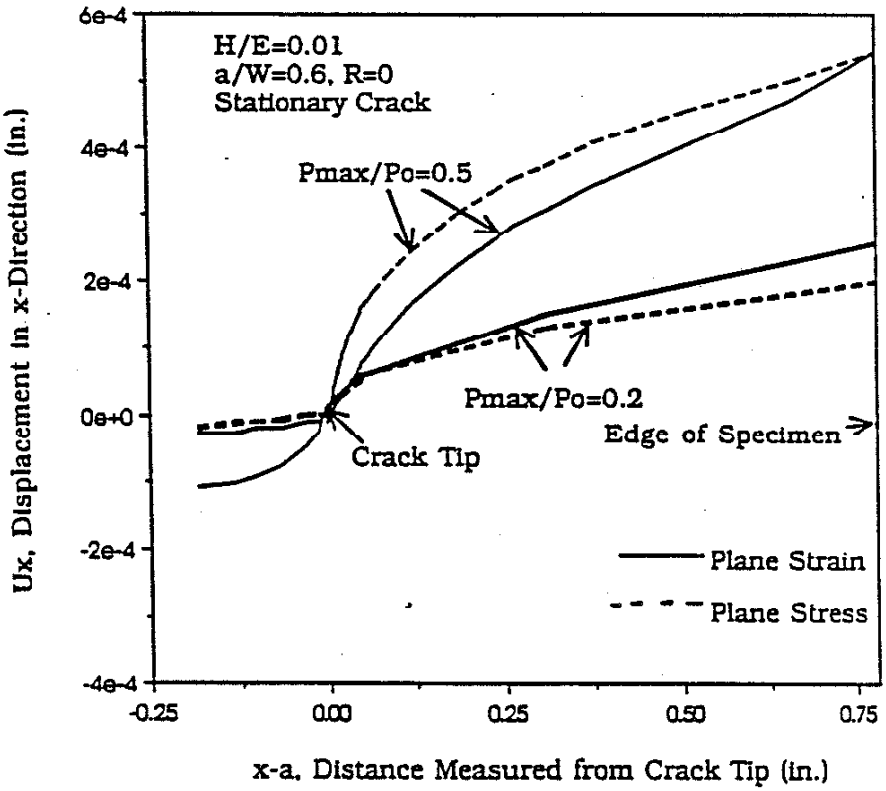

Figure 3.5 The displacements in the x direction in plane strain and plane stress for a stationary crack (first cycle).

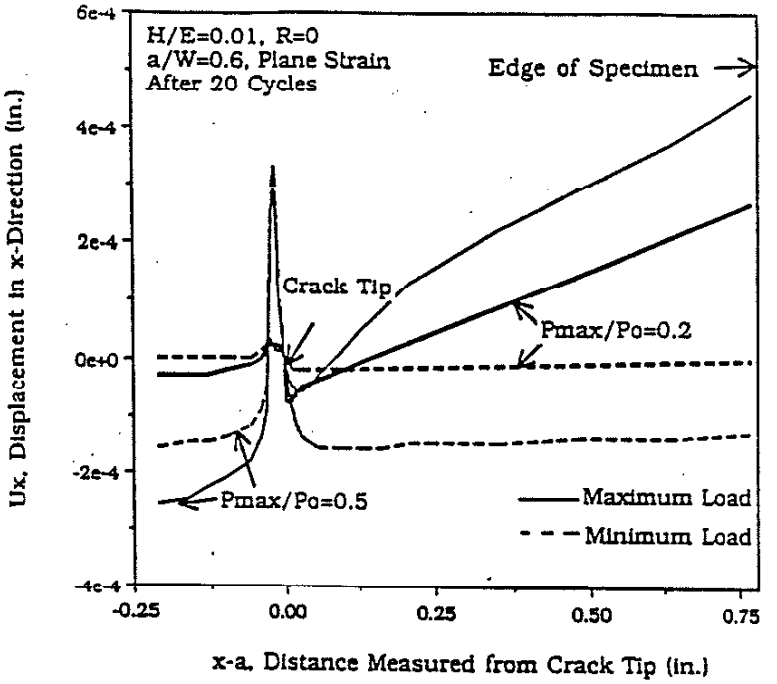

(a)

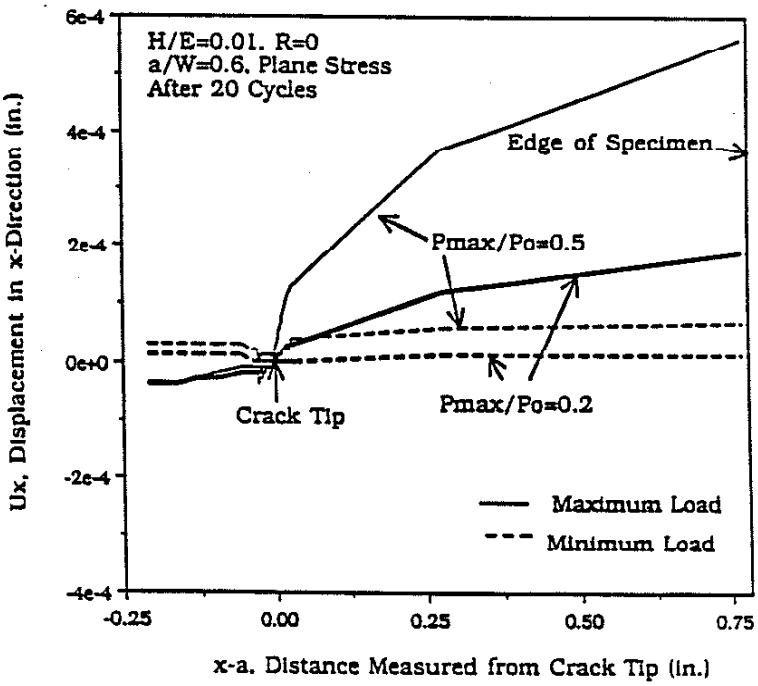

(b)

Figure 3.6 The displacement in the x direction on the crack plane after 20 cycles. (a) plane strain; (b) plane stress.

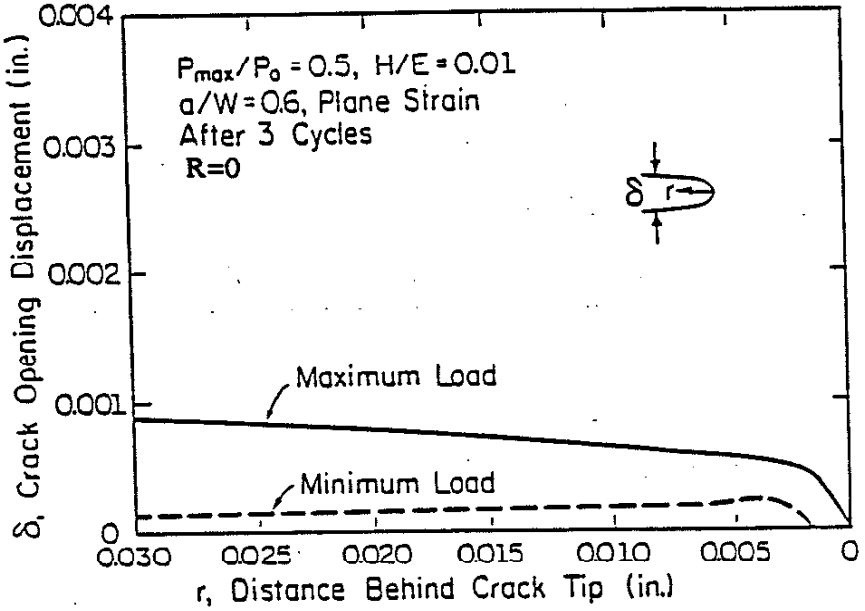

(a)

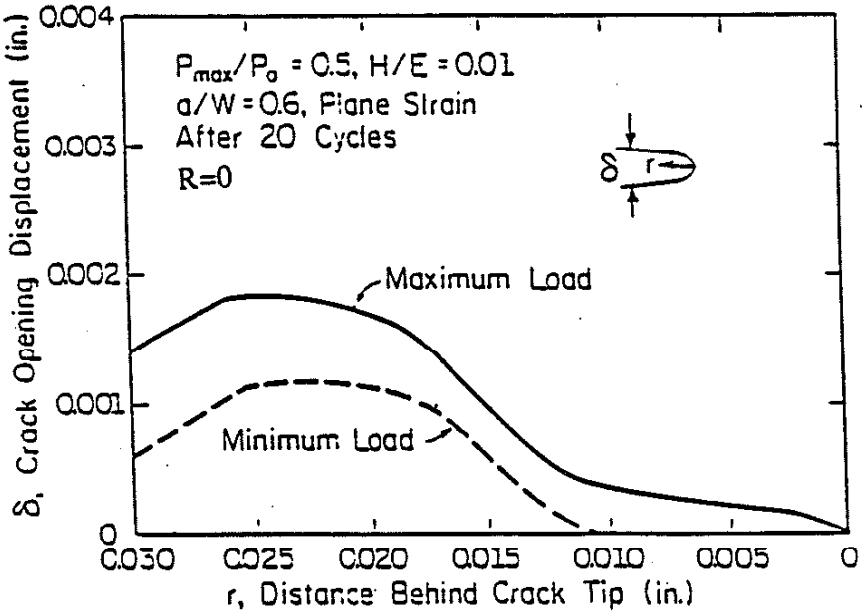

(b)

Figure 3.7 Crack tip opening displacements for plane strain case. (a) after 3 cycles; (b) after 20 cycles.

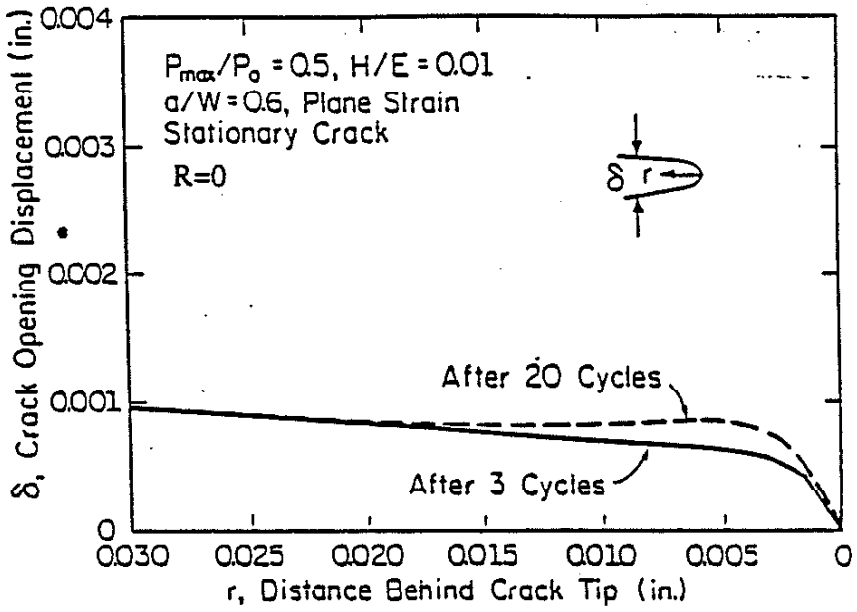

Figure 3.8 Crack tip opening displacements in the third cycle and in 20th cycle for stationary crack, $P_{max}/P_o = 0.5$, R = 0 case.

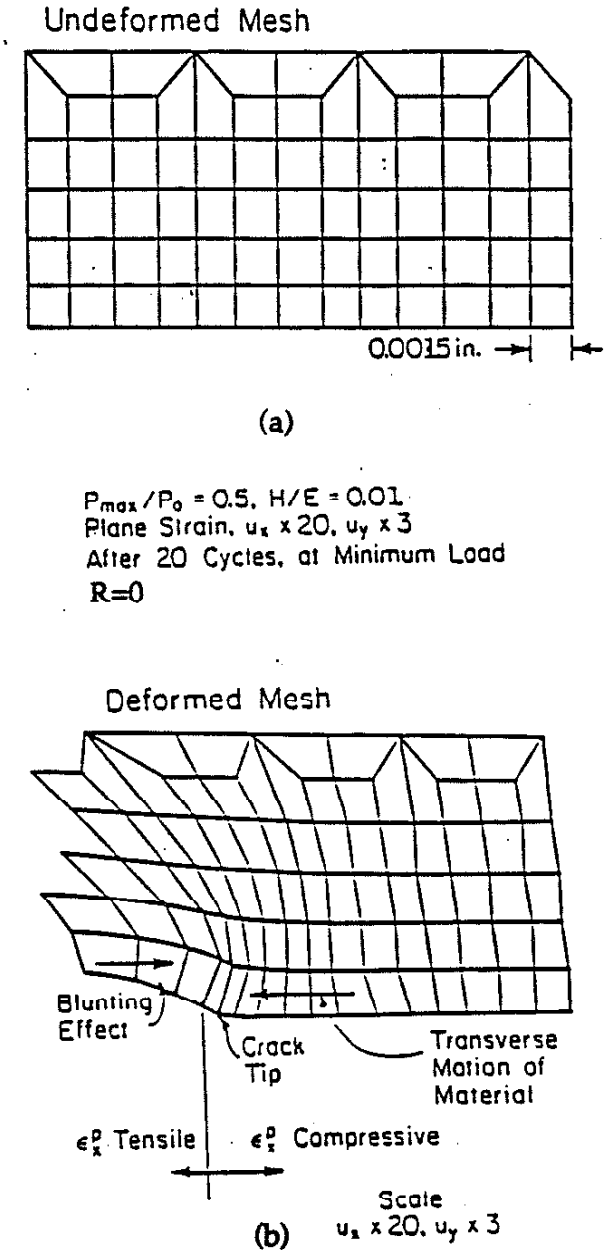

Figure 3.9 Finite element mesh near the crack tip. (a) undeformed mesh; (b) after 20 cycles under plane strain, R = 0 condition.

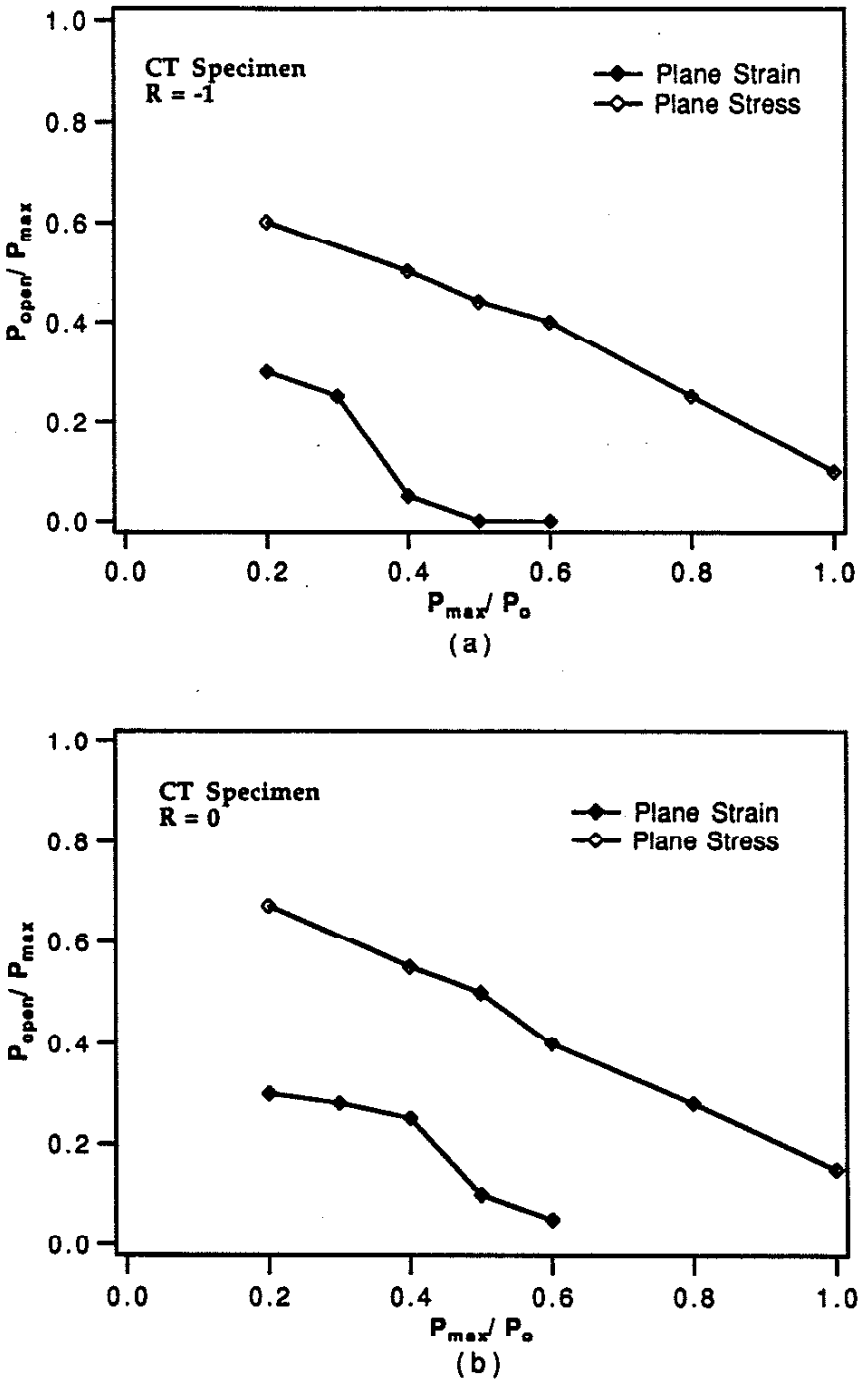

Figure 3.10 Summary of normalized crack opening load with increasing applied maximum load. (a) R = -1; (b) R = 0.

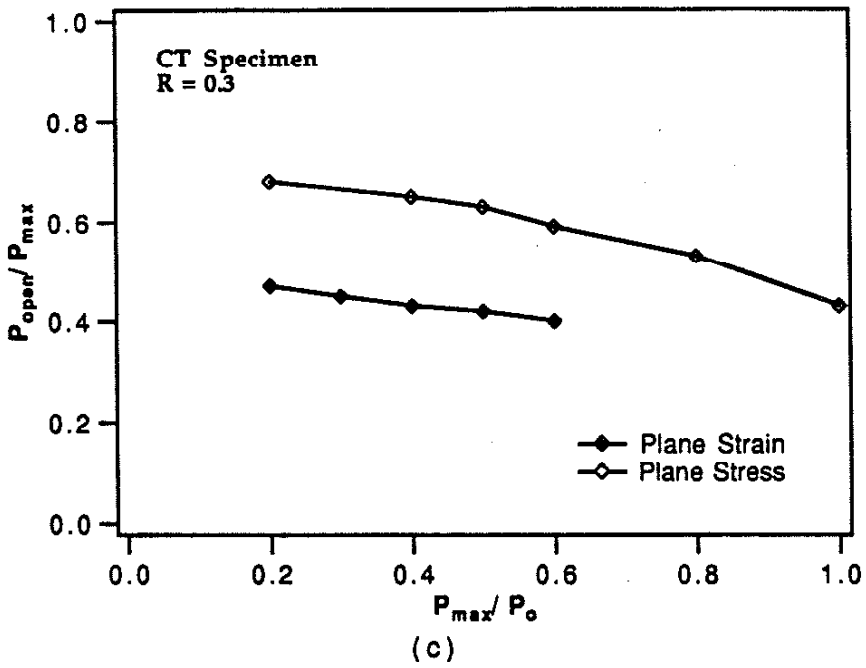

Figure 3.10 Summary of normalized crack opening loads with increasing applied maximum load. (c) R = 0.3.

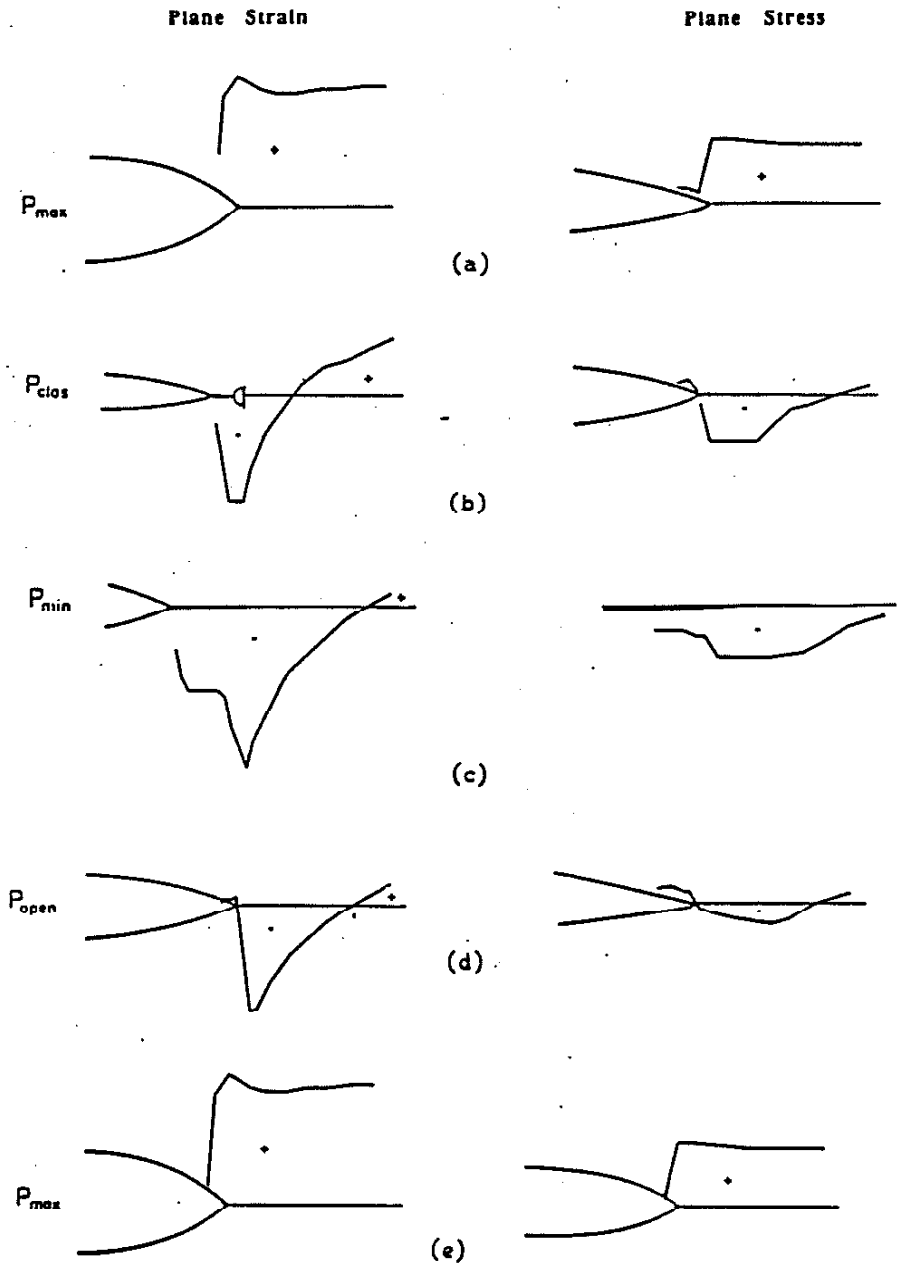

Figure 3.11 Schematic of stress distributions during an unloading and loading reversal under plane strain and plane stress conditions.

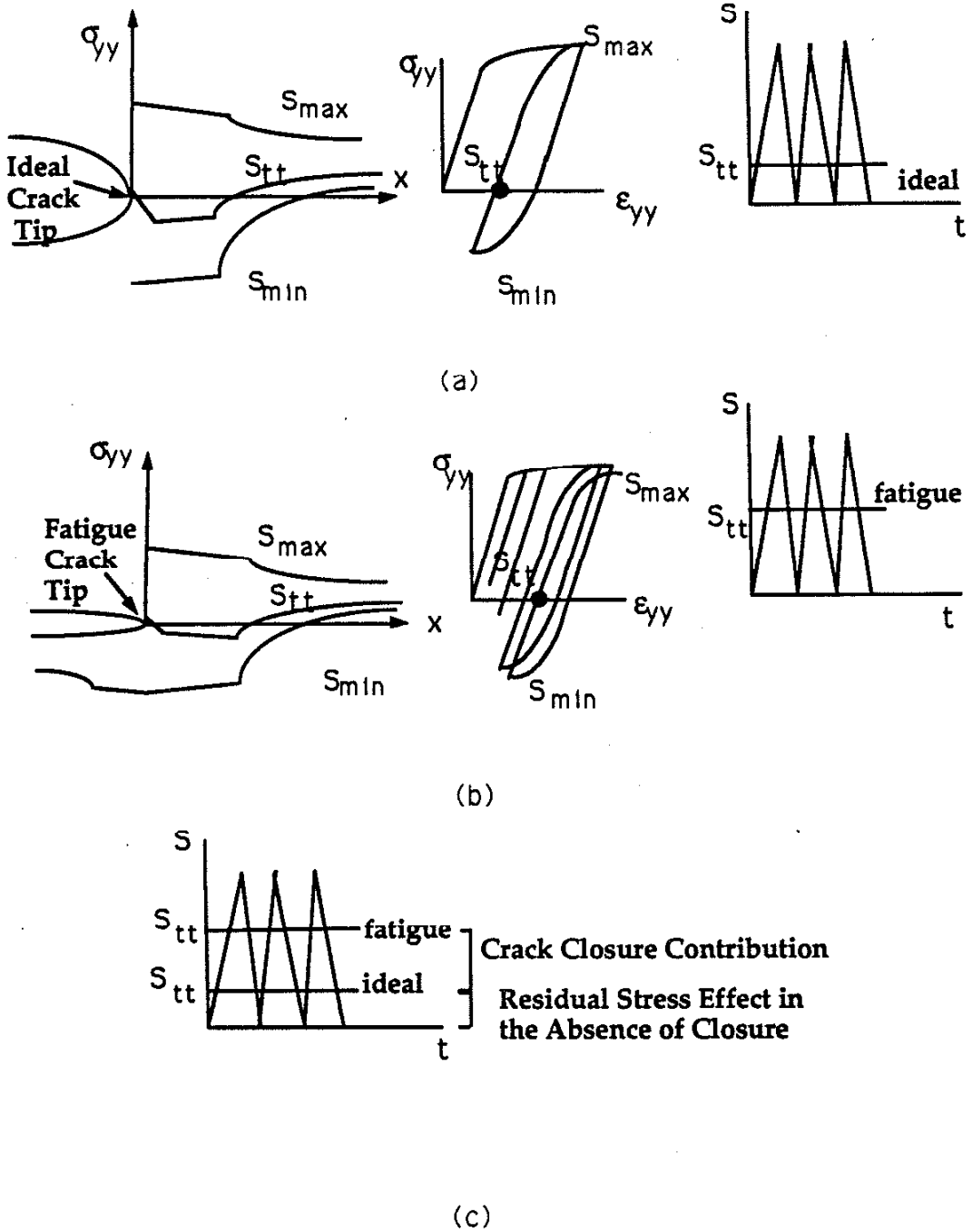

Figure 4.1 Schematics indicating the definition of S_{tt} for an (a) ideal crack and (b) for a fatigue crack. S_{tt} is the applied stress level when crack tip stress becomes tensile (c) the contribution to S_{tt} from crack closure and from residual stresses in the absence of closure.

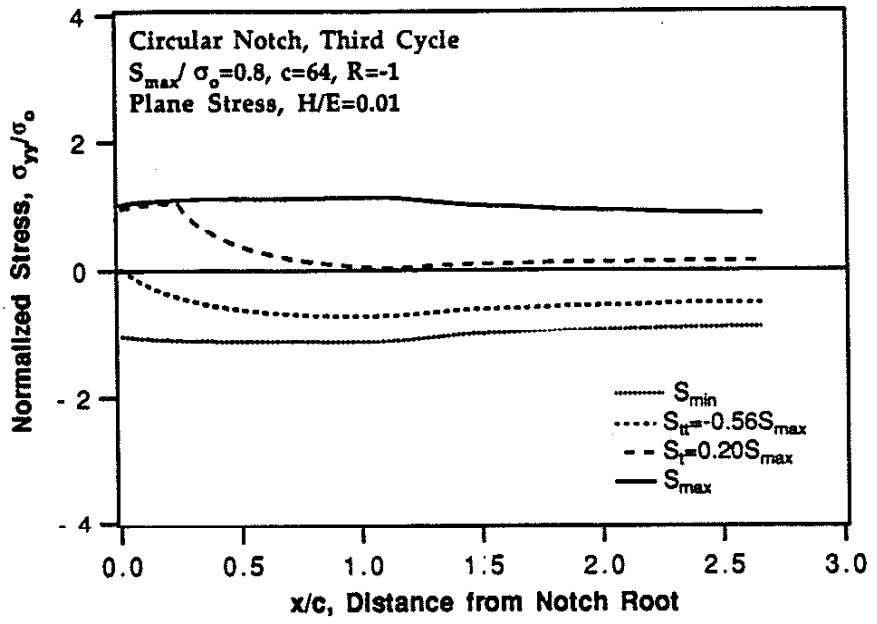

(a)

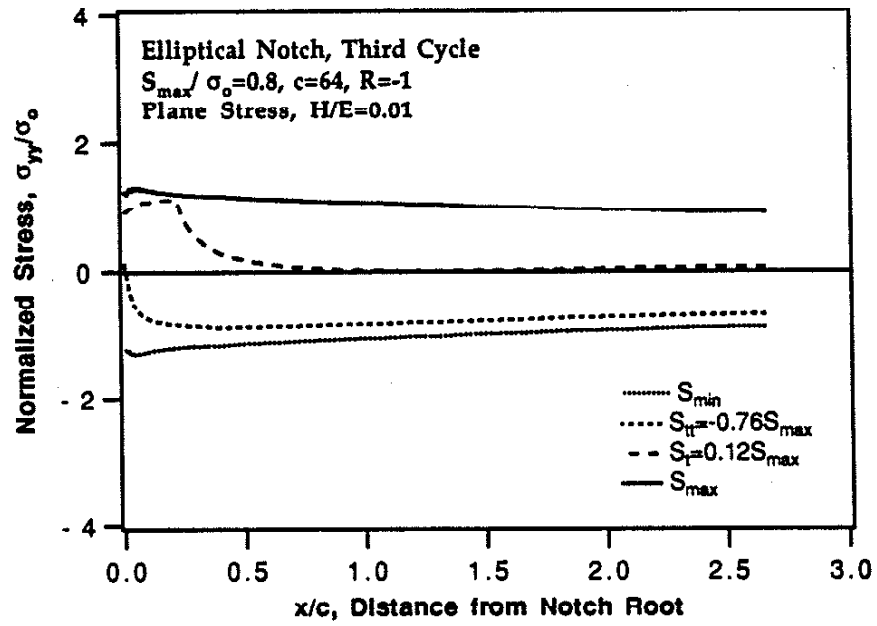

(b)

Figure 4.2. The stress distribution ahead of notch root at minimum load, crack tip tensile load, crack tensile load and maximum load for S_{max}/σ_o=0.8, R=-1, plane stress case. (a) circular notch, (b) elliptical notch

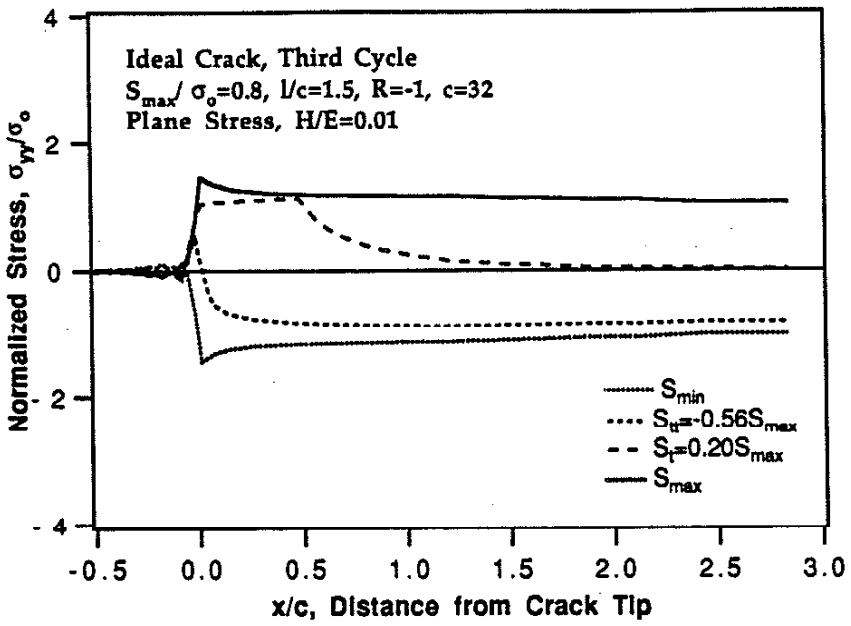

(c)

Figure 4.2. The stress distribution ahead of notch root at minimum load, crack tip tensile load, crack tensile load and maximum load for S_{max}/σ_o=0.8, R=-1, plane stress case. (c) ideal crack.

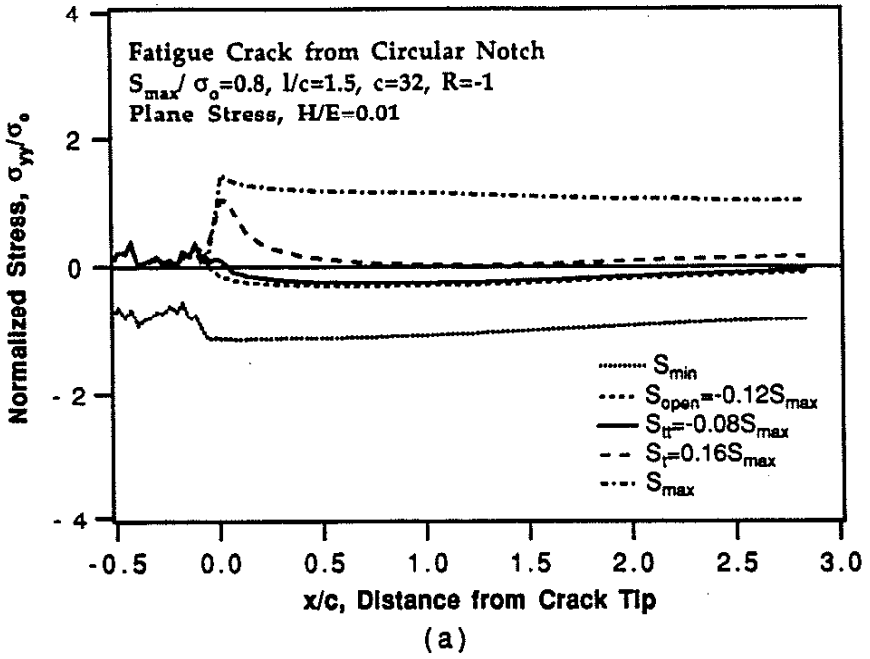

(a)

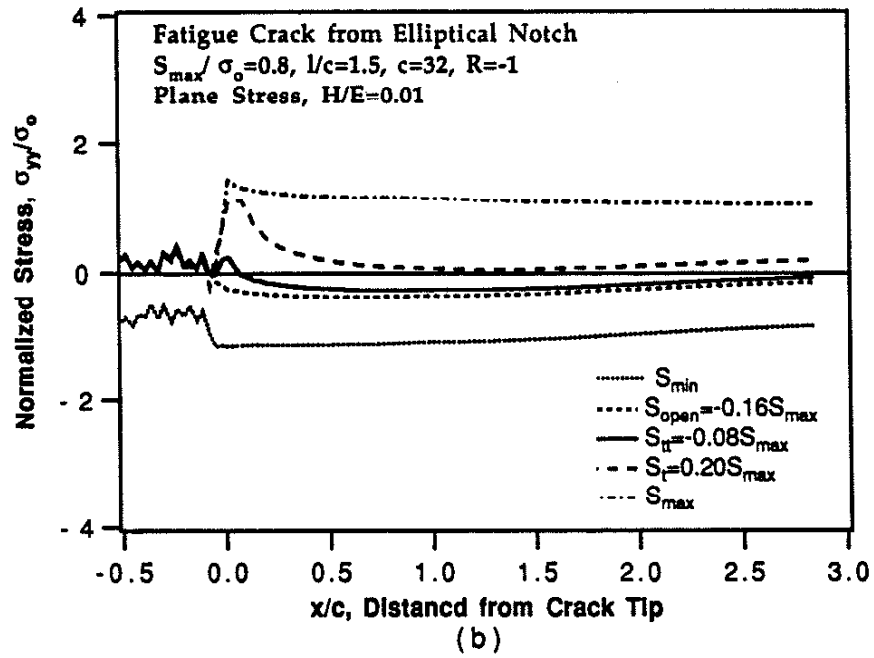

(b)

Figure 4.3 The stress distribution near fatigue crack tip at minimum load, crack opening load, crack tip tensile load, crack tensile load and maximum load for S_{max}/σ_o=0.8, R=-1, plane stress case. (a) fatigue crack from circular notch, (b) fatigue crack from elliptical notch.

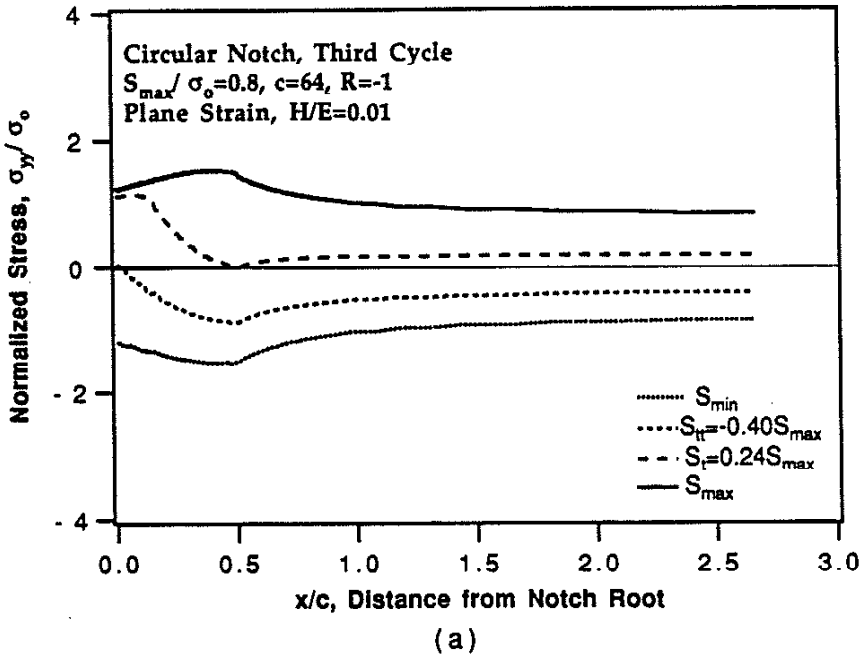

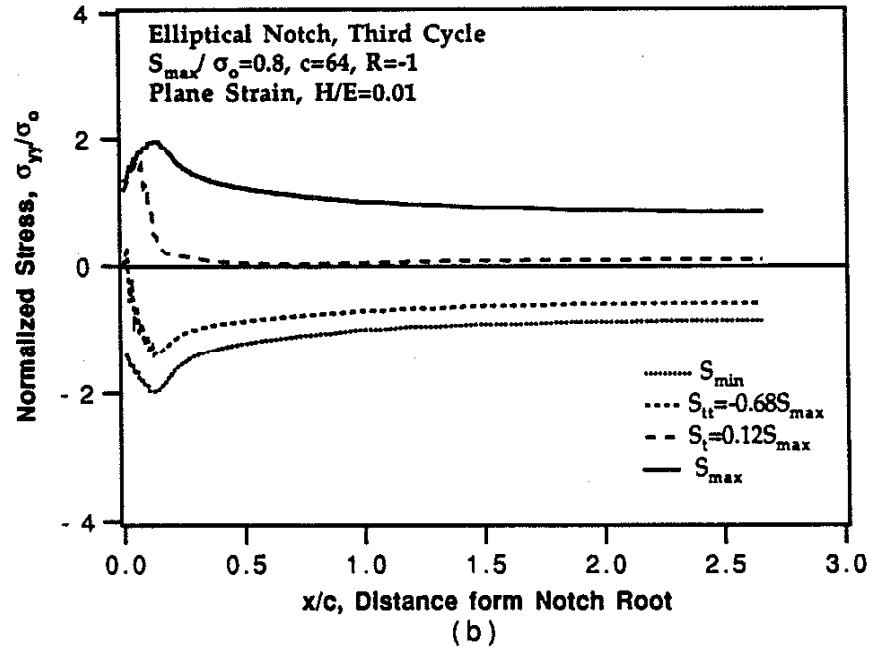

Figure 4.4. The stress distribution ahead of notch root and near crack tip at minimum load, crack opening load, crack tip tensile load, crack tensile load and maximum load for S_{max}/σ_o=0.8, R=-1, plane strain case. (a) circular notch, (b) elliptical notch

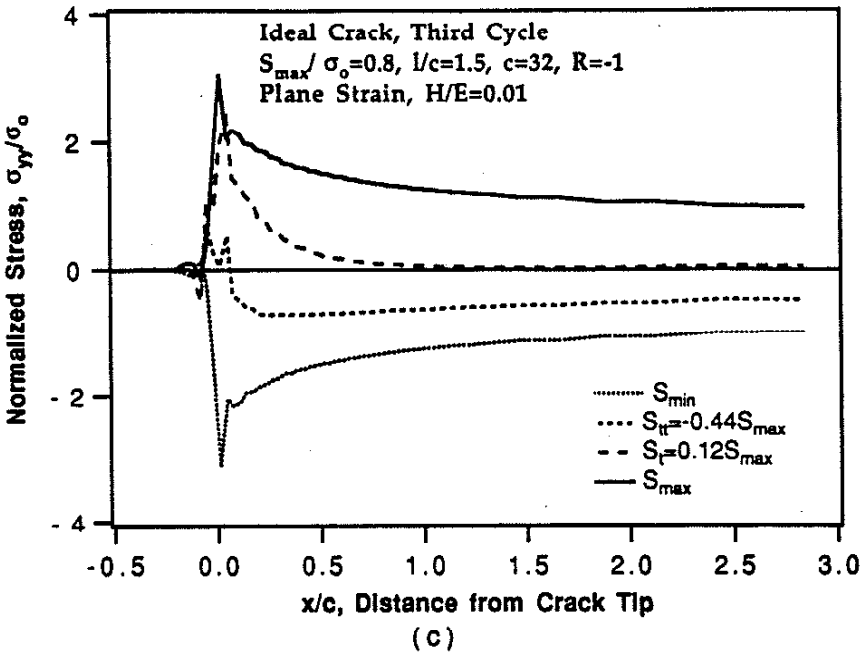

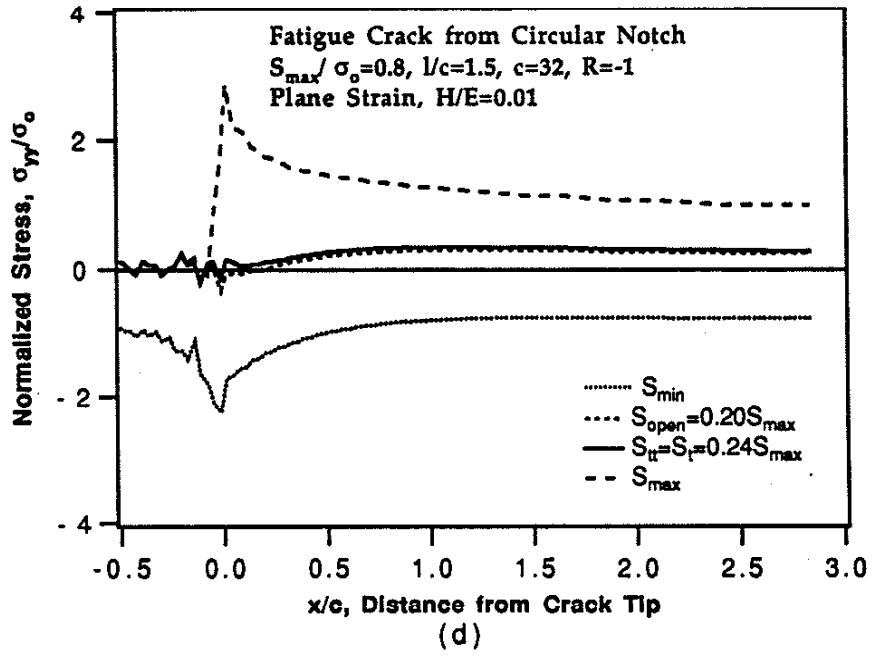

Figure 4.4. The stress distribution ahead of notch root and near crack at minimum load, crack opening load, crack tip tensilt load, crack tensile load and maximum load for S_{max}/σ_o=0.8, R=-1, plane strain case. (c) ideal crack, (d) fatigue crack from circular notch

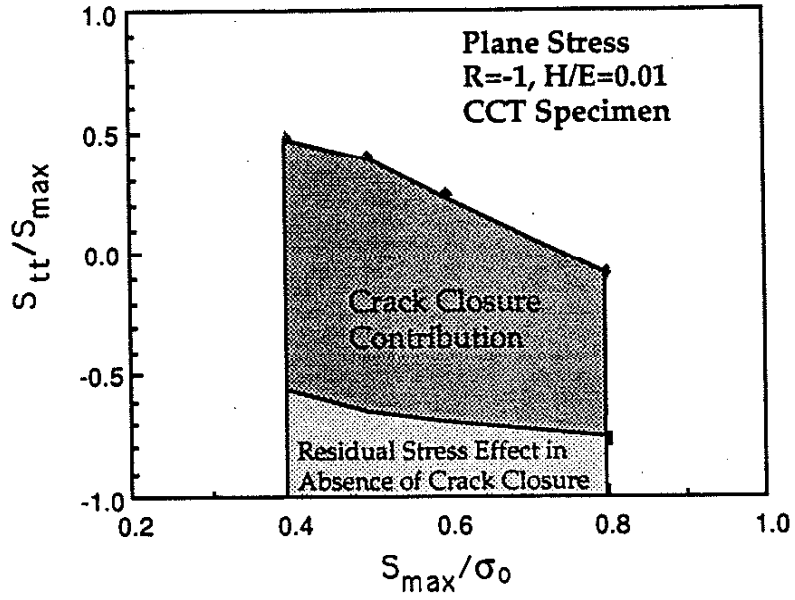

(a)

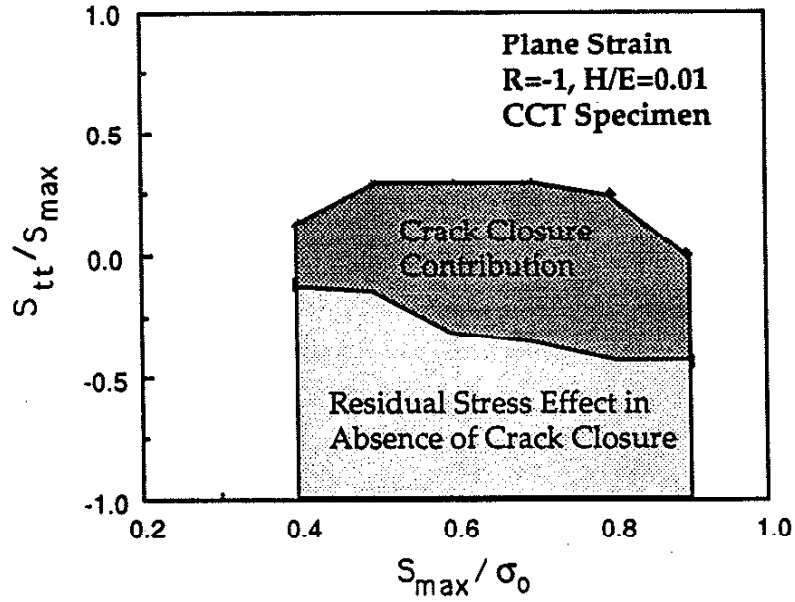

(b)

Figure 4.5. Crack closure contribution on S_{tt} and residual stress effect in absence of crack closure on S_{tt} for CCT specimen, R=-1
(a) plane stress, (b) plane strain

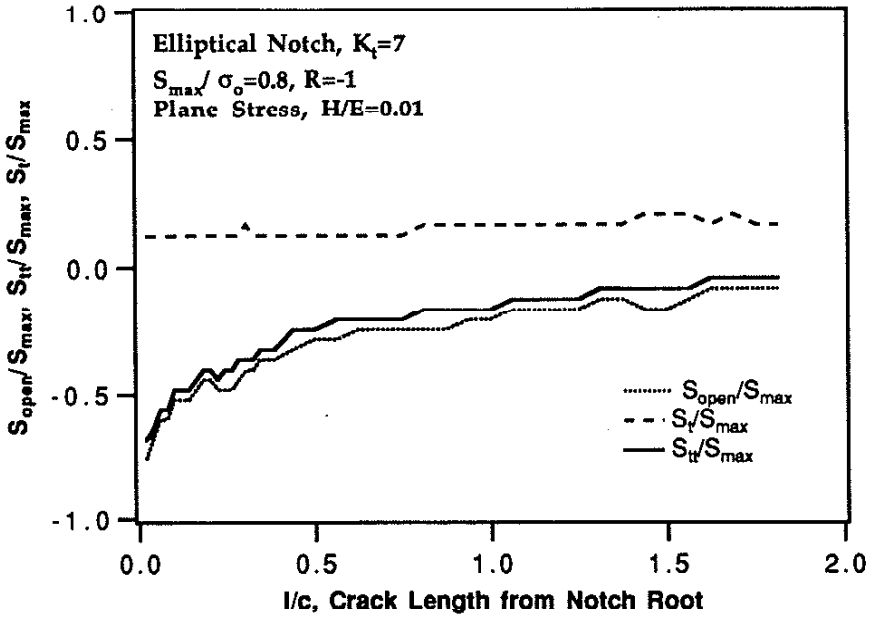

(a)

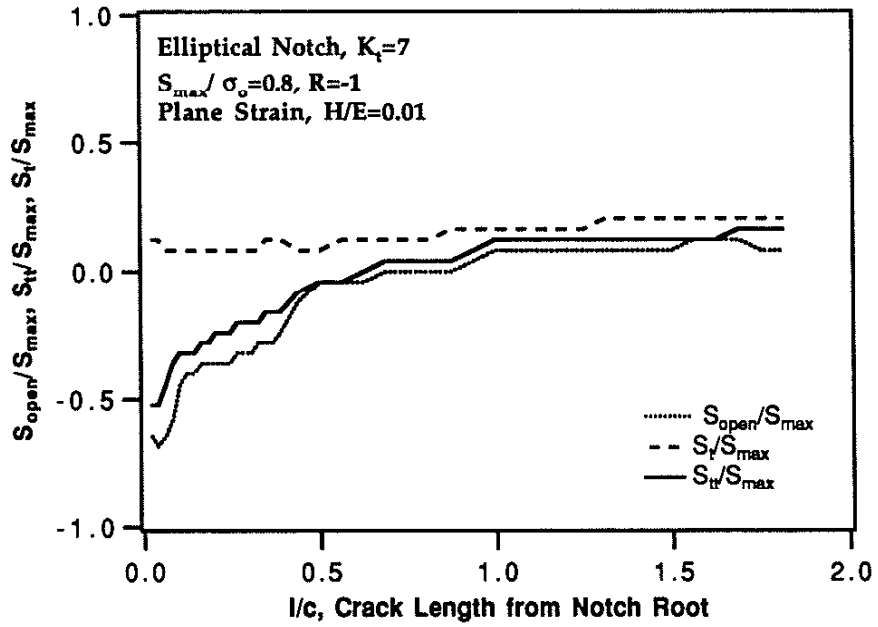

(b)

Figure 4.6. History of crack opening load, crack tip tensil load and crack tensile load when a fatigue crack grows from elliptical notch for S_{max}/σ_o=0.8, R=-1 case, CCT specimen. (a) plane stress (b) plane strain.

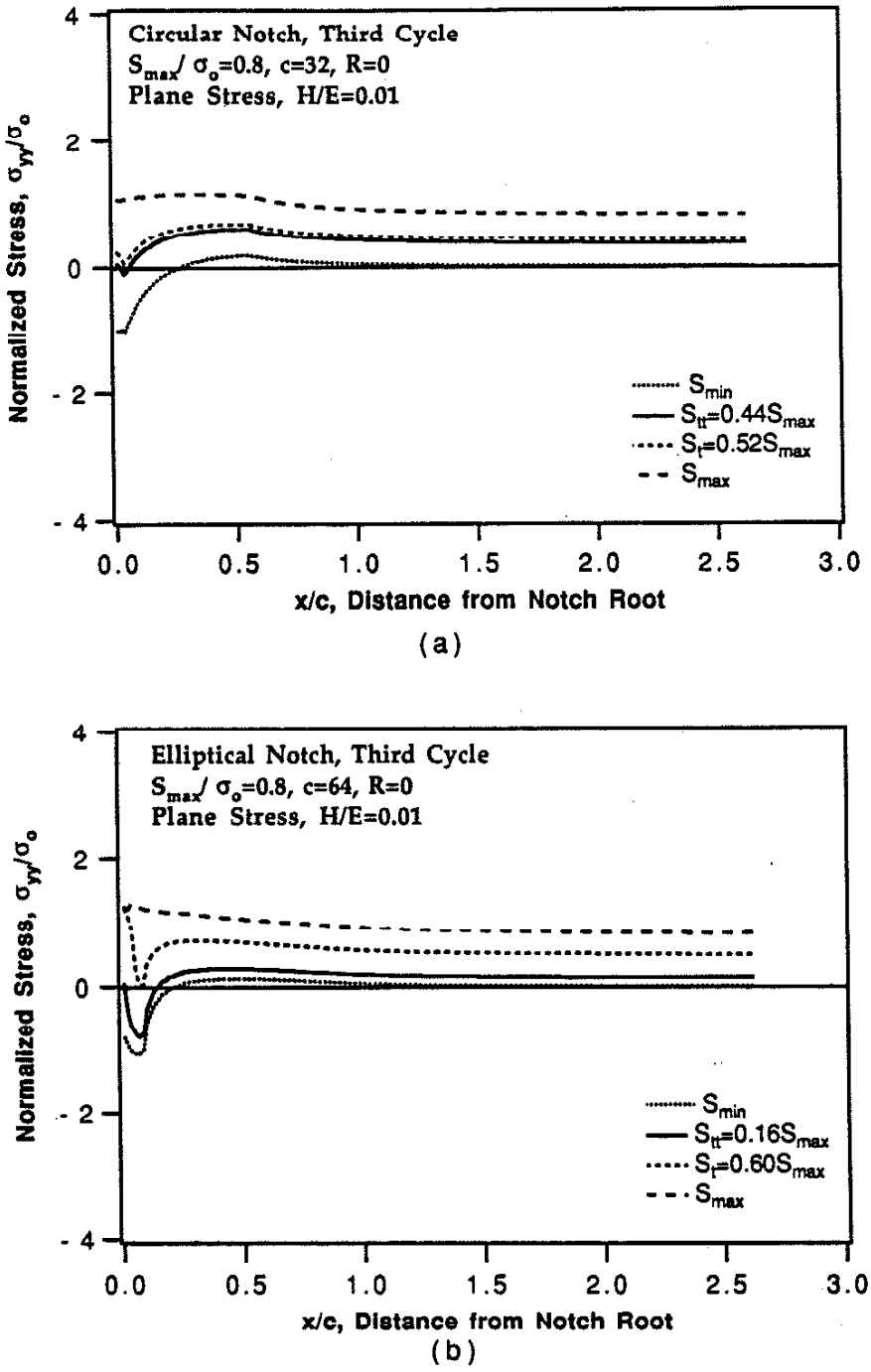

Figure 4.7. The stress distribution ahead of notch root at minimum load, crack tip tensile load, crack tensile load and maximum load for S_{max}/σ_o=0.8, R=0, plane stress case. (a) circular notch, (b) elliptical notch.

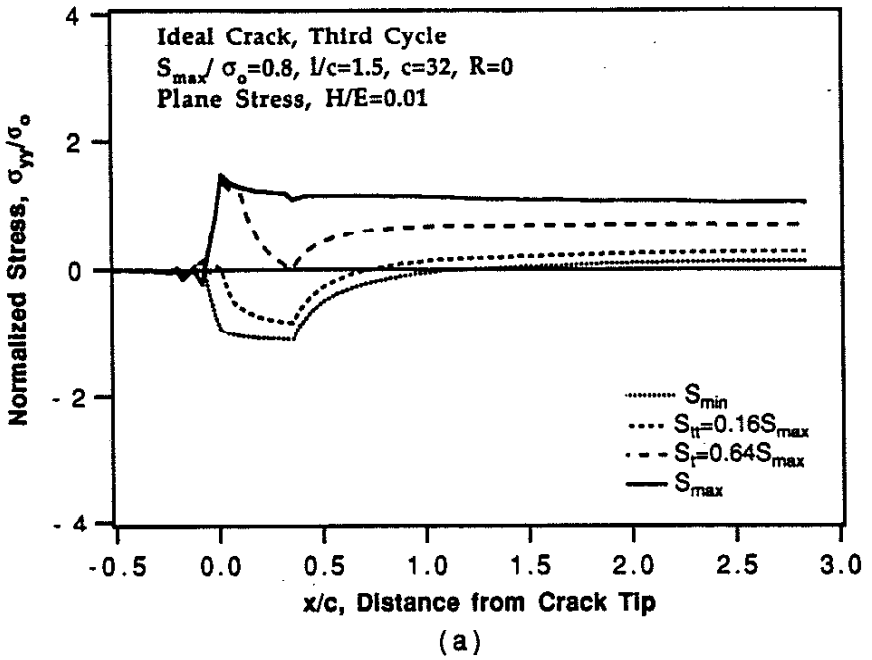

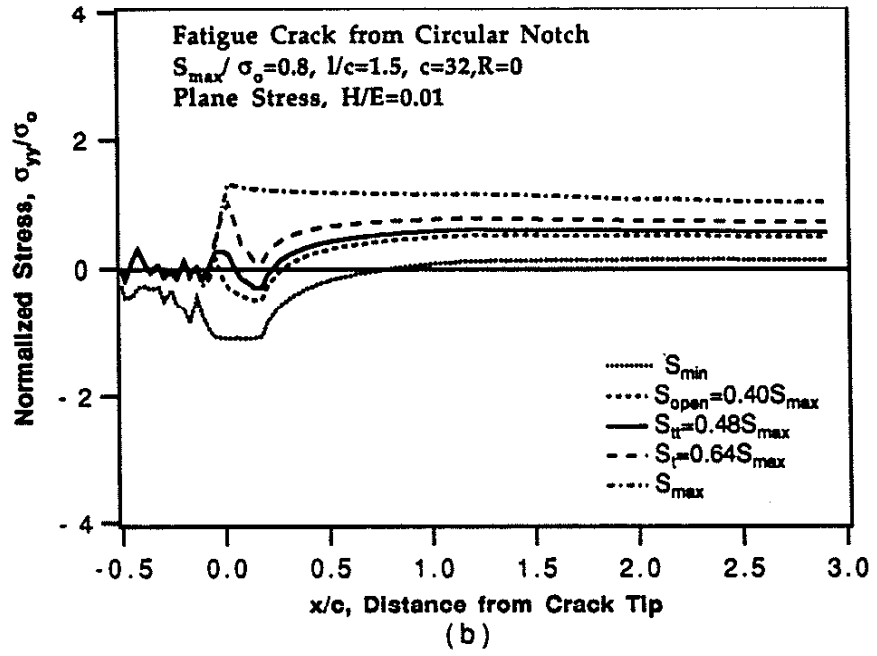

Figure 4.8. The stress distribution near crack tip at minimum load, crack tip tensile load, crack tensile load and maximum load for S_{max}/σ_o=0.8 R=0, plane stress case, CCT specimen. (a) ideal crack, (b) fatigue crack from circular notch.

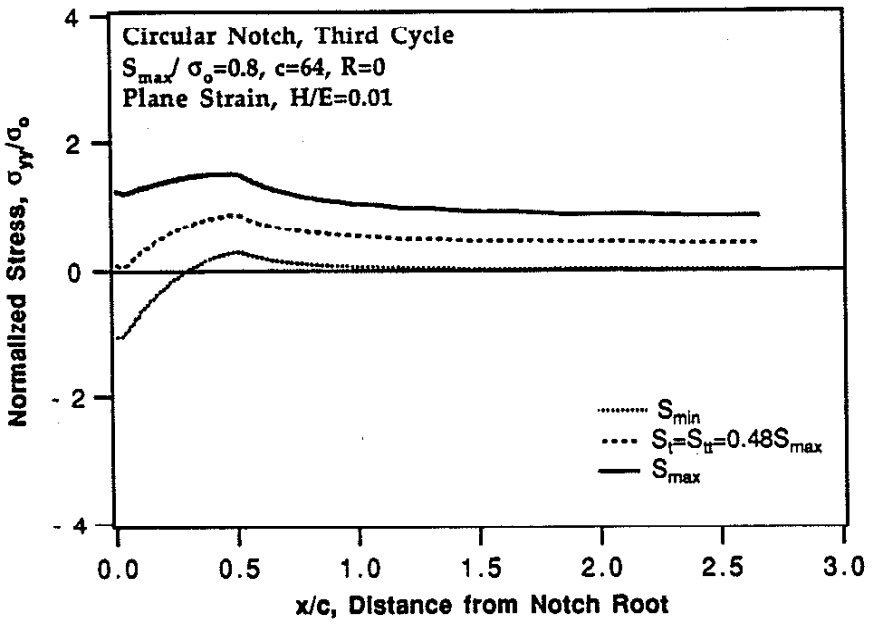

(a)

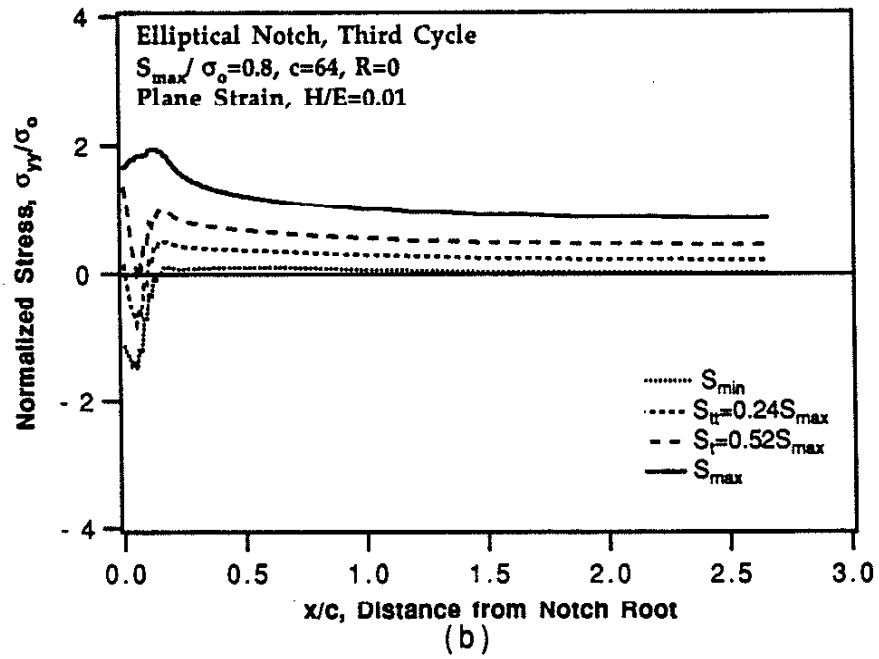

(b)

Figure 4.9. The Stress distribution ahead of notch root at minimum load, crack tip tensile load, crack tensile load and maximum load for S_{max}/σ_o=0.8, R=0, plane strain case. (a) circular notch, (b) elliptical notch.

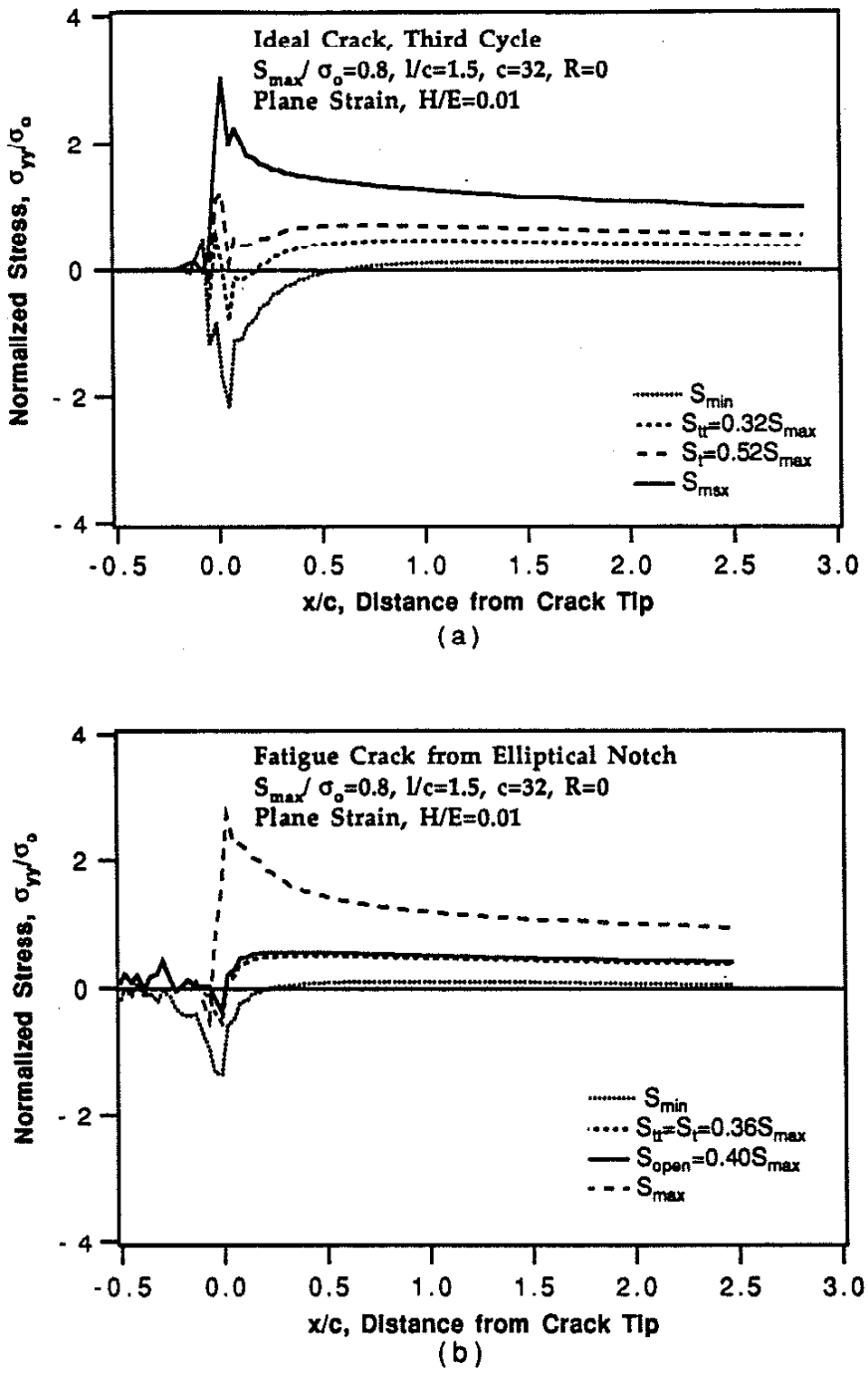

Figure 4.10. The stress distribution near crack tip at minimum load, crack tip tensile load, crack tensile load and maximum load for S_{max}/σ_o=0.8, R=0, plane strain case, CCT specimen. (a) ideal crack, (b) fatigue crack from elliptical notch.

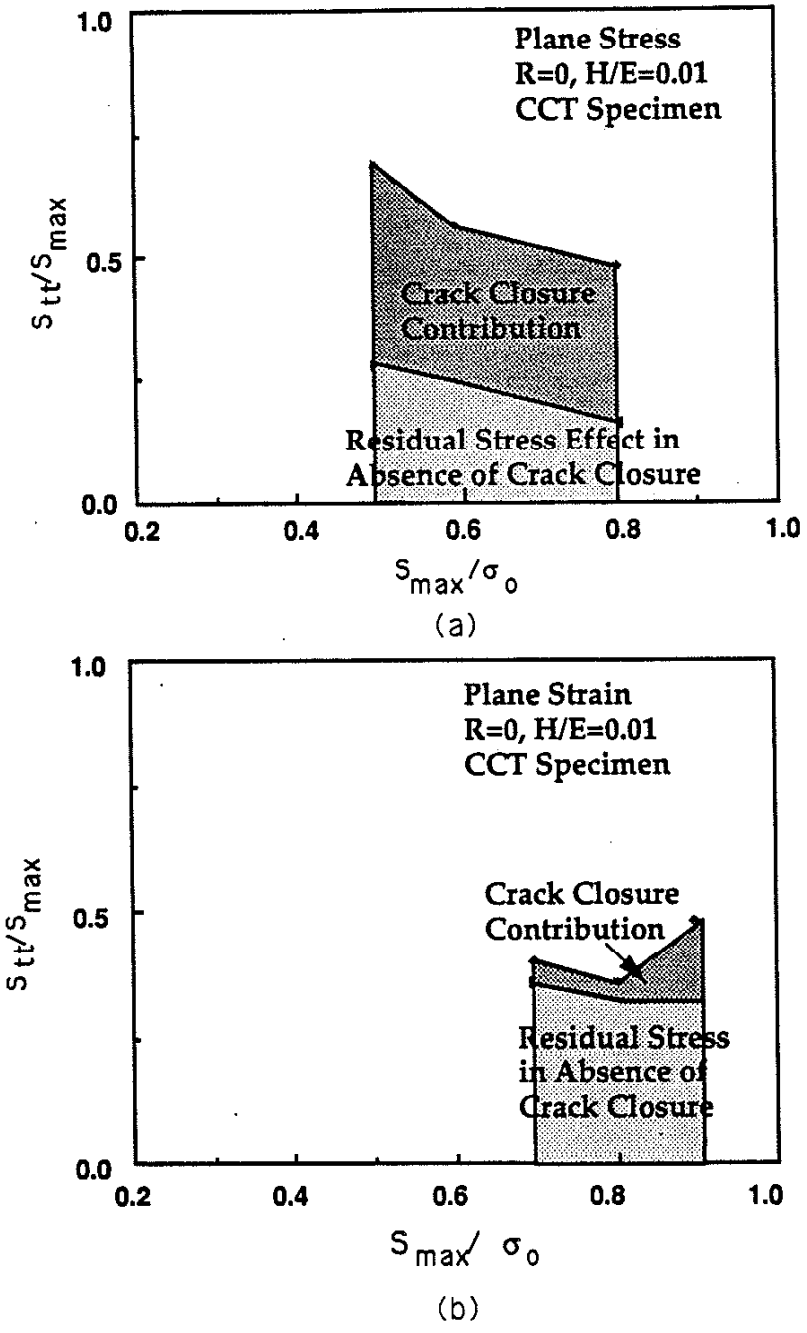

Figure 4.11. Crack closure contribution to S_{tt} and residual stress effect on S_{tt} in the absence of crack closure for R=0 case, CCT specimen (a) plane stress, (b) plane strain.

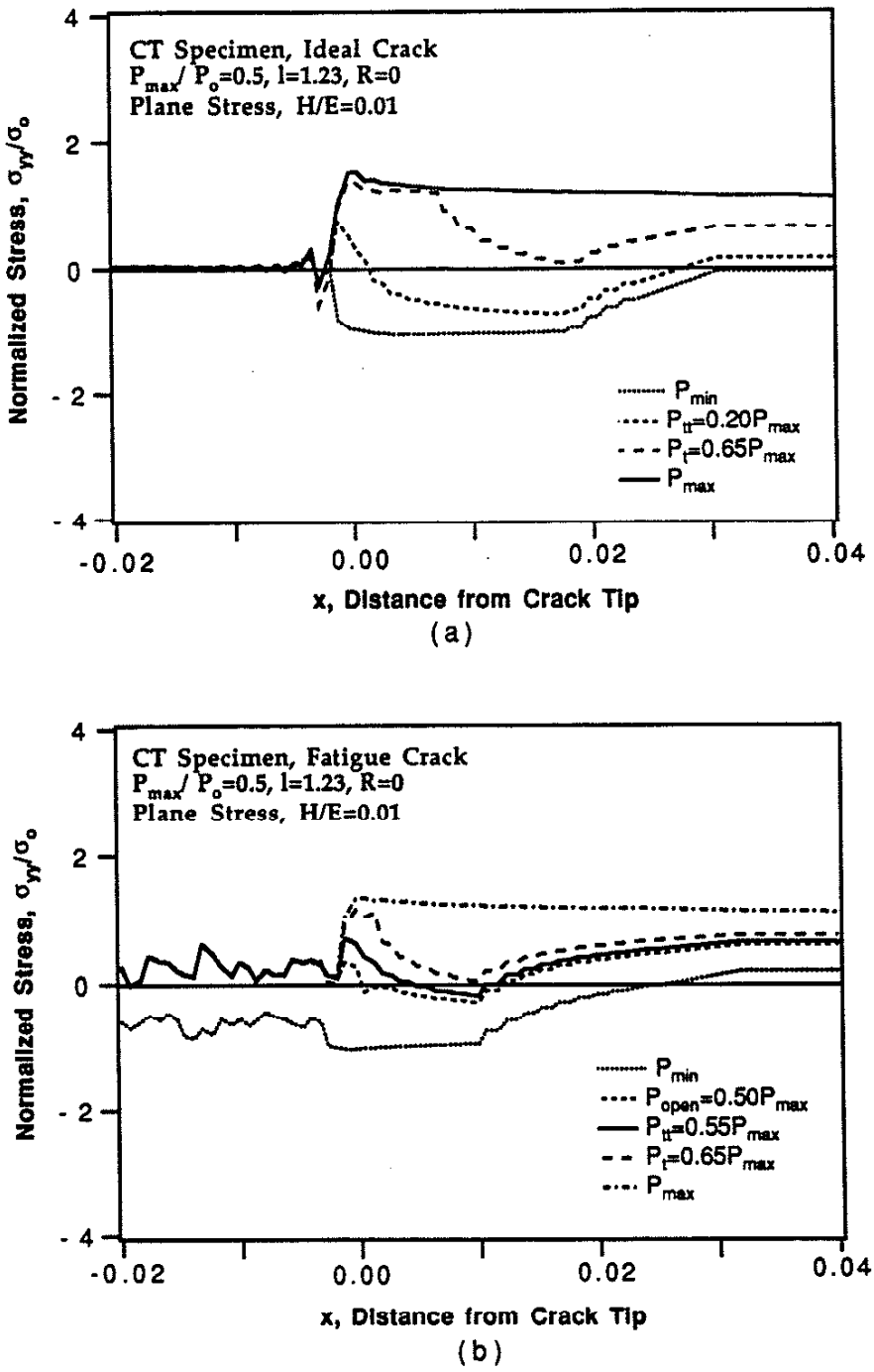

Figure 4.12. The stress distribution near crack tip at miimum load, crack opening load, crack tip tensile load, crack tensile load and maximum load for P_{max}/P_o=0.5, R=0, CT specimen, plane stress case. (a) ideal crack, (b) fatigue crack

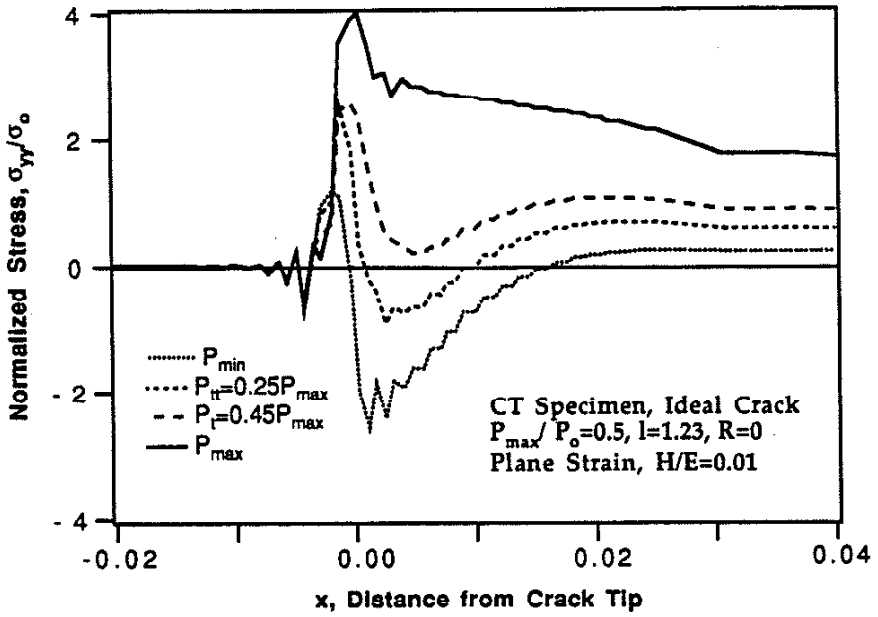

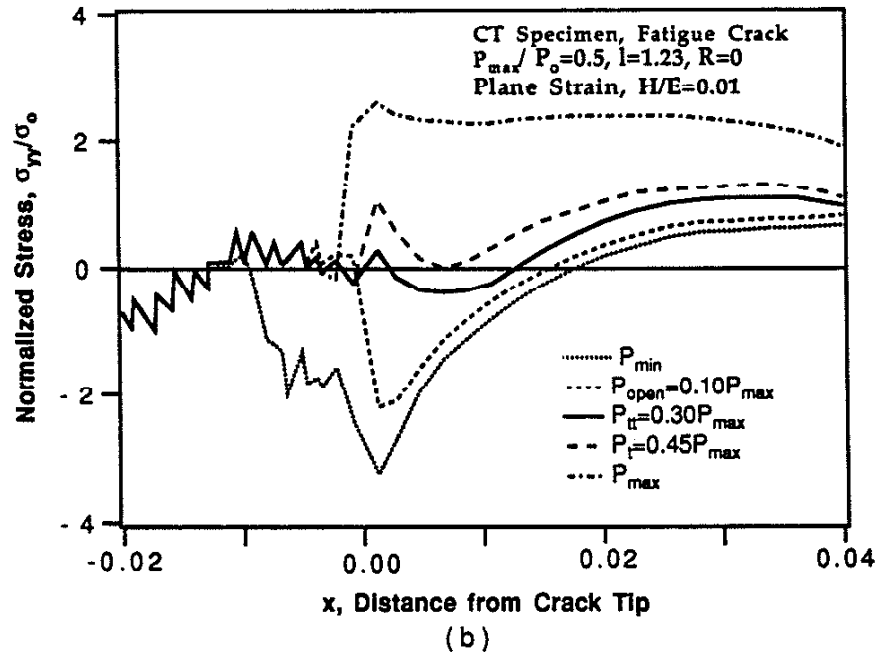

Figure 4.13. The stress distribution near crack tip at minimum load, crack opening load, crack tip tensile load, crack tensile load and maximum load for P_{max}/P_o=0.5, R=0, plane strain case, CT specimen. (a) ideal crack, (b) fatigue crack.

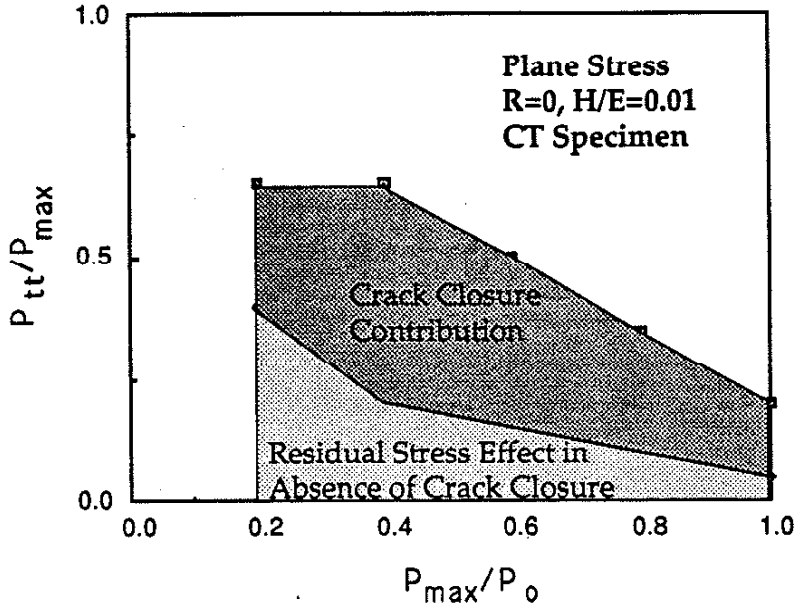

(a)

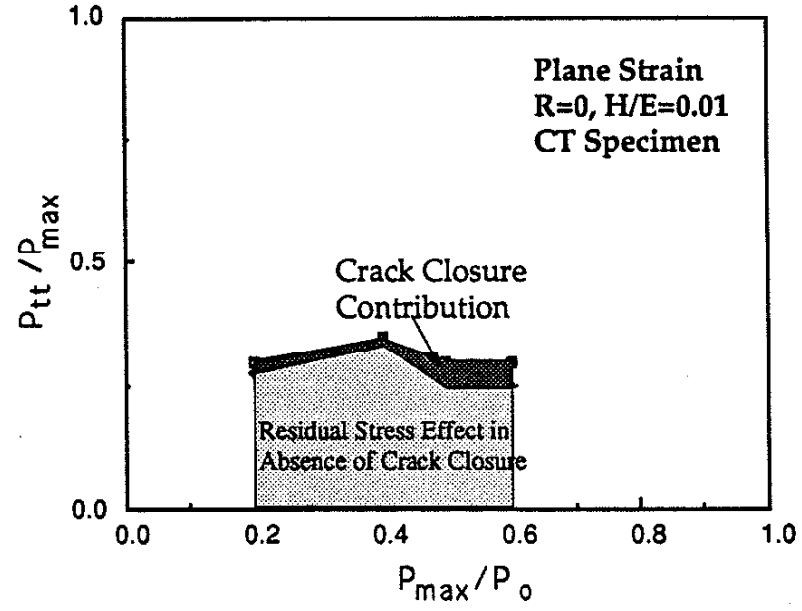

(b)

Figure 4.14. Crack closure contribution on S_{tt} and residual stress effect on S_{tt} in absence of crack closure, CT specimen
(a) plane stress, R=0, (b) Plane strain, R=0.

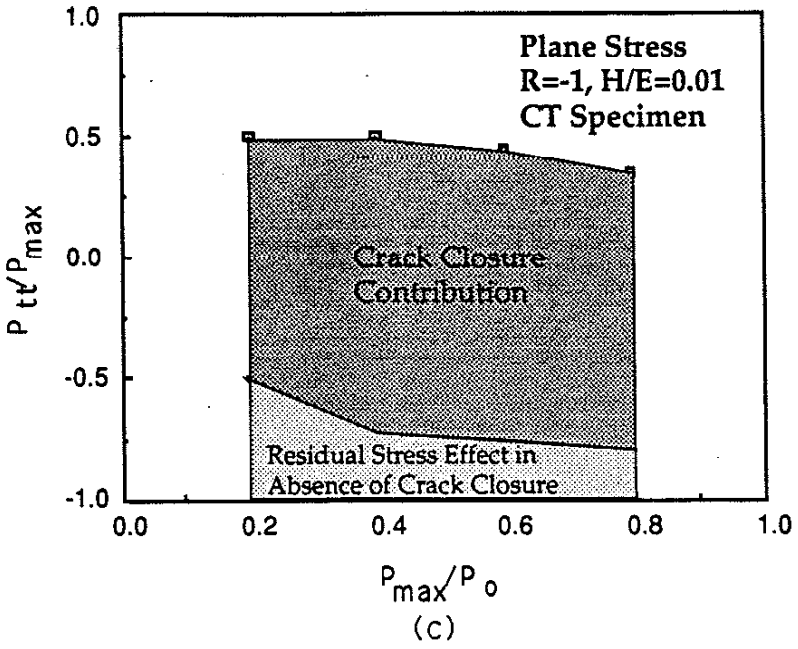

(c)

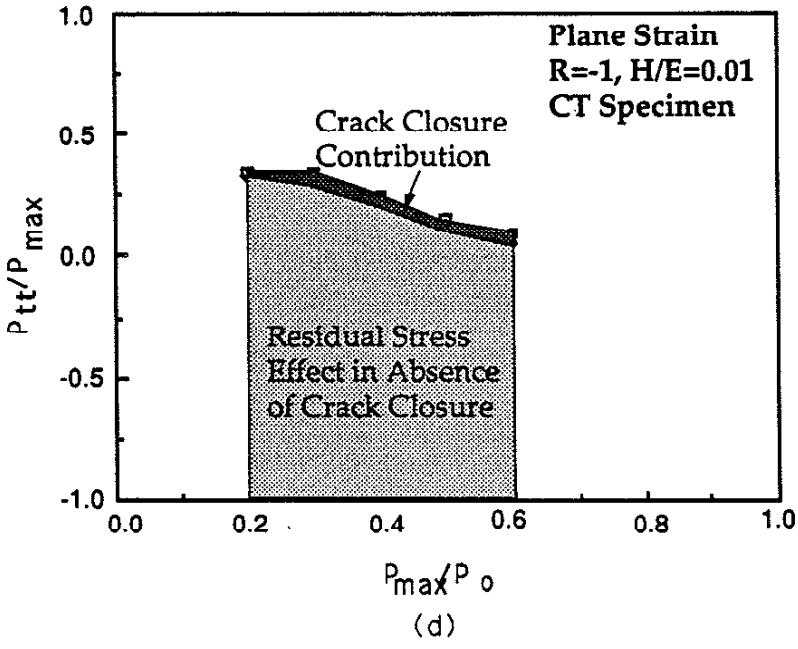

(d)

Figure 4.14. Crack closure contribution on S_{tt} and residual stress effect on S_{tt} in absence of crack closure, CT specimen.
(c) plane stress, R=-1, (d) plane strain, R=-1

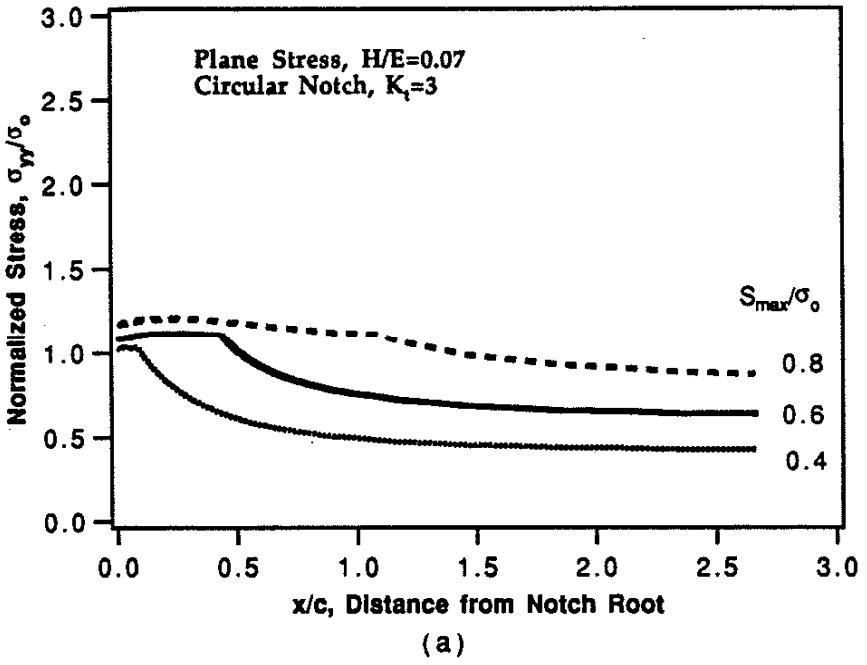

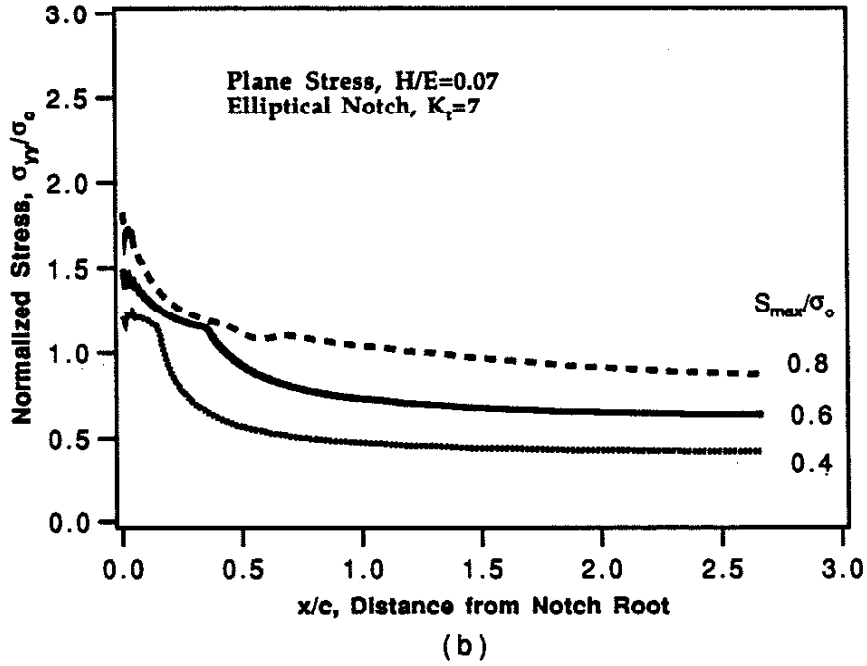

Figure 5.1 Stress distributions ahead of notch root under different applied load (H/E=0.07, plane stress)

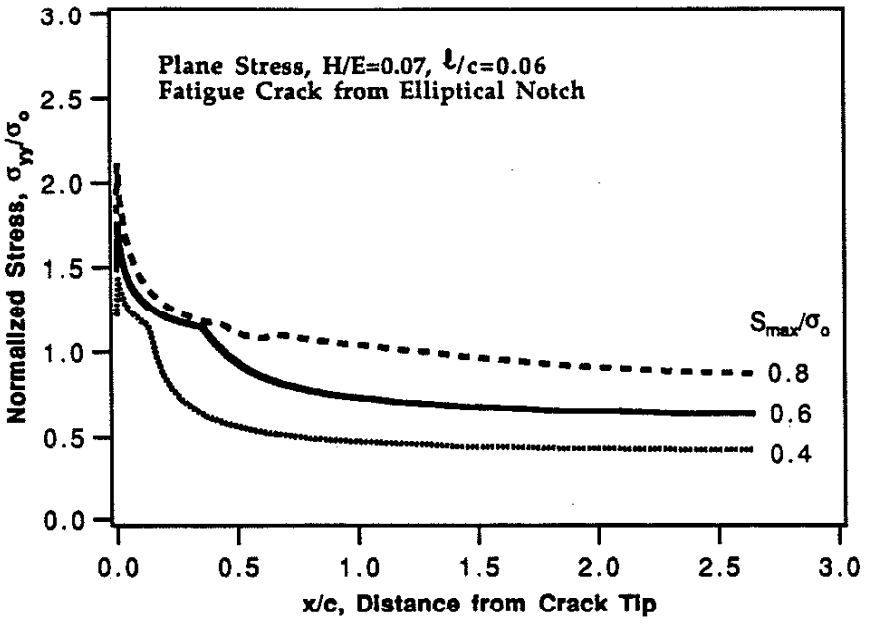

Figure 5.2 Stress distributions ahead of crack tip under different applied load (H/E=0.07, plane stress)

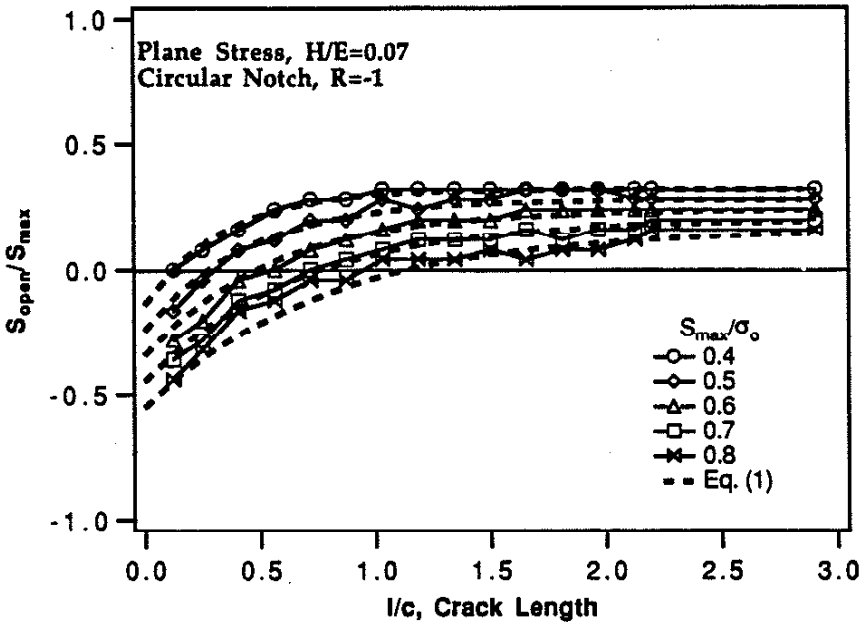

(a)

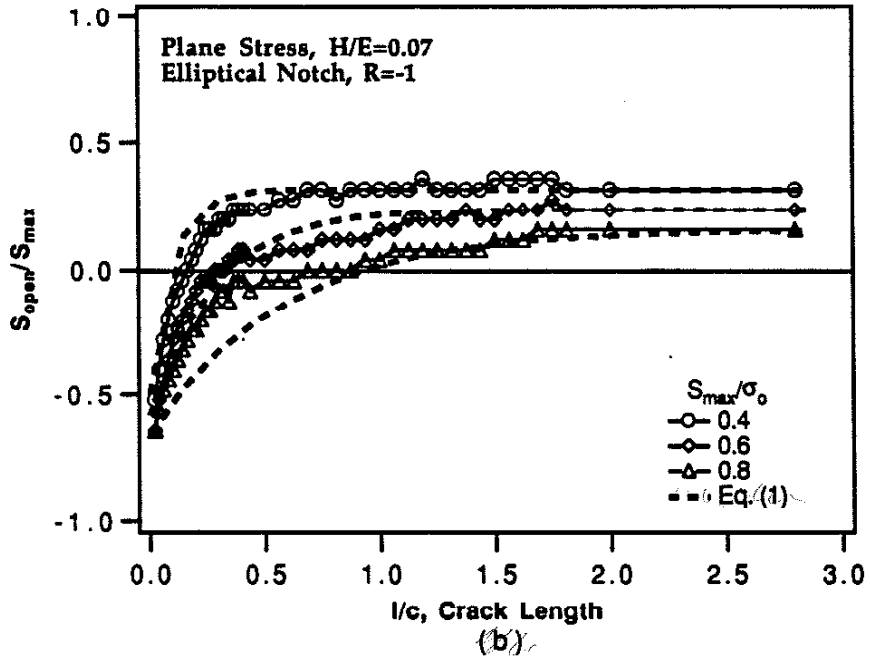

(b)

Figure 5.3. Comparison of crack opening stresses from finite element analysis and from predition model (H/E=0.07, plane stress).

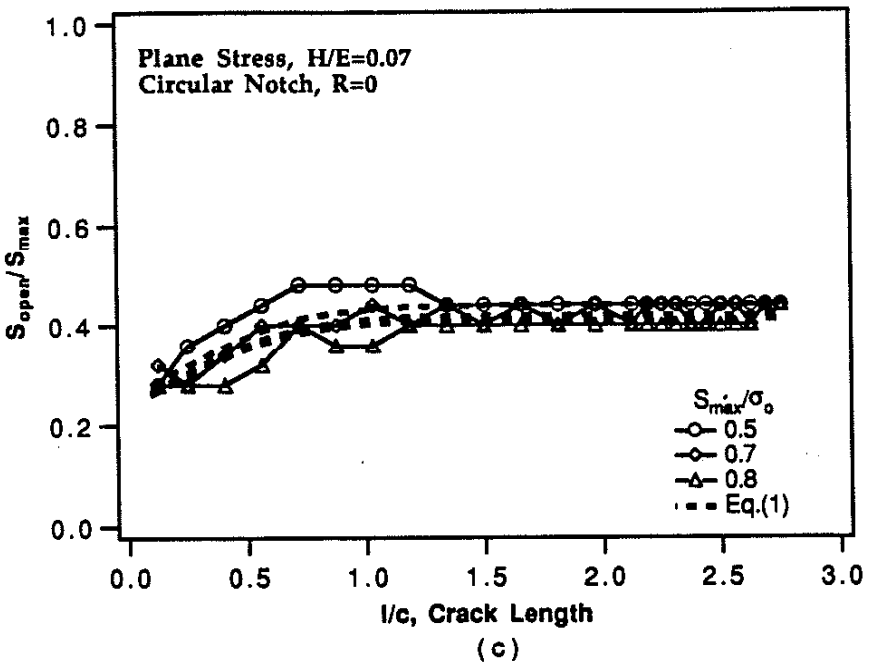

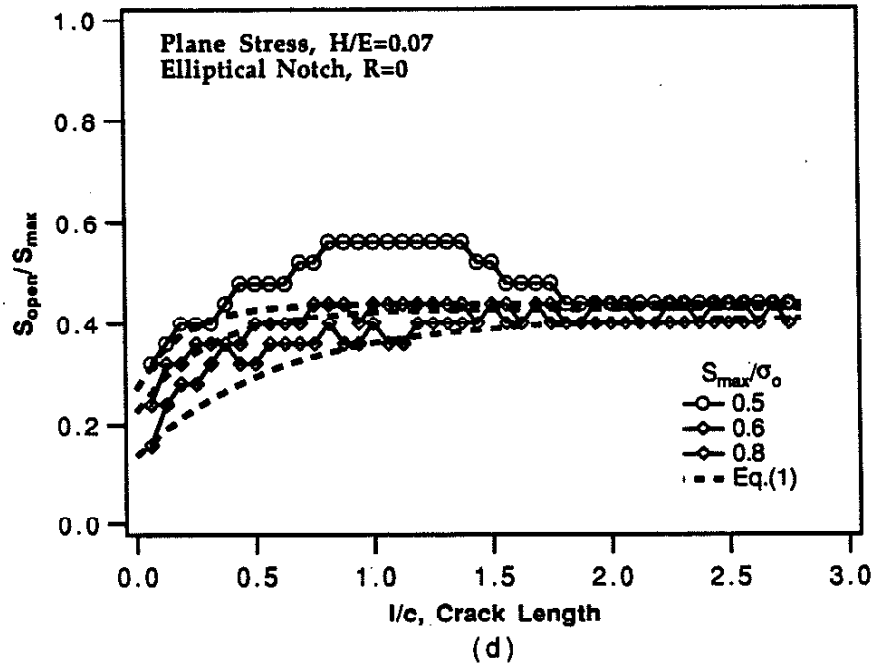

Figure 5.3. Comparison of crack opening stresses from finite element analysis and from prediction model (H/E=0.07, plane stress)

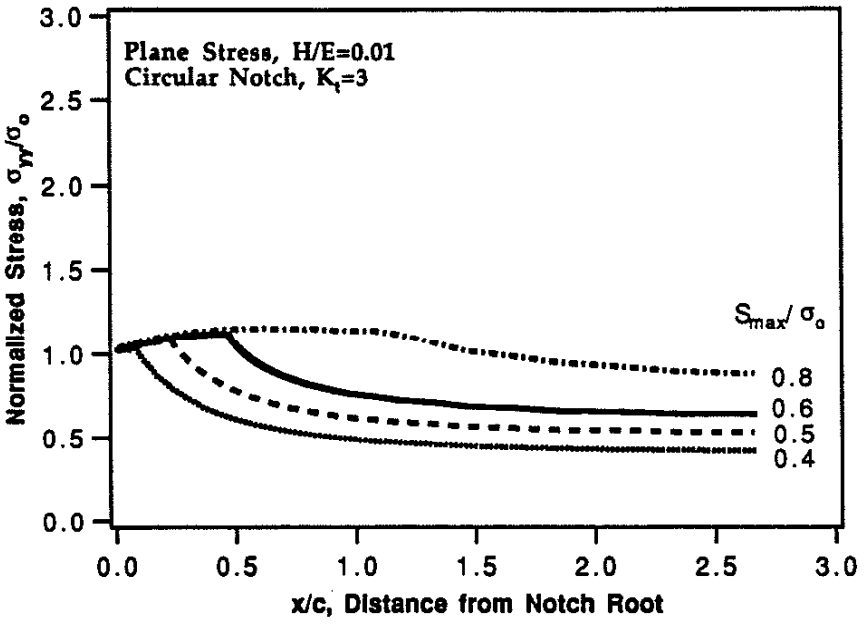

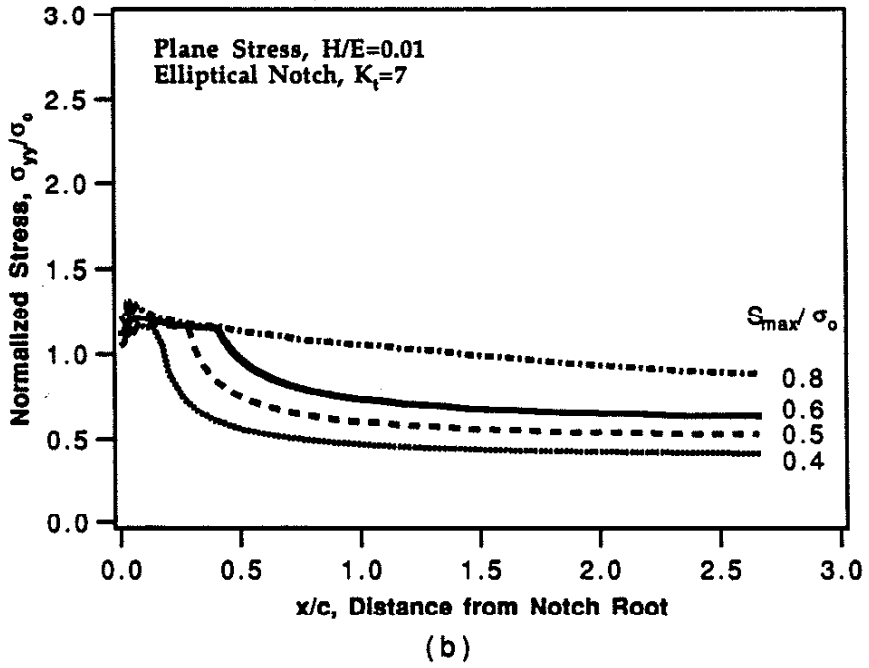

Figure 5.4 Stress distributions ahead of notch root under different applied load (H/E=0.01, plane stress)

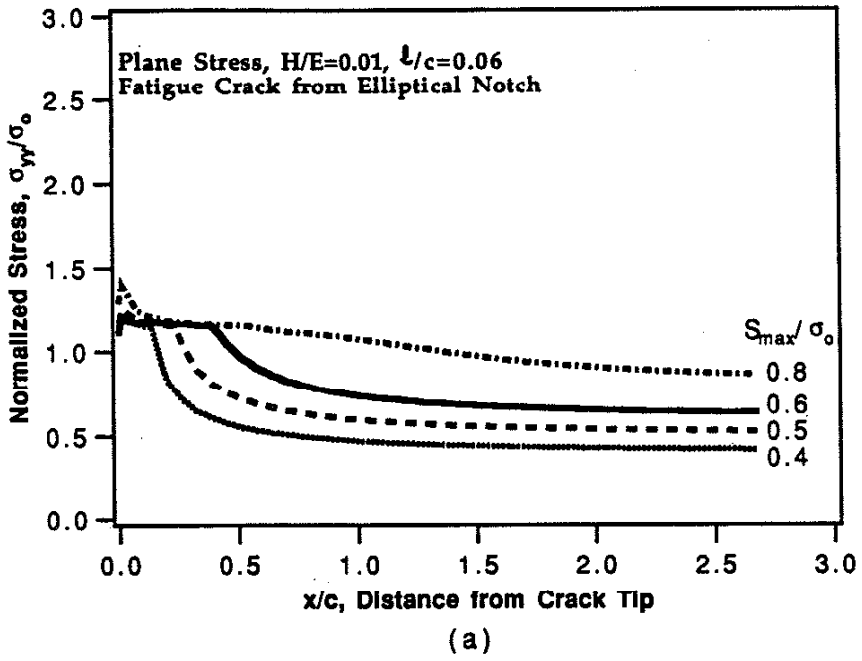

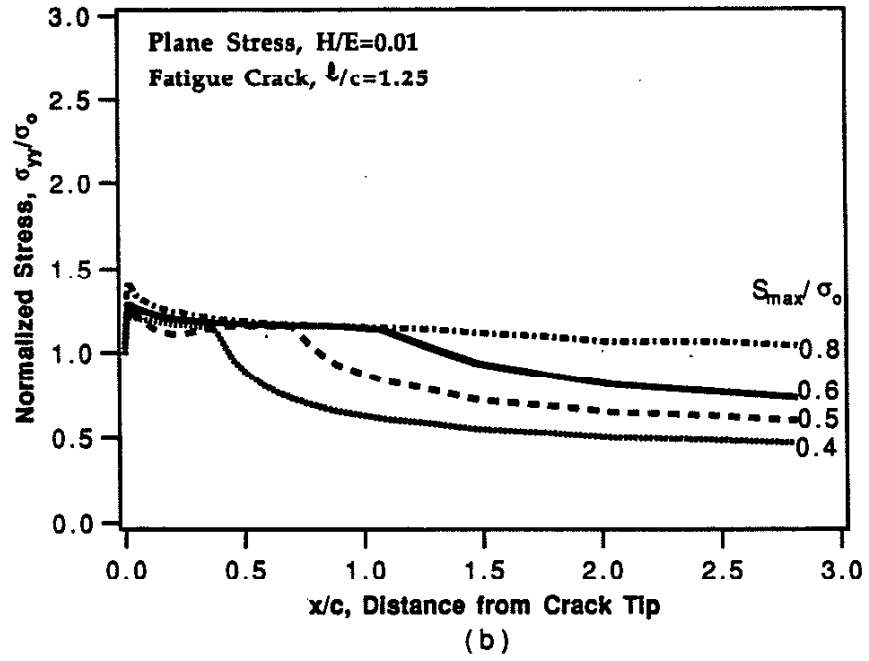

Figure 5.5 Stress distributions ahead of crack tip under different applied load (H/E=0.01, plane stress)

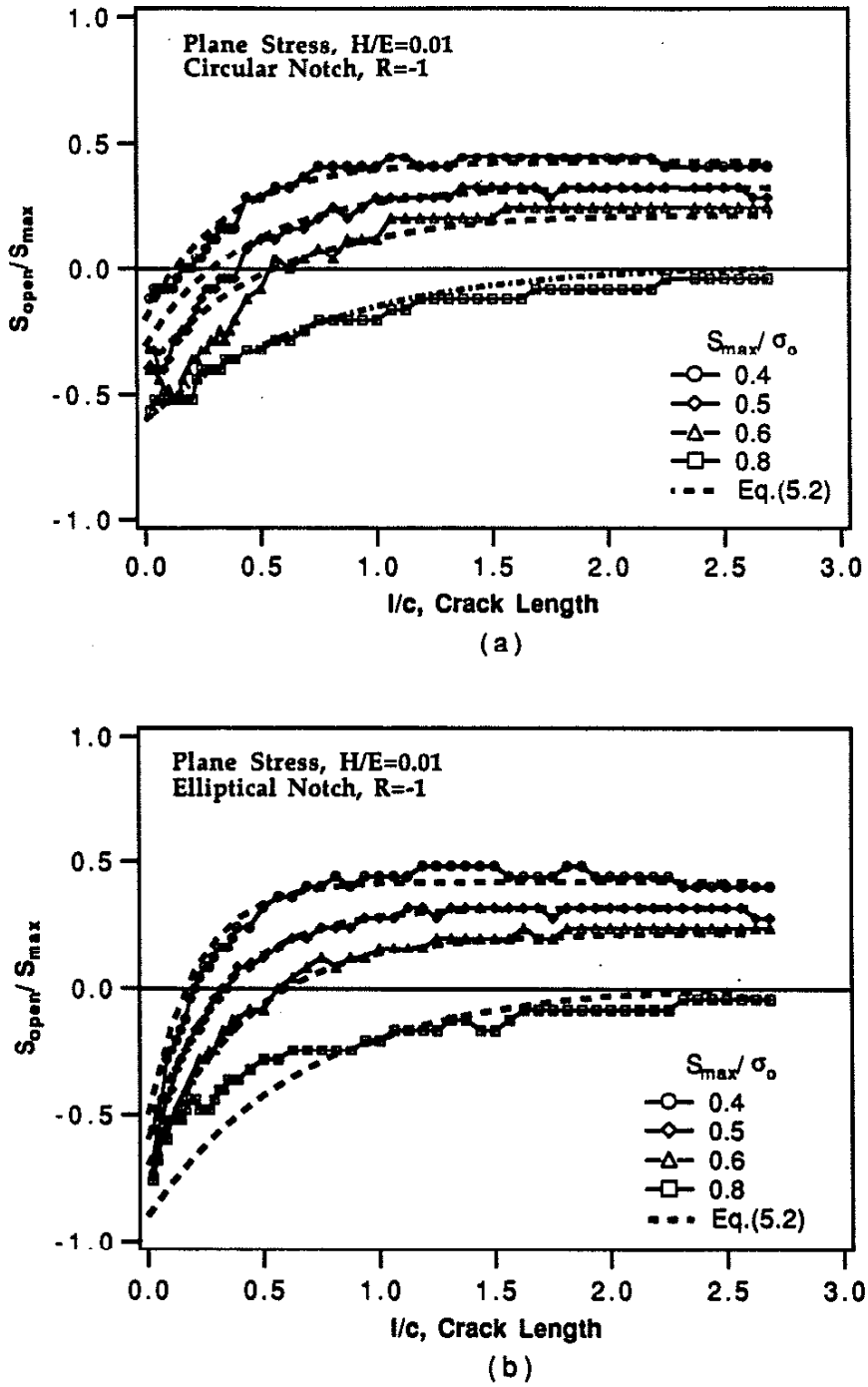

Figure 5.6 Comparison of crack opening stresses from finite element analysis and from prediction model, (H/E=0.01, plane stress, R=-1)

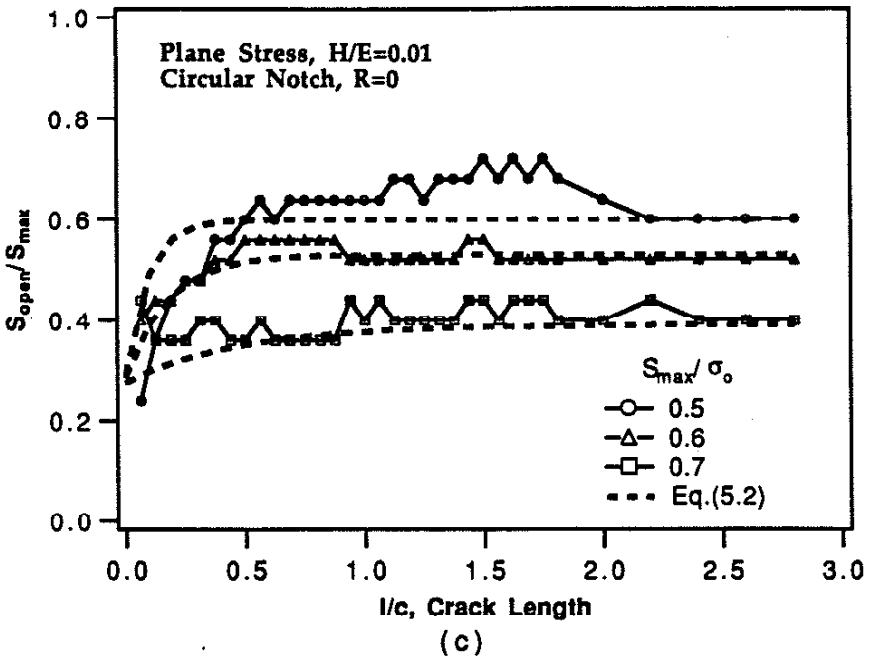

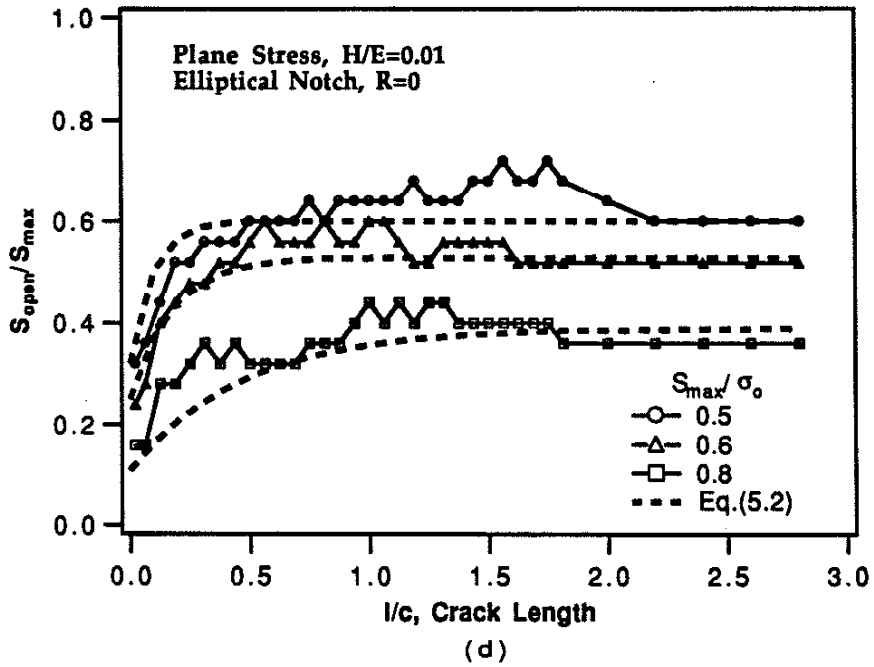

Figure 5.6 Comparison of crack opening stresses from finite element analysis and from prediction model, (H/E=0.01, plane stress, R=0)

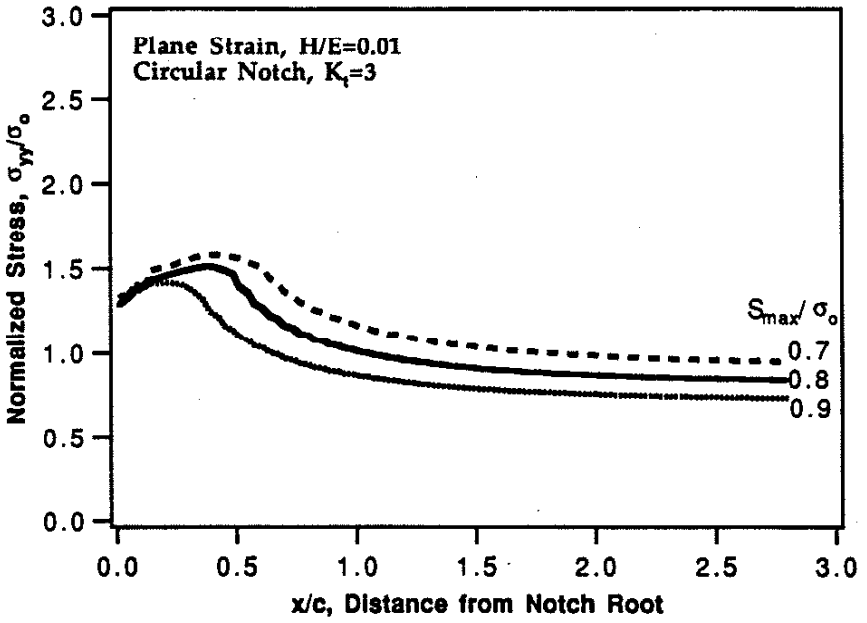

Figure 5.7 Stress distributions ahead of notch roots under different applied load (H/E=0.01, plane strain)

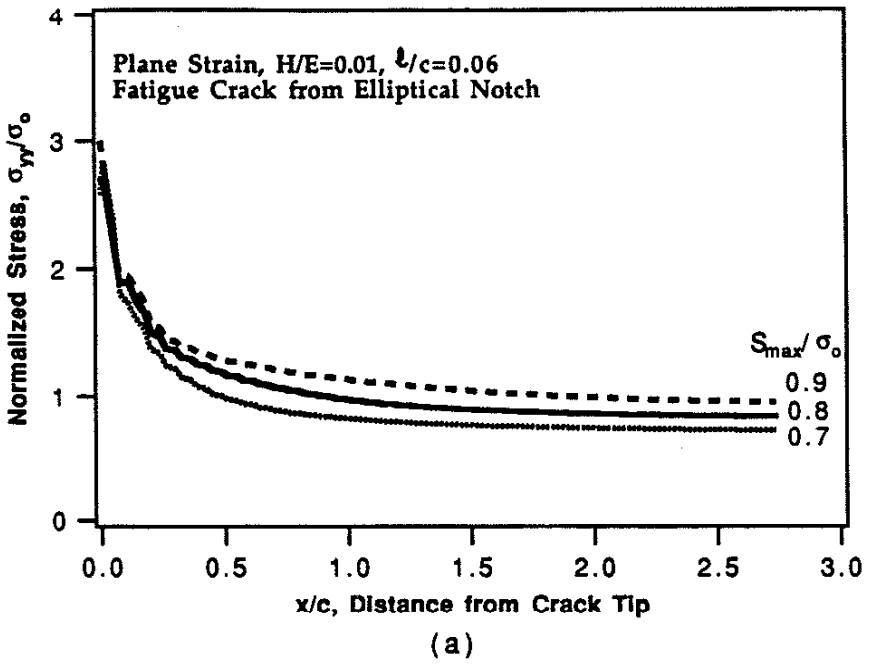

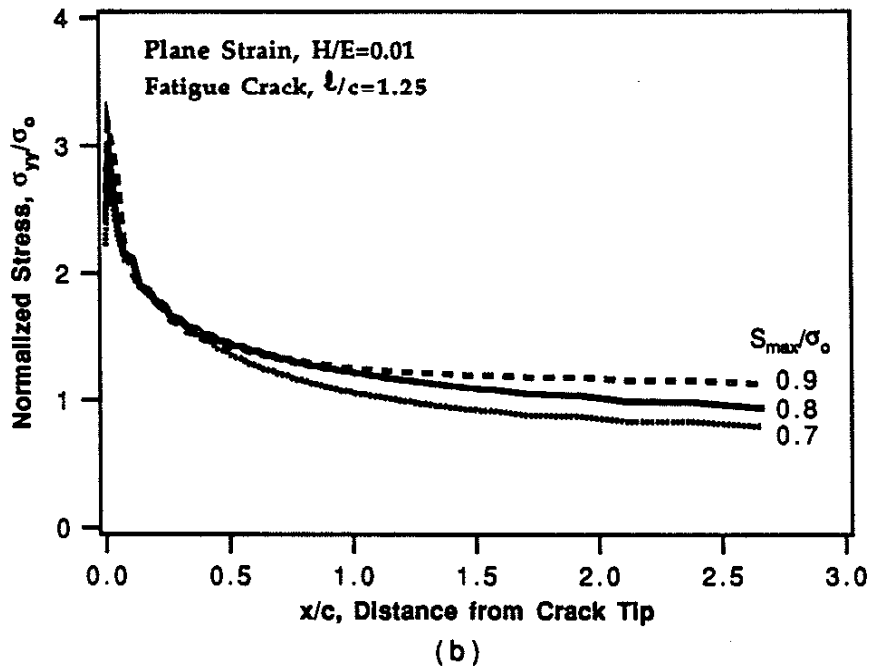

Figure 5.8 Stress distributions ahead of crack tip under different applied load (H/E=0.01, plane strain)

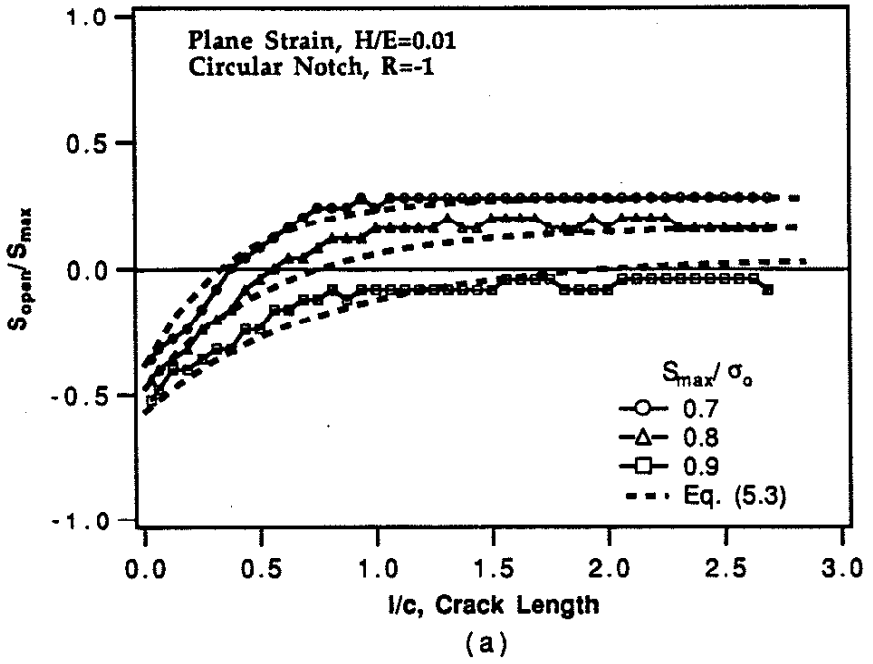

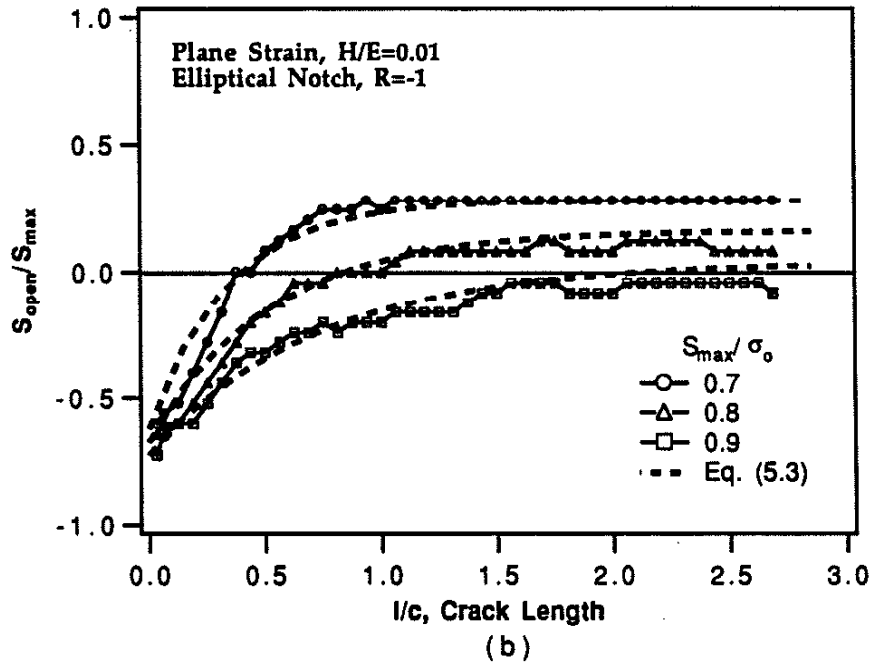

Figure 5.9 Comparison of crack opening stresses from finite sanalysis and from prediction model (H/E=0.01, plane strain)

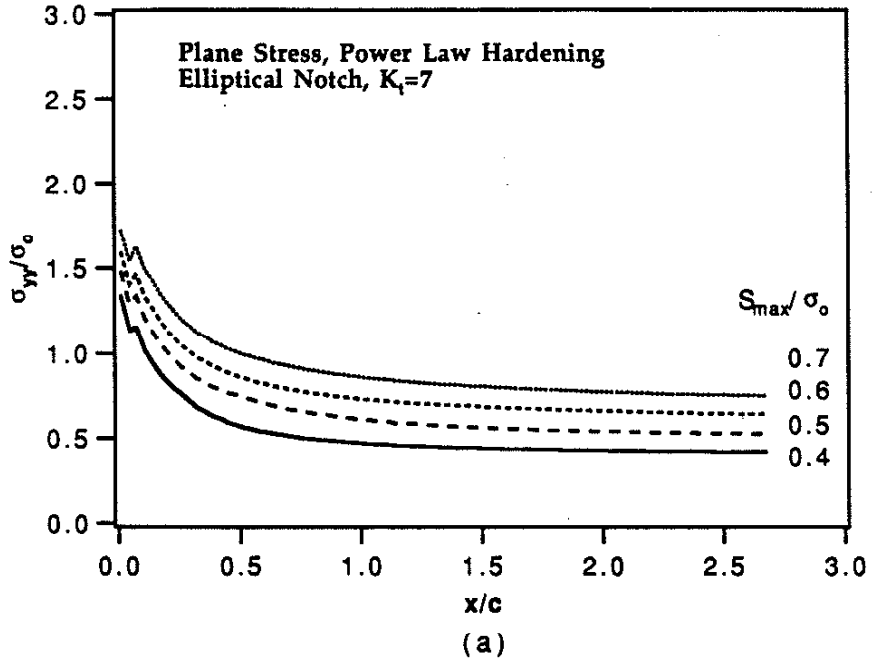

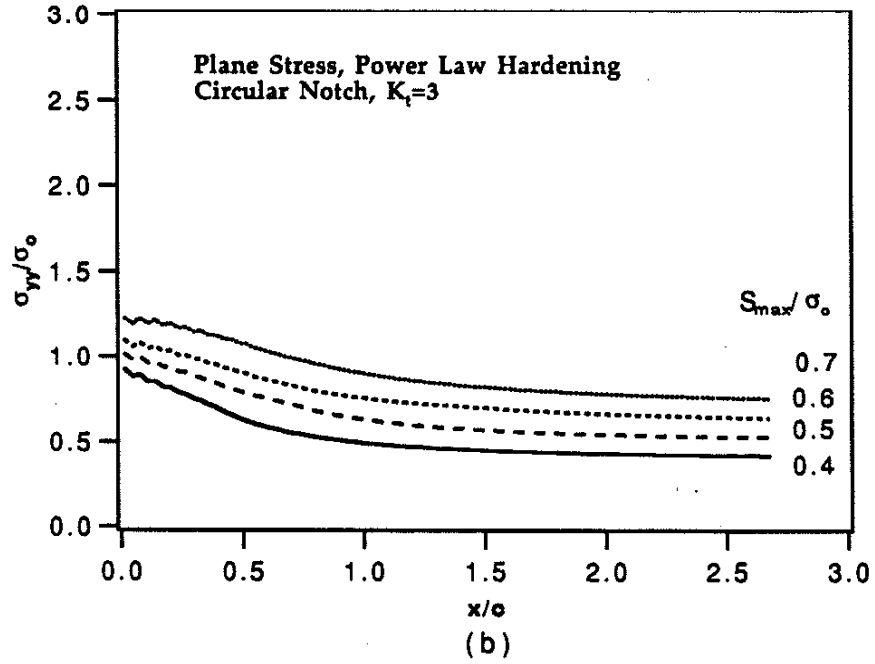

Figure 5.10 Stress distribution ahead of notch roots under different applied load (power law hardening)

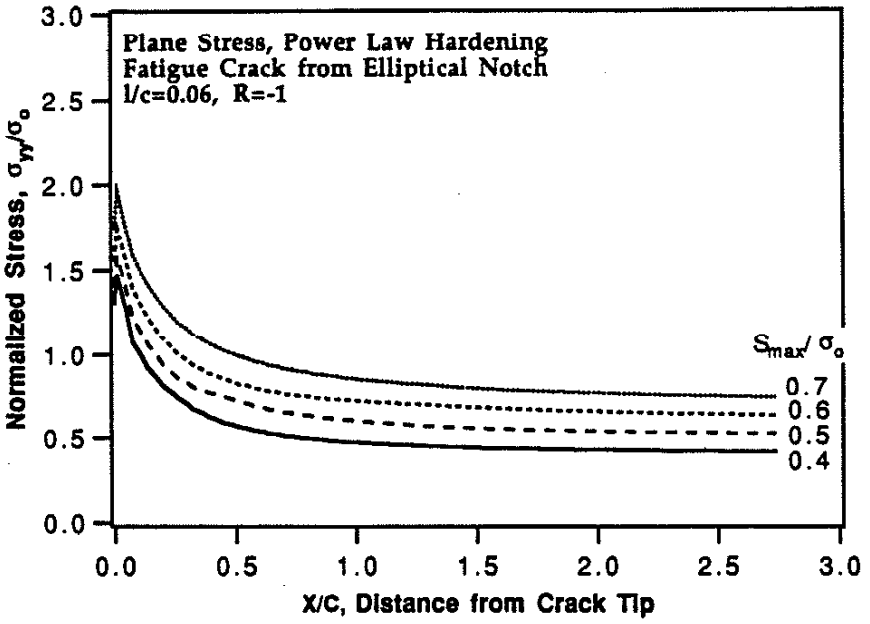

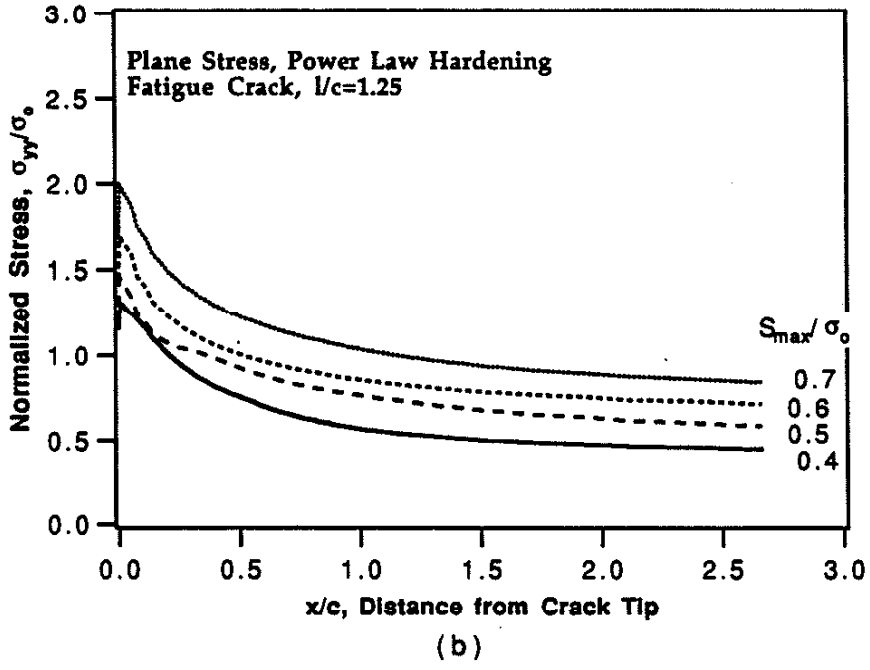

Figure5.11 Stress distribution ahead of fatigue crack tip under different applied load (power law hardening)

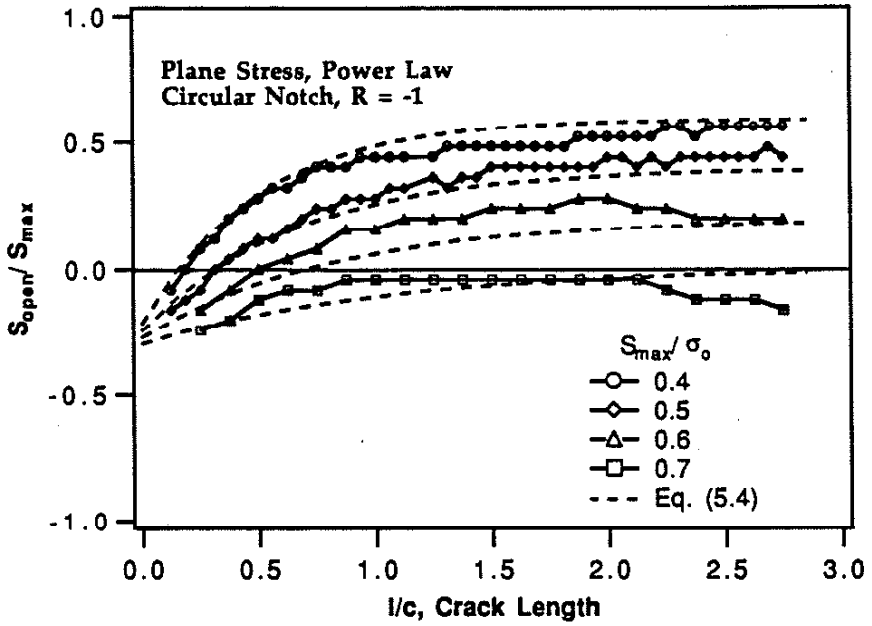

(a)

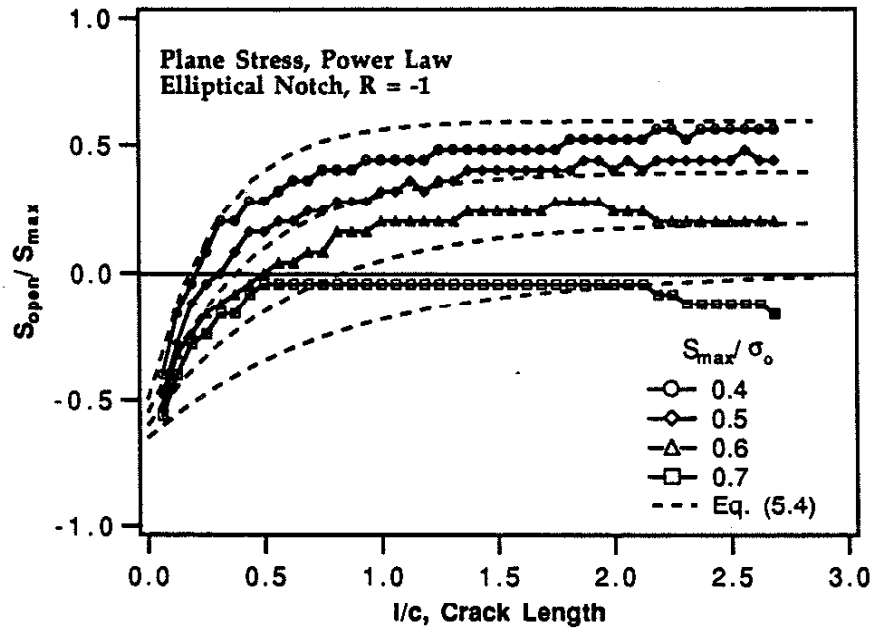

(b)

Figure 5.12 Comparison of crack opening stresses from finite element analysis and from predition model (power law hardening, plane stress, R = -1).

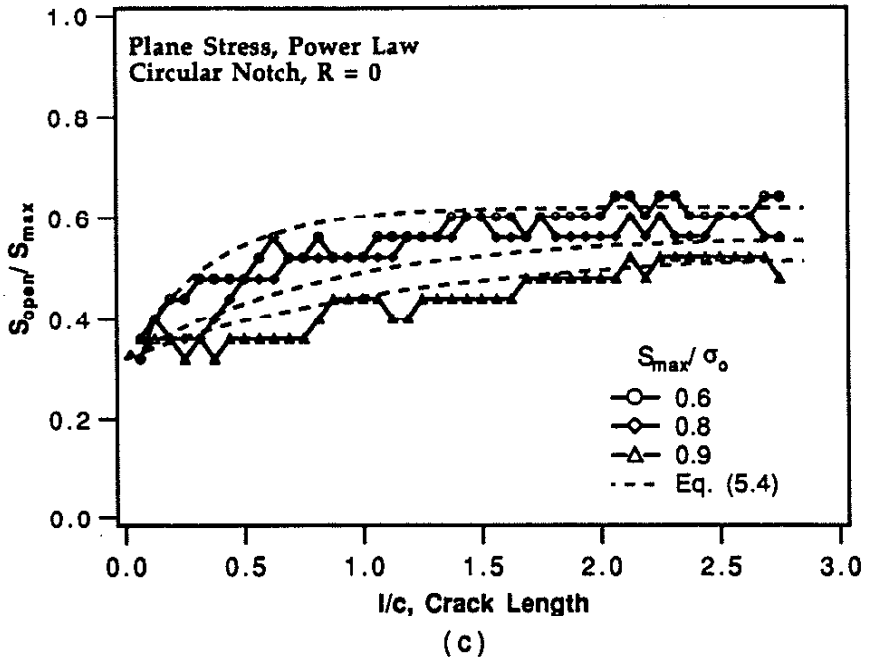

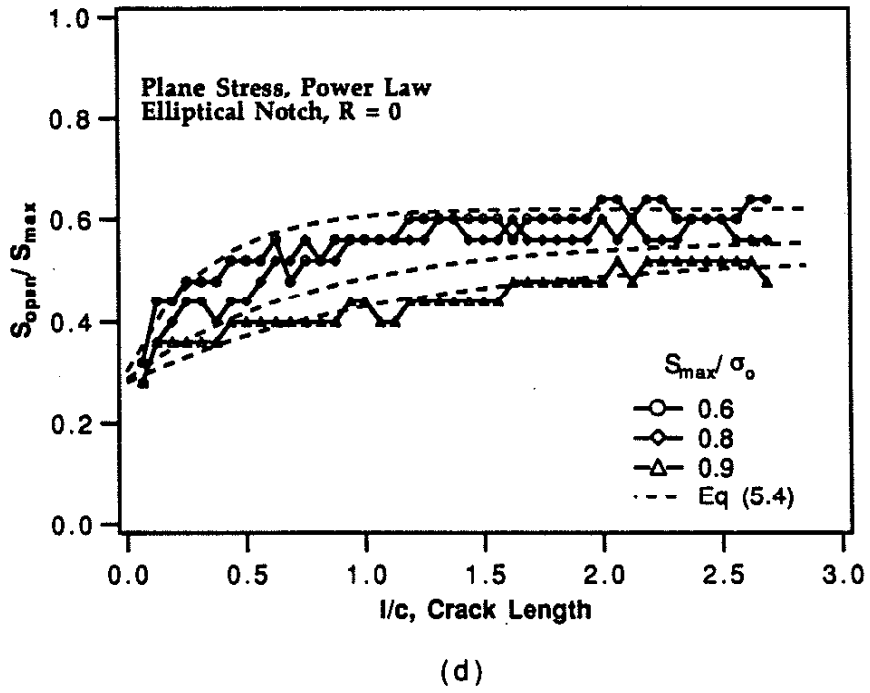

Figure 5.12 Comparison of crac k opening stresses from finite element analysis and from predition model (power law hardening, plane stress, R = 0)

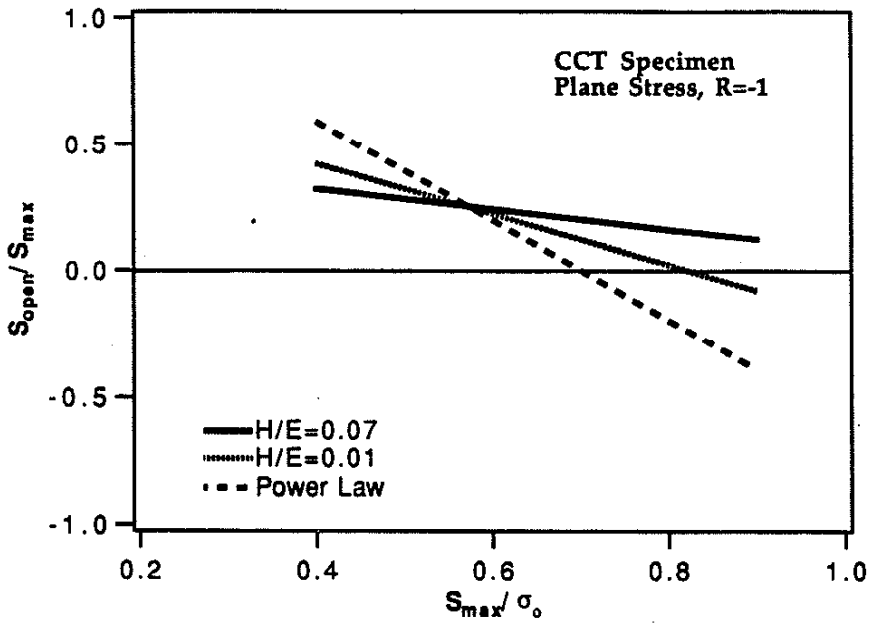

Figure 5.13 Comparison of crack opening stresses for different hardening models under plane stress condition, R=-1.

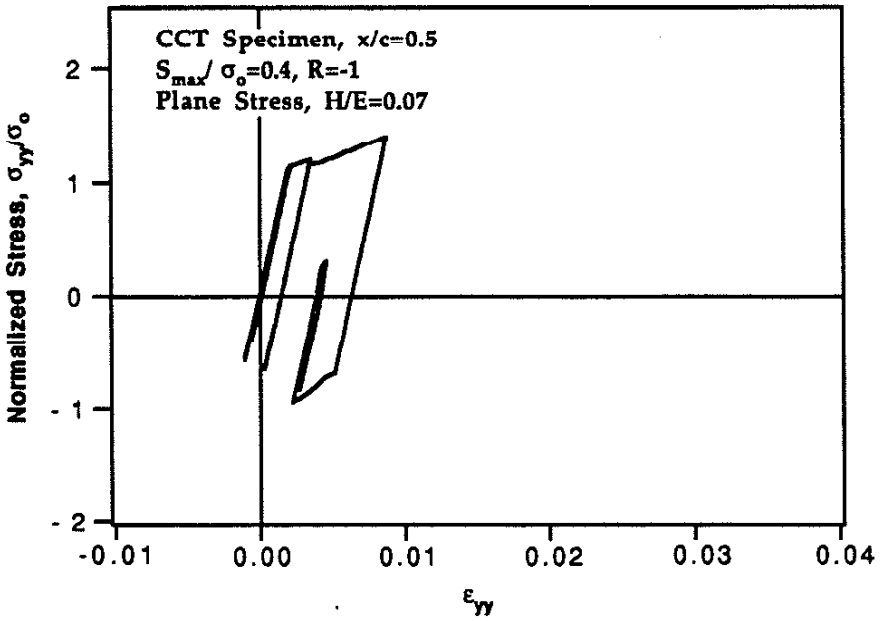

(a)

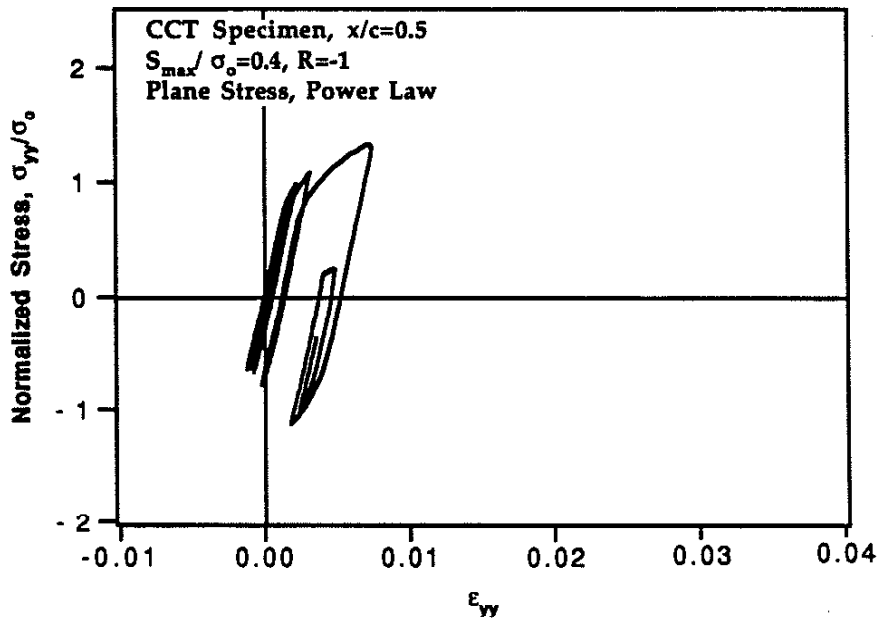

(b)

Figure 5.14 Stress-strain responds for CCT specimen, x/c=0.5, S_{max}/σ_o=0.4

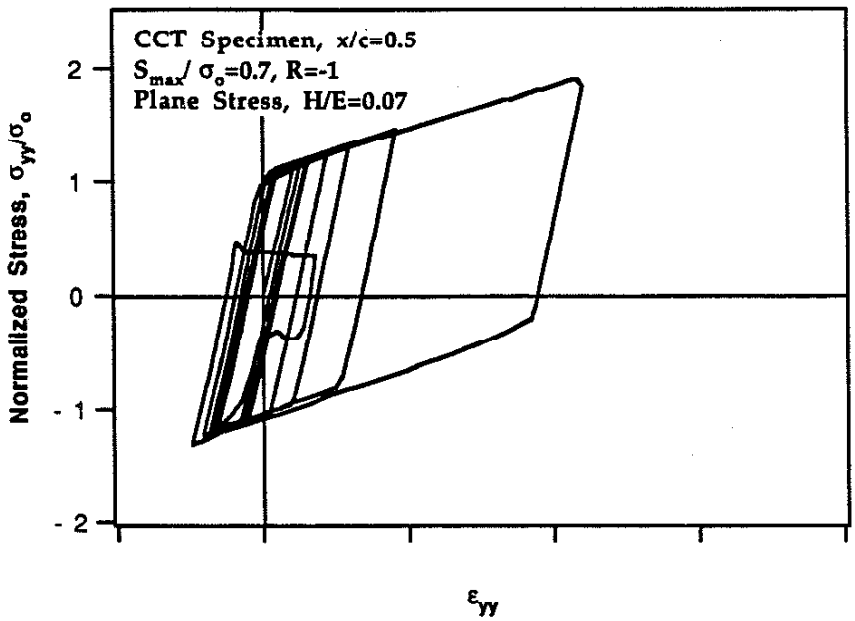

(c)

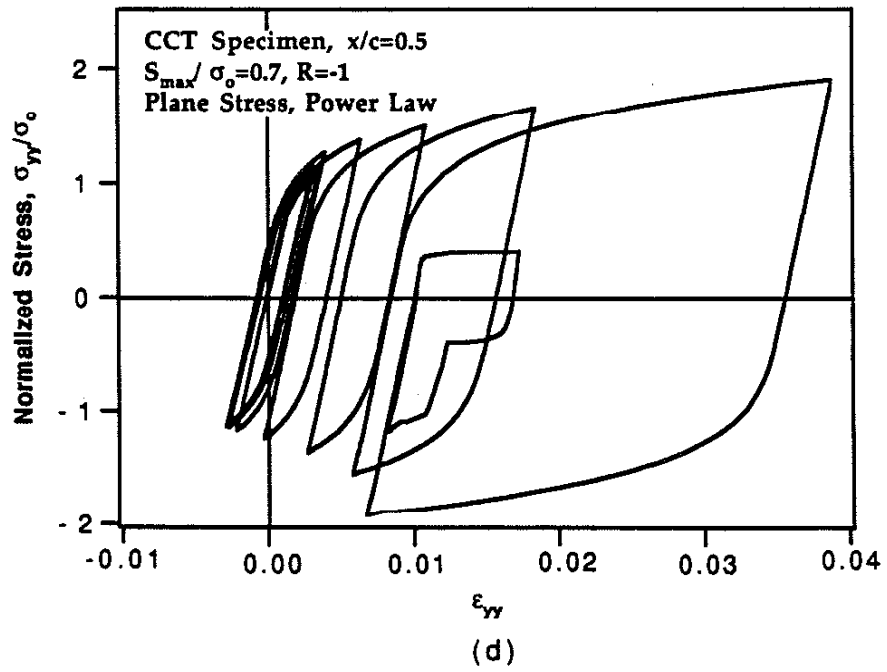

(d)

Figure 5.14. Stress-strain responds at a material point for CCT specimen, x/c=0.5, S_{max}/σ_o=0.7, R=-1

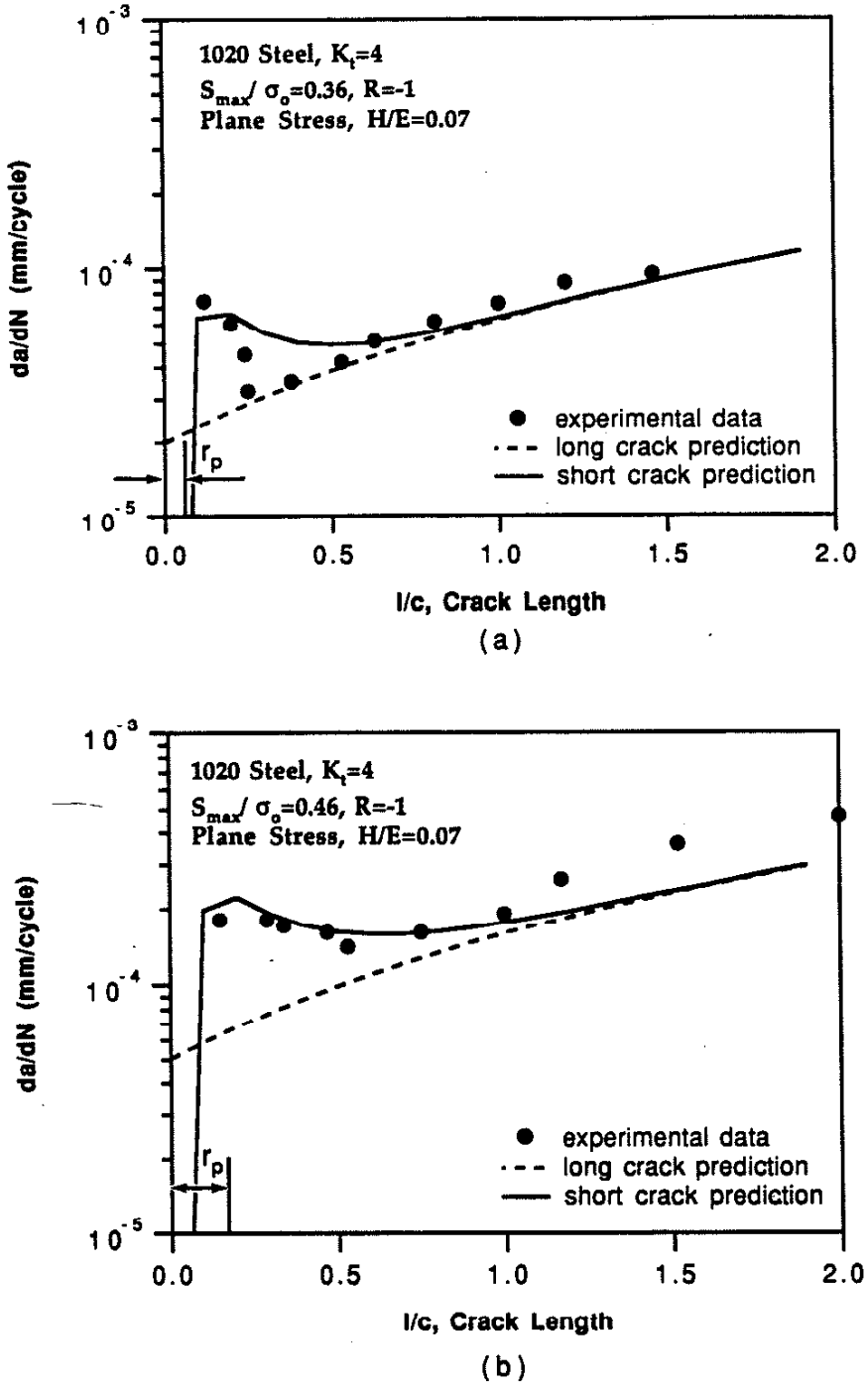

Figure 5.15 Comparison of the prediction and experimental cracks growth rate data for 1020 steel.

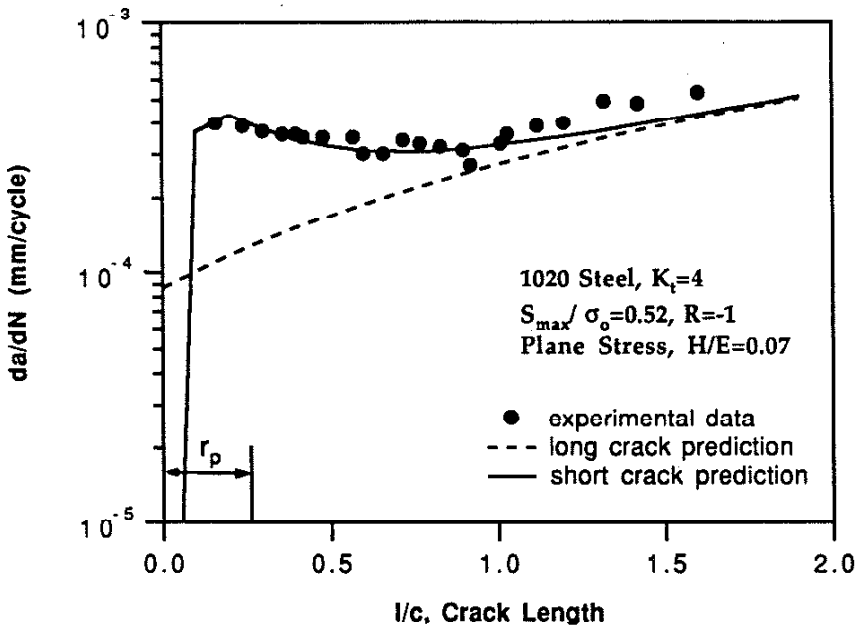

(c)

Figure 5.15 (continued)

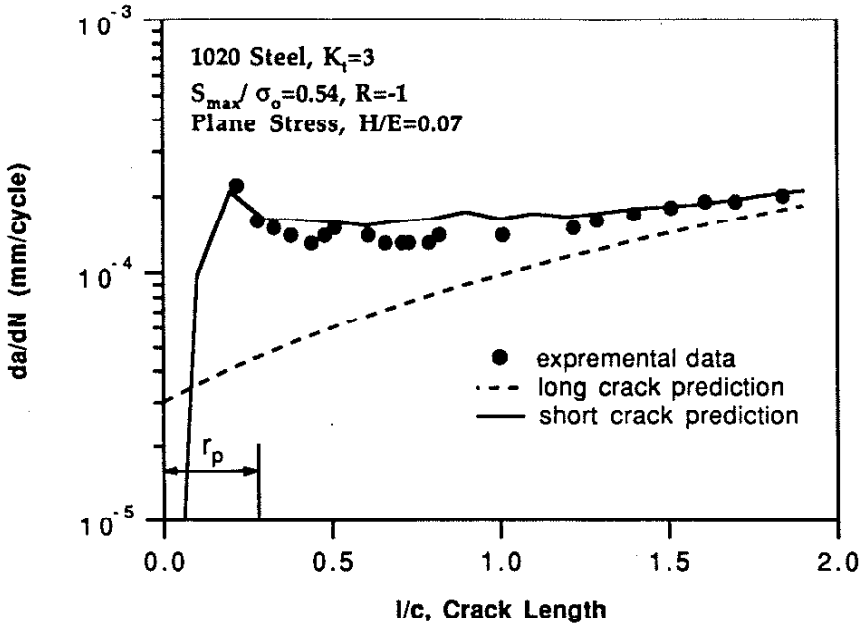

(d)

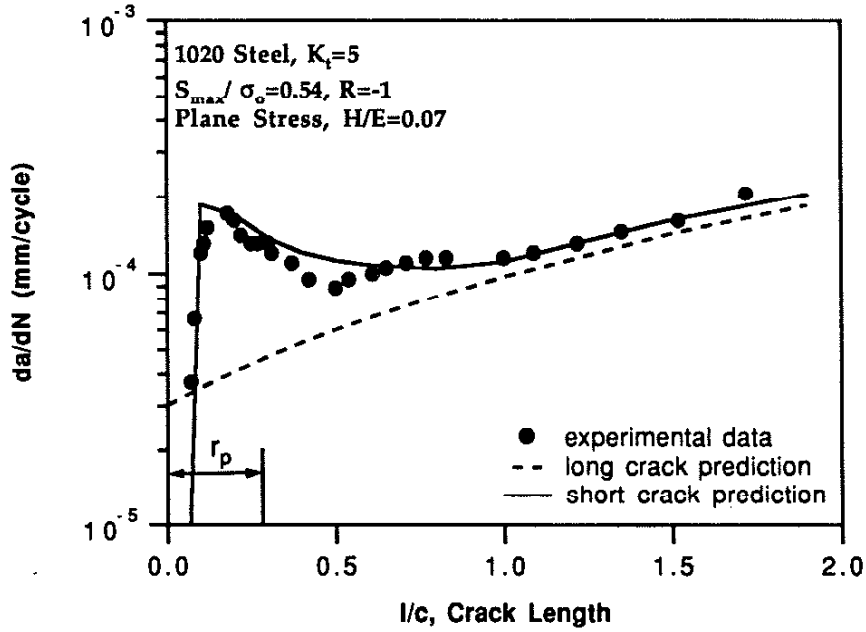

(e)

Figure 5.15 (continued)

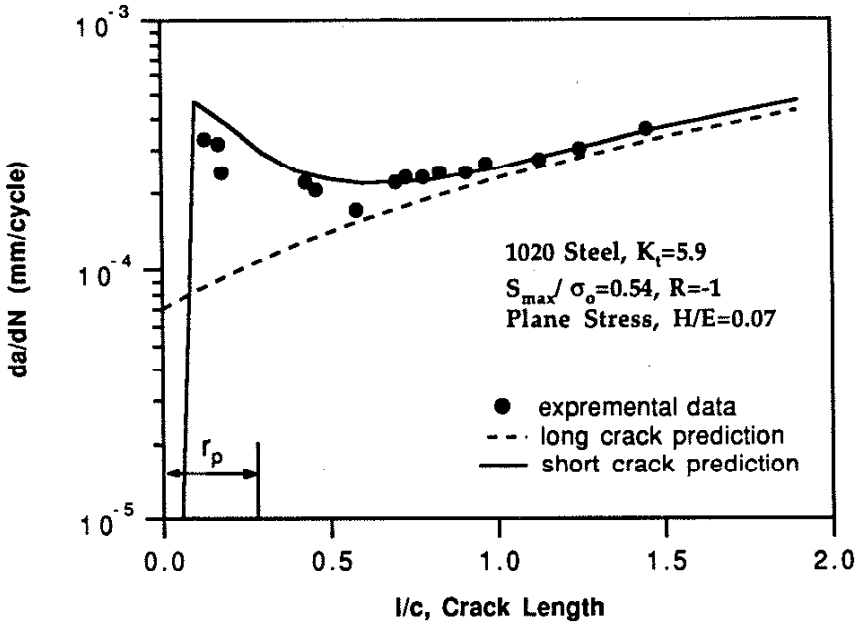

(f)

Figure 5.15 (continued)

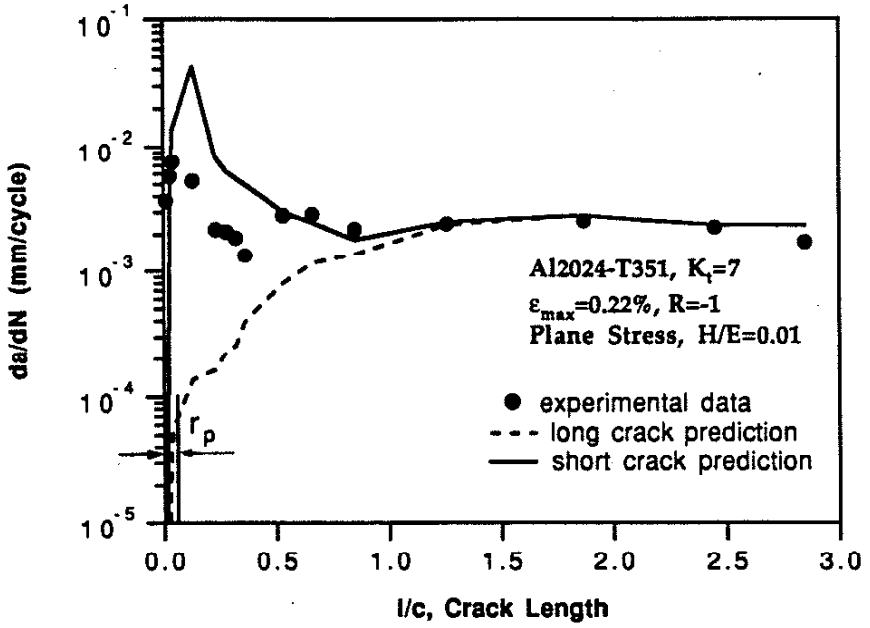

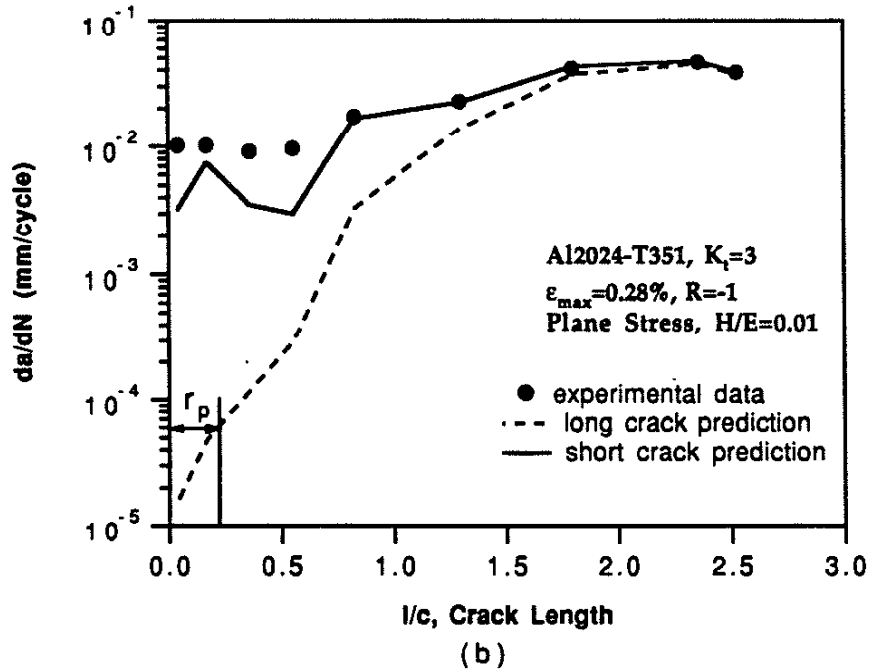

Figure 5.16 Comparison of the prediction and experimental crack growth rate data for 2024-T351 Aluminum.

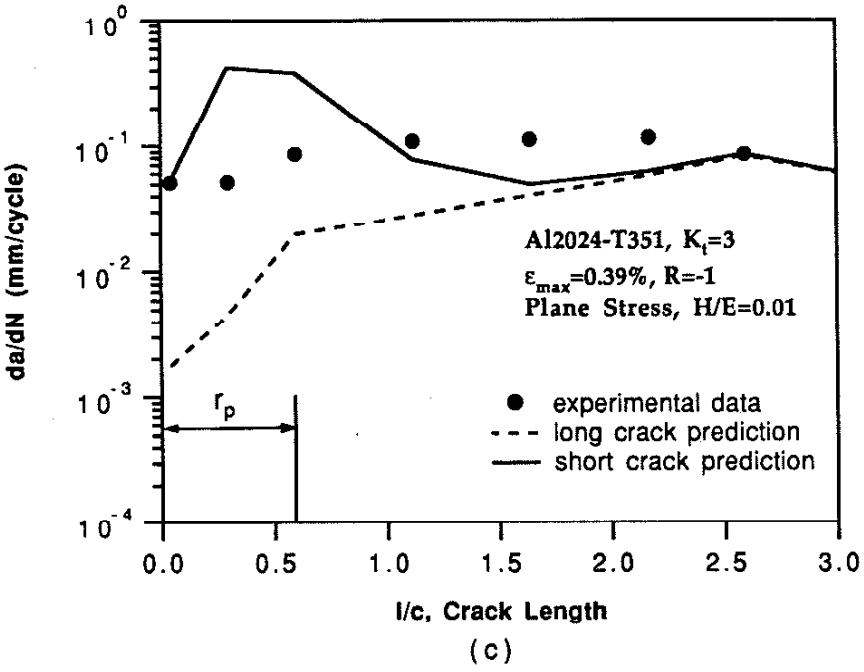

(c)

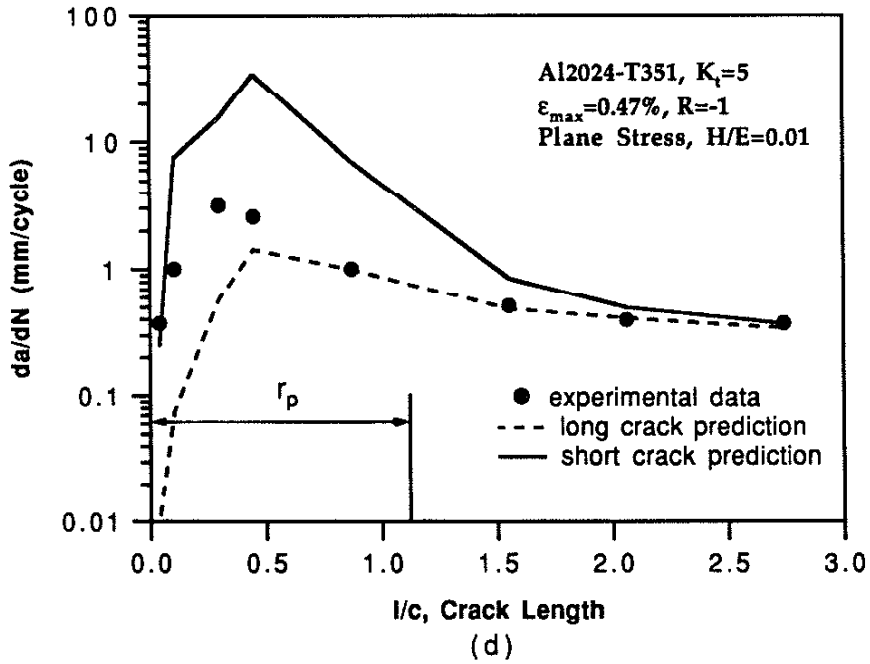

(d)

Figure 5.16 (continued)

References

1. Elber, W., "Fatigue Crack Propagation," Ph.D. Thesis, University of New South Wales, Australia, 1968.

2. Elber, W., "Fatigue Crack Closure under Cyclic Tension," *Engineering Fracture Mechanics*, Vol.2, 1970, pp. 37-45.

3. Elber, W., "The Significance of Fatigue Crack Closure," *Damage Tolerance in Aircraft Structures*, ASTM STP 486, 1971, pp. 230-242.

4. McEvily, A. J., 'On Crack Closure in Fatigue Crack Growth', *Mechanics of Fatigue Crack Closure*, ASTM STP 982, 1988, pp. 35-43.

5. Liaw, P. K., 'Overview of Crack Closure at Near-Threshold Fatigue Crack Growth Levels', *Mechanics of Fatigue Crack Closure*, ASTM STP 982, 1988, pp. 62-92.

6. Davidson, D. L., 'Fatigue Crack Closure', *Engineering Fracture Mechanics*, Vol. 38, No. 6, 1991, pp. 393-402.

7. Socie, D. F., 'Predict of Fatigue Crack Growth in Notched Members under Variable Amplitude Loading Histories', *Engineering Fracture Mechanics*, Vol. 9, 1977, pp. 849-865.

8. Lalor, P., H. Sehitoglu and R. C. McClung, 'Mechanics Aspects of Small Crack Growth from Notches ——— The Role of Crack Closure', *The Behavior of Short Fatigue Cracks*, EFG Pub. 1, Mechanical Engineering Publications, London, 1986, pp. 369-386.

9. McClung, R. C. and H. Sehitoglu, 'Closure Behavior of Small Cracks under High Strain Fatigue Histories', *Mechanics of Fatigue Crack Closure, ASTM STP 982*, 1988, pp. 279-299.

10. Newman, J. C. Jr., M. H. Swain and E. P. Phillips, 'An Assessment of the Small-Crack Effect for 2024-T3 Aluminum Alloy', *Small Fatigue Cracks*, Proceedings of the Second Engineering Foundation International Conference/Workshop, Santa Barbara, California, January 5-10, 1986, pp. 427-452.

11. Newman, J. C. Jr, E. P. Phillips, and M. H. Swain, 'Predicting the Growth of Small and Large Cracks Using a Crack-Closure Model', *Mechanical*

Behavior of Materials --- V, Proceedings of the Fifth International Conference, Beijing, China, pp. 51-60.

12. Bachmann, V. and D. Munz, 'Fatigue Crack Closure Evaluation with the Potential Method', *Engineering Fracture Mechanics*, Vol. 11, 1979, pp. 61-71.

13. McGowan, J. J. and H. W. Liu, 'The Role of Three-Dimensional Effects in Constant Amplitude Fatigue Crack Growth Testing', *Journal of Engineering Materials and Thechnology*, Vol. 102, 1980, pp. 341-346.

14. Kumar, R and S. B. L. Garg, 'Influence of Stress Ratio and Material Properties on Effective Stress Range Ratio and Crack Growth', *Engineering Fracture Mechanics*, Vol. 32, No. 2, 1989, pp. 195-202.

15. McEvily, A. J. and Z. Yang, 'The Nature of the Two Opening Levels Following an Overload in Fatigue Crack Growth', *Metallurgical Transactions*, Vol. 21A, 1990, pp. 2717-2727.

16. Fleck, N., 'Plane Strain Crack Closure', Ph. D. Thesis, University of Cambridge, England, 1984.

17. Ewalds, H. L. and R. T. Furnee, 'Crack Closure Measurement Along the Fatigue Crack Front of Center Cracked Specimens', *International Journal of Fracture*, Vol. 14, 1978, pp. R53-R55.

18. Mahulikar, D. S. , W. P. Slagle, and H. L. Marcus, 'Edge Effects on Fatigue Crack Closure of Aluminum Alloys', *Scripta Matallurgica*, Vol. 13, 1979, pp. 867-880.

19. Blom, A. F. and D. K. Holm, 'An Experimental and Numerical Study of Crack Closure', *Engineering Fracture Mechanics*, Vol. 22, No. 6, 1985, pp. 997-1011.

20. Ogura, K., Y. Miyoshi, and I. Nishikawa, "Fatigue Crack Growth and Closure of Small Cracks at the Notch Root," *Current Research on Fatigue Cracks*, MRS Vol. 1, Society of Materials Science, Japan, 1985, pp. 67-91.

21. Davidson, D. L., 'Plasticity Induced Fatigue Crack Closure', *Mechanics of Fatigue Crack Closure, ASTM STP 982*, American Society for Testing and Materials, 1988, pp. 44-61.

22. Sharpe, W. N. and X. Su, 'Closure Measurements of Natureally Initiating Small Cracks', *Engineering Fracure Mechanics*, Vol. 30, No. 3, 1988, pp. 275-294.

23. Nisitani, H. and K. Takao, 'Significance of Initiation Propagation and Closure of Microcracks in High Cycle Fatigue of Ductile Metals', *Engineering Fracture Mechanics*, Vol. 15, No. 3-4, 1981, pp. 445-446.

24. Sehitoglu, H., 'Crack Opening and Closure in Fatigue', *Engineering Fracture Mechanics*, Vol. 21, No. 2, 1985, pp. 329-339.

25. Allison, J. E., R. C. Ku, and M. A. Pompetzki, 'A Comparison of Measurement Methods and Numerical Procedures for the Experimental Characterization of Fatigue Crack Closure', *Mechanics of Fatigue Crack Closure, ASTM STP 982*, 1988, pp. 171-185.

26. Vazquez, J. A., A. Morrone, and H. Ernst, 'Experimental Results on Fatigue Crack Closure for Two Aluminum Alloys', *Engineering Fracture Mechanics*, Vol. 12, 1979, pp. 231-140.

27. Vazquez, J. A., A. Morrone, and J. C. Gasco, 'A comparative Experimental Study on the Fatigue Crack Closure Behavior Under Cyclic Loading for Steels and Aluminum Alloys', *Fracture Mechanics, ASTM STP 677*, 1979, pp. 187-197.

28. Larsen, J. M., 'The Effects of Slip Character and Crack Closure on the Growth of Small Fatigue Cracks in Titanium-Alluminum Alloys', Ph.D. Thesis, Air Force Wright Aeronautical Laboratories (AFSC), 1988.

29. Lalor, P., and H. Sehitoglu, "Crack Closure Outside Small Scale Yielding Regime," *American Society for Testing and Materials,* STP 982, 342-360, 1988.

30. Lalor, P., 'Mechanics Aspects of Crack Closure', M. S. Thesis, University of Illinois at Urbana-Champaign, 1986.

31. McClung, R. C., and H. Sehitoglu, "Finite Element Analysis of Fatigue Crack Closure 1. Basic Modelling Issues," *Engineering Fracture Mechanics*, Vol. 33, No. 2, pp. 237-252, 1989.

32. McClung, R. C., and H. Sehitoglu, "Finite Element Analysis of Fatigue Crack Closure 2. Numerical Results," *Engineering Fracture Mechanics*, Vol. 33, No. 2, pp. 253-272, 1989.

33. McClung, R. C., 'Fatigue Crack Closure and Crack Growth Outside the Small Scale Yielding Regime', Ph. D. Thesis, University of Illinois at Urbana-Champaign.

34. Fleck, N., 'Finite Element Analysis of Plasticity Induced Crack Closure under Plane Strain Conditions', *Engineering Fracture Mechanics*, Vol. 25, 1986, pp. 441-449.

35. Chermahini, R. G., 'Three Dimensional Finite Element Analysis of Fatigue Crack Growth and Closure', Ph. D. Thesis, Old Donimion University, Norfolk, VA, 1986.

36. Llorca, J. and V. S. Galvez, 'Modelling Plasticity-Induced Fatigue Crack Closure', *Engineering Fracture Mechanics*, Vol. 37, No. 1, 1990, pp. 185-196.

37. Nakagaki, M. and S. N. Atluri, 'Fatigue Crack Closure and Delay Effects Under Mode I Spectrum Loading: An Efficient Elastic-Plastic Analysis Procedure', *Fatigue of Engineering Materials and Structures*, Vol. 1, 1979, pp. 421-429.

38. Newman, J. C. Jr., 'A Finite-Element Analysis of Fatigue Crack Closure', *Mechanics of Crack Growth, ASTM STP 590*, 1976, pp. 281-301.

39. Shiratori, M., T. Miyoshi, H. Miyamoto and T. Mori, 'A Computer Simulation of Fatigue Crack Propagation Based on the Crack Closure Concept', *Advances in Research on the Strength and Fracture of Materials*, Fourth International Conference on Fracture, June, 1977, Waterloo, Canada, Vol. 2B, pp. 1091-1098.

40. Fuhring, H. and T. Seeger, 'Dugdale Crack Closure Analysis of Fatigue Cracks Under Constant Amplitude Loading', *Engineering Fracture Mechanics*, Vol. 11, 1979, pp. 99-122.

41. Ibrahim, F. K., J. C. Thompson and T. H. Topper, 'A Study of the Effect of Mechanical Variables on Fatigue Crack Closure and Propagation', *International Journal of Fatigue*, Vol. 8, No. 3, 1986, pp. 135-142.

42. Budiansky, B. and J.Hutchinson, 'Analysis of Closure in Fatigue Crack Growth', *Journal of Applied Mechanics*, Transaction of ASME, Vol. 45, 1978, pp.267-276.

43. Newman, J. C. Jr., and H. Armen, Jr., 'Elastic-Plastic Analysis of Propagating Crack Under Cyclic Loading', *AIAA Journal*, Vol. 13, No. 8, 1975, pp. 1017-1023.

44. Kumar, V., M. D. German and C. F. Shih, 'An Engineering Approach for Elastic-Plastic Fracture Analysis', Topical Report of General Electric Company, NP-1931, Research Project 1237-1, 1981.

45. Nagtegaal, J. C., D. M. Parks and J. R. Rice, 'On Numerically Accurate Finite Element solution in the Fully Plastic Range', *Computer Methods in Applied Mechanics and Engineering*, Vol. 4, 1974, pp. 153-177.

46. McClung, R. C. and D. L. Davidson, 'High Resolution Numerical and Experimental Studies of Fatigue Cracks', *Engineering Fatigue Mechanics*, 1990.

47. Fleck, N. and Newman, J. C. Jr., 'Analysis of Crack Closure under Plane Strain Conditions', *Mechanism of Fatigue Crack Closure*, ASTM STP982, 1988, pp. 319-341.

48. Ritchie, R. O., W. Yu, A. F. Blom and D. K. Holm, Response to a Discussion by A. J. McEvily, *Fatigue of Engineering Materials and Structures*, Vol. 12, No. 1, 1989, pp. 73-75.

49. Sehitoglu, H. and W. Sun, "Mechanisms of Crack Closure in Plane Strain and Plane Stress," Fatigue under *Biaxial/Multiaxial*, ESIS10 (Edited by K. Kussmail), Mechanical Engineering Publications, London, 1991.

50. Sun, W., 'Mechanisms of Crack Closure ——— Creep and Constraint Effects', M. S. Thesis, University of Illinois at Urbana-Champaign, 1989.

51. Buck, O., 'Recent Advances in Fracture Mechanics Testing', Proceeding of ASM Materials Science Seminar: *Fracture Mechanics: Microstructures and Micromechanisms*, 1989.

52. McClung, R. C., 'The Influence of Applied Stress, Crack Length, and Stress Intensity Factor on Crack Closure', to be published, 1991.

53. Staal, H. U., and J. D. Elen, 'Crack Closure and Influence of Cycle Ratio R on Fatigue Crack Growth in Type 304 Stainless Steel at Room Temperature', *Engineering Fracture Mechanics*, Vol. 11, 1979, pp. 275-283.

54. Davidson, David L., 'Determination of The Local Driving Force for Fatigue Crack Growth under Variable Amplitude Loading', *Spring Meeting, French Metallurgical Society*, June 1988.

55. Welsch, E., D. Eifler, B. Xcholtes and E. Macherauch, 'Influence of a Residual Surface Stress Field Near The Crack Tip on Crack Propagation', *Fracture Control of Engineering Structures*, 6th European Conference on Fracture, 1986, pp.1303-1320.

56. Honda, Kazuo, Tashiyudi Torii and Norihiko Toi, 'Relation Between Fatigue Crack Propagation and Residual Stress Distribution near Crack Measured by X-Ray', *Zairyo, Journal of the Society of Materials Science,* Japan, Vol. 33, No. 365, Feb. 1984, pp.103-109.

57. Kunz, L., Z. Knesl and P. Lukas, 'Macroscopic Residual Stress Distribution at a Fatigue Crack Tip', *Fatigue of Engineering Materials and Structures,* Vol. 2, 1979, pp. 279-287.

58. Schlosberg, W. H. and J. B. Cohen, 'The Plastic Zone and Residual Stress near a Notch and a Fatigue Crack in HSLA Steel', *Metallurgical Transactions A,* Vol. 13a, 1982, pp. 1987-1995.

59. Taira, Shuji and Keisuke Tanaka, 'Study of Fatigue Crack Propagation by X-Ray Diffraction Approach', *Engineering Fracture Mechanics,* Vol. 4, 1972, pp. 925-938.

60. Blyumenauer, Kh. and B. Zutkhoff, 'X-Ray Diffraction determination of Stress Distribution in Specimens with Fatigue Cracks', *Strength of Materials,* Vol. 13, No. 3, 1981, pp. 281-283.

61. Allison, J. E., 'Measurement of Crack-Tip Stress Distributions by X-Ray Diffraction', *Fracture Mechanics. ASTM STP 677,* 1979, pp. 550-562.

62. Macherauch, E. and U. Wolfstieg, 'Recent German Activities in the Field of X-Ray Stress Analysis', *Materials Science and Engineering,* Vol. 30, 1977, pp. 1-13.

63. Lindley, T. C. and C. E. Richards, 'The Relevance of CRack Closure to Fatigue Crack Propagation', *Materials Science and Engineering,* Vol. 14, 1974, pp. 281-293.

64. Mills, W. J. and R. W. Hertzberg, 'The Effect of Sheet Thickness on Fatigue Crack Retardation in 2024-T3 Aluminum Alloy', *Engineering Fracture Mechanics,* Vol. 7, 1975, pp. 705-711.

65. Minakawa, K., G. Levan, and A. J. McEvily, 'The Influence of Load Ration on Fatigue Crack Growth in 7090-T6 and IN9021-T4 P/M Aluminum Alloys', *Metallurgical Transactions A,* Vol. 17A, October 1986, pp. 1787-1795.

66. McEvily, A. J., Discussion, *Fatigue and Fracture of Engineering Materials and Structures,* Vol. 12, No. 1, 1989, pp. 71-72.

67. Fleck, N. A. and R. A. Smith, 'Crack Closure - Is It Just a Surface Phenomenon', *International Journal of Fatigue,* Vol. 4, 1982, pp. 157-160.

68. Shercliff, H. R. and N. A. Fleck, 'Effect of Specimen Geometry on Fatigue Crack Growth in Plane Strain ——— I. Constant Amplitude Response, II. Overload Response', *Fatigue and Fracture on Engineering Material and Structure*, Vol. 13, No. 3, pp. 287-310.

69. Damri, D. and J. F. Knott, 'Transient Retardations in Fatigue Crack Growth Following a Single Peak Overload', *Fatigue and Fracture on Engineering Material and Structure*, Vol. 14, No. 7, 1991, pp. 709-719.

70. Williams, D. R., D. L. Davidson, and J. Lankford, 'Crack Tip Stresses as Computed from Strains Determined by Stereo imaging', *Experimental Mechanics*, V.23, 1983, pp.242-248

71. Sehitoglu, Huseyin and Wei Sun, 'Modelling of Plane Strain Fatigue Crack Closure', *ASME Journal of Engineering Materials and Technology*, Vol. 113, No. 1, 1990, pp. 31-40.

72. Sehitoglu, Huseyin and Wei Sun, 'Mechanisms of Crack Closure in Plane Strain and Plane Stress', 3rd Conference on Biaxial/Multiaxial Fatigue, Stuttgart, Germany, 1989.

73. Rice, J. R., 'Mechanics of Crack Tip Deformation and Extension by Fatigue', *Fatigue Crack Propagation*, ASTM STP 415, 1967, pp. 281 - 301.

74. Broek, D., "The Propagation of Fatigue Cracks Emanating from Holes," Report NLR TR-72134C, National Aerospace Laboratory, Amsterdam, The Netherlands, 1972.

75 Truyens, P., "Crack Growth under Variable Load in Ships," Ph.D. Thesis, State University of Ghent, Belgium, Nov. 1976 (in Dutch). Also see Nibbering, J. J. W., "Vermoeiing van gelaste constructies," Parts 1, 2, 3, Lastijdschrift nos. 1, 2, 3, 1978 (in Dutch).

76. El Haddad, M. H., K. N. Smith, and T. H. Topper, "A Strain Based Intensity Factor Solution for Short Fatigue Cracks Initiating from Notches," *Fracture Mechanics*, ASTM STP 677, American Society for Testing and Materials, 1979, pp. 274-289.

77. Leis, B. N., and T. P. Forte, "Fatigue Growth of Initially Physically Short Cracks in Notched Aluminum and Steel Plates," *Fracture Mechanics: Thirteenth Conference, ASTM STP 743*, American Society for Testing and Materials, 1981, pp. 100-124.

78. Leis, B. N., and R. D. Galliher, "Growth of Physically Short Corner Cracks at Circular Notches," *Low-Cycle Fatigue and Life Prediction, ASTM STP 770*, American Society for Testing and Materials, 1982, pp. 399-421.

79. Leis, B. N., "Fatigue Crack Propagation Through Inelastic Gradient Fields," *International Journal of Pressure Vessels and Piping*, Vol. 10, No. 2, March 1982, pp. 141-158.

80. Leis, B. N., "Microcrack Initiation and Growth in a Pearlitic Steel Experiments and Analysis," Fracture Mechanics: *Fifteenth Symposium, ASTM STP 833*, American Society for Testing and Materials, 1984, pp. 449-480.

81. Leis, B. N., "Displacement Controlled Fatigue Crack Growth in Inelastic Notch Fields: Implications for Short Cracks," *Engineering Fracture Mechanics*, Vol. 22, No. 2, 1985, pp. 279-293.

82. Tanaka, K., and Y. Nakai, "Propagation and Non-Propagation of Short Fatigue Cracks at a Sharp Notch," *Fatigue of Engineering Materials and Structures*, Vol. 6, No. 4, 1983, pp. 315-327.

83. Usami, S., "Short Crack Fatigue Properties and Component Life Estimation," *Current Research on Fatigue Cracks*, MRS Vol. 1, Society of Materials Science, Japan, 1985, pp.

84. Shin, C. S., and R. A. Smith, "Fatigue Crack Growth from Sharp Notches," *International Journal of Fatigue*, Vol. 7, No. 2,1985, pp. 87-93.

85. Shin, C. S., and R. A. Smith, "Fatigue Crack Growth at Stress Concentrations--The Role of Notch Plasticity and Crack Closure," *Engineering Fracture Mechanics*, Vol. 29, No. 3, 1988, pp. 301-315.

86. Sehitoglu, H., "Fatigue Life Prediction of Notched Members Based on Local Strain and Elastic-Plastic Fracture Mechanics Concepts," *Engineering Fracture Mechanics*, Vol. 18, No. 3,1983, pp. 609-621.

87. Sehitoglu, H., "Characterization of Crack Closure," *Fracture Mechanics: Sixteenth Symposium, ASTM STP 868*, American Society for Testing and Materials, 1985, pp. 361-380.

88. Suresh, S., and R. O. Ritchie, "Propagation of Short Fatigue Cracks," *International Metals Reviews*, Vol. 29, No. 6,1984, pp. 445-476.

89. Sehitoglu, H., "Crack Opening and Closure in Fatigue," *Engineering Fracture Mechanics*, Vol. 21, No. 2,1985, pp. 329-339.

90. R. C. McClung and H. Sehitoglu, "Fatigue Crack Growth From Notches", ASME, J.Eng. Mats., To be published 1991.

91. Newman, J. C., Jr., 'A Nonlinear Fracture Mechanics Approach to the Growth of Small Cracks', Proc. of the 55th AGARD Meeting on Behaviour of Short Cracks in Airframe Components, Toronto, 1982.

92. Hammouda, M. M., and K. J. Miller, "Elastic Plastic Fracture Mechanics Analysis of Notches," *Elastic-Plastic Fracture, ASTM STP 668*, American Society for Testing and Materials, 1979, pp. 703-719.

93. Hammouda, M. M., R. A. Smith, and K. J. Miller, "Elastic-Plastic Fracture Mechanics for Initiation and Propagation of Notch Fatigue Cracks," *Fatigue of Engineering Materials and Structure*, Vol. 2,1979, pp. 139-154.

94. Keyvanfar, F., 'Effects of Residual Stresses on Fatigue Crack Propagation', Ph. D Thesis, Stanford University, 1985.

95. Lalor, P., H. Sehitoglu, and R. C. McClung, "Mechanics Aspects of Small Crack Growth from Notches--The Role of Crack Closure," *The Behavior of Short Fatigue Cracks*, EGF Pub. 1, Mechanical Engineering Publications, London, 1986, pp. 369-386.

96. Newman, J. C., Jr., "An Improved Method of Collocation for the Stress Analysis of Cracked Plates with Various Shaped Boundaries," NASA TN D- 6376, Aug. 1971.

97. Topper, T. H. and B. I. Sandor, 'Effects of Mean Stress and Prestrain on Fatigue-Damage Summation', Effects of Environment and Complex Load History on Fatigue Life, ASTM STP 462, 1970, pp. 93-104.

98. Topper, T. H., B. I. Sandor and JoDean Morrow, 'Cumulative Fatigue Damage Under Cyclic Strain Control', Journal of Materials, JMLSA, Vlo. 4, No. 1, 1969, pp. 189-199.

99. Nihei, M., P. Heuler, Ch. Boller and T. Seeger, 'Evaluation of Mean Stress Effect on Fatigue Life By Use of Damage Parameters', International Journal of Fatigue, Vol. 8, No. 3, 1986, pp. 119-126.

100. Hatanaka, K, T. Fujimitsu and H. Ichiyama, 'The Effect of Mean Stress and Strain on Crack Growth and Crack Closure in Low-Cycle Fatigue', JSME International Journal, Series I, Vol. 31, No. 2, 1988, pp. 280-286.

101. Kllman, V. and M. Bily, 'Influence of Mode Control, Mean Value and Frequency of Loading on the Cyclic Stress-Strain Curve', Material Science and Engineering, Vol. 44, 1980, pp. 73-79.

102. Koh, S. K. and R. I. Stephens, 'Mean Stress Effects on Low Cycle Fatigue for a High Strength Steel', Fatigue and Fracture on Engineering Material and Structure, Vol. 14, No. 4, 1991, pp. 413-428.

103. Fash, J. and D. F. Socie, 'Fatigue Behaviour and Mean Effects in Grey Cast Iron,' International Journal of Fatigue, 1982, pp. 137-142.

104. Dowling, N. E., 'Notched Member Fatigue Life Predictions Combining Crack Initiation and Propagation', *Fatigue of Engineering Materials and Structures,* Vol. 2, No. 2, pp. 129-138, 1979.